ABSTRACT

HUAYTA RAMIREZ, JAVIER. Quantitative Analysis of the Effects of Environmental Factors on Lifespan and Stress Resistance of *C. elegans*. (Under the direction of Dr. Adriana San Miguel Delgadillo).

In developing countries, the number of elderly adults will continue to increase in the near future, causing a higher impact on society. Amongst the causes for these population tendencies is the improvement on health services experienced during the previous decades. Consequently, this has caused a rise in lifespan, defined as the maximum amount of time an organism in a species can live . Furthermore, elderly adults have a higher risk of exhibiting diseases such as Alzheimer's disease, Parkinson's disease, and several forms of dementia ; this underscores the relevance of performing studies on the effect of environmental stressors and their influence in the aging process. For that purpose, we have a powerful model organism for in *C. elegans*, a microscopic nematode that has been important in elucidating genetic and environmental factors affecting lifespan. This work would be the first of its kind to use an integrated approach using CRISPR/Cas9, deep learning, and machine learning tools to characterize lifespan and healthspan, while associating this metric to the spatiotemporal activity of longevity genes. Our systems biology approach will enable the advancement of our to understanding of the fundamental mechanisms by which genetic pathways regulate the lifespan and stress resistance.

In **Chapter 2** we modify and improve an existing CRISPR/Cas9 approach to allow us the generation of transgenic lines. These strains will enable tracking of endogenous levels of expression of transcription factors that regulate the stress response in *C. elegans*. We will also demonstrate that DAF-16 and PHA-4 have different responses to

the same stimuli, giving insights on how a change in food source induces stress in these animals.

In **Chapter 3**, we use our DAF-16 strain to explore further the response of *C. elegans* to dietary restriction and its role in dietary restriction. For this purpose, we describe the use of a custom/made MATLAB algorithm and deep learning tools to track endogenous DAF-16. To achieve this we expose the animals to various dietary restriction regimes and quantify the DAF-16 response and lifespan extension conveyed by its activity. We show that by combining these metrics, we are able to account for up to 78% of lifespan variation by using only DAF-16 activity as input. Furthermore, we describe that the main contributors to lifespan extension are neuron and intestinal cells. Finally, we describe a new interaction of DAF-16 in the cell nucleoli, where we observed DAF-16 migration, indicating a possible mechanism for lifespan extension in nucleolus previously undescribed.

In **Chapter 4** we describe the development of our custom-made MATLAB algorithm and other deep learning, and machine learning tools that we sued to extract the data in Chapter 3. This includes a new algorithm that is able to track the subtle translocation patterns of endogenous single-copy DAF-16, a Fine Tree Classifier that enables assessment of tissue contribution to DAF-16 activity, and a Mask R-CNN that can see potential use to track morphological changes of *C. elegans* pharynx.

In **Chapter 5** we develop a platform for the evaluation of combinatorial exposure to xenobiotics and environmental factors, by using a simplex centroid design. This experimental approach enables us to evaluate the oxidative response in *C. elegans* under conditions of food limitations and heat-shock. We determined that dietary restriction

enhances the effect of ternary mixtures of naphthoquinones while heat-shock abrogates the oxidative response to these chemicals. This puts in perspective the importance of performing these combinatorial analyses using our approach.

In **Chapter 6**, we explore methods and techniques for the assessment of healthspan and lifespan in short-lived *C. elegans* mutants. We describe that these metrics are robust to indicate that the strains evaluated not only have a diminished longevity but also have an early onset of aging phenotypes in the pharynx and their locomotion.

Quantitative Analysis of the Effects of Environmental Factors on Lifespan and Stress Resistance of *C. elegans*

by
Javier Huayta Ramirez

A dissertation submitted to the Graduate Faculty of
North Carolina State University
in partial fulfillment of the
requirements for the degree of
Doctor of Philosophy

Chemical Engineering

Raleigh, North Carolina
2022

APPROVED BY:

_____	_____
Dr. Adriana San Miguel Delgadillo Committee Chair	Dr. Balaji Rao
_____	_____
Dr. Albert Keung	Dr. Kevin Flores

DEDICATION

I would like to dedicate this to my parents, who introduced me to math and sciences since I was a child. They made sure that I had access to education and supported me in every step I took during my career.

BIOGRAPHY

Javier Huayta was born in Lima, Peru in 1982. Since a young age, his parents instill in him a love for reading and the mathematics. During his time in high school, he develop a particular passion for science courses and classes, especially chemistry and biology. However, he also kept an interest in history, in particular the study of the long nineteenth century. After graduating from high school in 1997, he decided to pursue a degree in engineering. Is in this way that Javier was accepted to the Chemical Engineering undergraduate program at National University of San Marcos (UNMSM) in Peru. While here, Javier grew an interest in research of environmental sciences, led by his thesis advisor Dr. Jorge Loayza. After graduating with his bachelor degree, he started a fruitful and long tenure at INSUMEX S.A., a Peruvian company specialized in the extraction and processing of non-metallic mineral. It is here that Javier discover that his true passion and the one he decided to further pursue was in teaching and training new engineers that join his place of work. With this in mind. Javier decided to apply to the PhD program in Chemical Engineering at North Carolina State University after working in industry for 13 years. At the end of 2016, Javier joined the research group of Dr. Adriana San Miguel Delgadillo as her third graduate student. Here he completed his thesis research on the study of *C. elegans* and the effects of stressors in its lifespan and healthspan. Javier is looking forward at joining the research group of Dr. Joel Meyer at Duke University in Summer of 2022 as a postdoctoral researcher.

ACKNOWLEDGMENTS

First I want to thank my mom, my dad, and my sister (and now my brother-in-law and niece). Without their support and encouragement, it would have not been possible to move to a different country, with a different language, and different customs. I also want to thank my fiancée, Sarah Rosenzweig, whose patience I have tested multiple times, but who is always ready to support and find ways to keep me in the right track.

I want to thank my advisor, Dr. Adriana San Miguel for instilling in me a passion for *C. elegans* research that I hope I can keep for many more years. Without her support from day 1 I would not be here today. I also want to thank my collaborators and committee members, Dr. Kevin Flores, Dr. Albert Keung, and Dr. Balaji Rao. I want to thank The Director of Graduate Programs Dr. Saad Khan and the best Student Services Specialist Sandra Bailey. I also want to thank all of my group members, past and present but especially Dr. Sahand Saberi with whom we always held the most particular lunch conversations, Dr. Daniel Midkiff for been such a funny person to be around, Karthik Suresh Arulalan who is like my little brother, Andrew Clark, James Lichty, Victoria Karakis (the elder), Victoria Yarmey (the younger), Kin Gomez, Hrishikesh Mane, Mariam Shah, Zachary Kalmanson, Sreevansh Mareddy, Daisy Aguilar, Darlene Salvador, Joey Crapster, Morgan Stephens, Rita Tejada, Carolina Lopez, Mohammad Omary, Riley Reid, Zack Crawford, Sean Engels, Josh Currens, and Ori Soker.

Finally, I want to thank to all the friends I made along the way and who made my time at NC State a great one, Tommy Rudibaugh with whom I am looking forward to keep our social media partnership, Ryan Tam who taught me that it is never late to try new things, Chris Estridge who taught me that there is nothing better than winning at Fantasy

Football, Ryan Barton, Daniel Cardenas, Natasha Castellanos, Taylor Neumann, Ryan Dudek, Seif Yusuf, Zach Campbell, Jennifer Clark, Begum Yagci, Scott Collins, Dilara Sen Peers, Eliezer Reyes, Emily Facchine, Emily Krzystowcyk, Fausto Ortiz, Hadel Al Asafen, Jenna Meanor, Jiaqi Yan, John van Schaik, Kristine Smith, Michael Mantini, Rajesh Paul, Robbie Epps, Rachel Nye, Salvatore Luiso, Seungkeun Song, Kaihang Shi, Siyao Wang, and Shravan Pradeep. I hope I did not forget anyone!

TABLE OF CONTENTS

LIST OF FIGURES

Chapter 1: Motivation and Introduction

1.1 Motivation for aging studies

In modern society, the number of elderly adults will continue to increase in the near future, causing higher economic and social impacts on countries. Amongst the causes for these population tendencies is the improvement on health services experienced during the previous decades. Consequently, this has caused a rise in lifespan, defined as the maximum amount of time an organism in a species can live[1]. Furthermore, elderly adults have a higher risk of exhibiting diseases such as Alzheimer's disease, Parkinson's disease, and several forms of dementia[2]; this highlights the relevance of performing aging studies. For that purpose, we have a powerful model organism for aging research in *C. elegans*, a microscopic nematode that has been important in elucidating genetic and environmental factors affecting lifespan[3]. Our work would be the first of its kind to use integrate metrics such as exposure time and concentration and to characterize lifespan, while associating this metric to the spatiotemporal endogenous activity of a transcription factor. Moreover, our systems biology approach will enable the prediction of lifespan by using metrics such as gene activity and food availability. Finally, our findings and results will help to understand the fundamental mechanisms by which these players regulate the aging process.

1.2 *C. elegans* as a model organism for aging

C. elegans is a microscopic free-living nematode; it has a rapid life cycle, going from egg to adult in 3 days at 25°C. It has a relatively short lifespan of 3 weeks, which makes lifelong experiments possible in a timely manner. Its newly hatched larvae are 250μm long and an average adult is 1mm long[3]. Because *C. elegans* has a transparent

body, individual cells and tissues are easily observed using differential interference contrast (DIC) microscopy[4]. Moreover, fluorescent proteins can be used to tag proteins or subcellular compartments to screen and track protein activity *in vivo*[5]. *C. elegans* is primarily a self-fertilizing hermaphrodite, with males appearing at a rate lower than 0.2%, this enables maintenance of isogenic populations[3]. Additionally, *C. elegans* has an invariant number of 959 somatic cells, which has enabled researchers to map a complete cell lineage and wiring diagram of its nervous system[6]. Finally, at least 38% of the *C. elegans* protein-coding genes have predicted orthologs in the human genome, 60%-80% of human genes have orthologs in the *C. elegans* genome, and 40% of genes known to be associated with human diseases have clear orthologs in the *C. elegans* genome[7,8]. Using this nematode, a number of genetic factors have been shown to play an important role in regulating the aging process. These genetic factors are related to a number of environmental stressors, and their interplay regulates longevity in *C. elegans*[1,9]. Some of the pathways involved include insulin/insulin-like growth factor-1 signaling (IIS), TOR signaling, sirtuins, AMP-activated protein kinases, mitochondrial activity, hypoxia inducible factor-1 (HIF-1), and a number of epigenetic mechanisms[9]. These characteristics make *C. elegans* a powerful model organism to study the interplay between aging-regulating genes, environmental factors, and lifespan.

C. elegans has played an important role in elucidating the function of genetics in determining an organism's lifespan and healthspan. Seminal work by Cynthia Kenyon demonstrated that one mutation in the *daf-2* gene was enough to double the lifespan of these mutant nematodes[10]. This was achieved because *daf-2* is the upstream regulator of the Insulin/IGF-1 signaling pathway, whose downstream regulator is *daf-16*, a

transcription factor that governs the Insulin/IGF-1 signaling pathway. When active, DAF-16 translocates to cell nuclei where it enables activation of other aging-regulating and cell-protection genes. Furthermore, studies using *C. elegans* have shown the beneficial effects of hormetic stress in lifespan extension and increased resilience to stressors[11–14]. For example, exposure to various types of dietary restriction (DR), oxidative stress, and heat-shock in low doses provides these nematodes with longer lifespan[15]. Finally, similar studies performed in other organisms indicate that these effects of stress are also present in other organisms such as *D. melanogaster*, mice and primates[12,16,17], displaying the relevance of performing longitudinal studies with *C. elegans*.

These characteristics and developments of *C. elegans* highlight its importance as a model organism to quantify the effects of environmental stressors in its longevity and stress response, while performing these longitudinal studies in a timely manner.

1.3 Challenges in the assessment of gene activity in *C. elegans*

Various approaches have been successfully used to assess gene expression in *C. elegans* cells, tissues, and at different developmental stages, such as DNA microarrays, real-time PCR, RNAseq, and serial analysis of gene expression (SAGE)[18,19]. Nevertheless, these methods are not suitable for *in vivo* analysis of gene expression, since these techniques are destructive in nature, as they require extraction of DNA and RNA[20–22]. Furthermore, these techniques do not provide the spatial information required to assess nuclear translocation of cytoplasmic DAF-16 to cell nuclei, or to evaluate the different migrating patterns of DAF-16 in various tissues.

An alternative to the previously mentioned methods is to employ a *C. elegans* strain with a fluorescent tag attached to the gene of interest. Previous studies have used

said strains with fluorescently tagged DAF-16[23]. However, this introduces further problems as these strains are traditionally generated by injecting a plasmid mix in the gonad of adult worms, inducing the formation of extrachromosomal arrays in its progeny, carrying the fluorescent tag[5,24]. The strains produced in this manner can carry transgenic arrays that typically have hundreds of copies of the gene[25], possibly introducing overexpression effects, mosaicism, or being silenced in the *C. elegans* germline[25,26]. Additionally, these strains could be labeling only specific isoforms or tracking the gene of interest only in specific tissues[27].

A more recent method consists of taking advantage of the mobilization of the Mos1 transposon to insert a single copy of a transgene, named Mos1-mediated Single Copy Insertion (MosSCI). This technique avoids some of the problems of working with extrachromosomal arrays, but it is limited to the number and location of the Mos1 transposon in the *C. elegans* genome, and it removes the endogenous cis- or trans-regulatory elements associated with its genomic location[28,29]. This last hurdle is overcome by using a CRISPR/Cas9 approach, which enables targeting of almost any genomic location[30–33].

1.4 Tracking of *gene* activity enabled by CRISPR and machine learning

In developing countries, the nu Recent studies have developed methods for using CRISPR/Cas9 genome editing in *C. elegans*[30,32,34]. In all cases, these require the injection of adult worms in their gonads with a mix containing Cas9, a single-guide RNA (sgRNA), and repair templates, usually contained in plasmids. Once delivered to the gonad, Cas9 generates breaks in the target location indicated with the sgRNA. The repair templates contain a cassette with the fluorophore sequence, selection markers, and is flanked by

homology arms corresponding to the section of *C. elegans* genome that is being targeted[33]. This exploits the homology direct repair (HDR) mechanism used by cells to repair double-strand DNA lesions[35]. Homologous recombination paired with CRISPR/Cas9 thus enables introduction of a fluorescent tag at the endogenous loci of the target gene.

Using this approach overcomes all the problems commonly found in the assessment of gene activity with fluorescent-tagged strains developed with traditional methods. A CRISPR/Cas9 approach enables tracking of endogenous levels of expression by keeping single copies of the fluorophore in the endogenous loci[34]. Additionally, the flexibility in choosing the editing location provided by this approach, permits the tagging of all the isoforms of our target genes. This is achieved by making the edit at the C-terminus of the gene, before the stop codon, shared by all isoforms.

1.5 References

1. Kenyon, C. J. The genetics of ageing. *Nature* **464**, 504–512 (2010).
2. Arey, R. N. & Murphy, C. T. Conserved regulators of cognitive aging: From worms to humans. *Behavioural Brain Research* **322**, 299–310 (2017).
3. Corsi, A. K., Wightman, B. & Chalfie, M. A transparent window into biology: A primer on Caenorhabditis elegans. *Genetics* **200**, 387–407 (2015).
4. Porta-de-la-Riva, M., Fontrodona, L., Villanueva, A. & Cerón, J. Basic Caenorhabditis elegans methods: Synchronization and observation. *J. Vis. Exp.* e4019 (2012). doi:10.3791/4019
5. Boulin, T. Reporter gene fusions. *WormBook* 1–23 (2006). doi:10.1895/wormbook.1.106.1
6. Alper, S. & Podbilewicz, B. Cell fusion in Caenorhabditis elegans. *Methods in Molecular Biology* **475**, 53–74 (2008).
7. Markaki, M. & Tavernarakis, N. Modeling human diseases in Caenorhabditis elegans. *Biotechnology Journal* **5**, 1261–1276 (2010).
8. Kaletta, T. & Hengartner, M. O. Finding function in novel targets: C. elegans as a model organism. *Nature Reviews Drug Discovery* **5**, 387–399 (2006).
9. Uno, M. & Nishida, E. Lifespan-regulating genes in C. elegans. *Aging Mech. Dis.* **2**, 16010 (2016).
10. Lin, K., Hsin, H., Libina, N. & Kenyon, C. Regulation of the Caenorhabditis elegans longevity protein DAF-16 by insulin/IGF-1 and germline signaling. *Nature Genetics* **28**, 139–145 (2001).
11. Schulz, T. J. *et al.* Glucose Restriction Extends Caenorhabditis elegans Life Span

by Inducing Mitochondrial Respiration and Increasing Oxidative Stress. *Cell Metab.* **6**, 280–293 (2007).

12. Masoro, E. J. Overview of caloric restriction and ageing. *Mechanisms of Ageing and Development* **126**, 913–922 (2005).
13. Przybysz, A. J., Choe, K. P., Roberts, L. J. & Strange, K. Increased age reduces DAF-16 and SKN-1 signaling and the hormetic response of Caenorhabditis elegans to the xenobiotic juglone. *Mech. Ageing Dev.* **130**, 357–369 (2009).
14. Kumsta, C., Chang, J. T., Schmalz, J. & Hansen, M. Hormetic heat stress and HSF-1 induce autophagy to improve survival and proteostasis in C. Elegans. *Nat. Commun.* **8**, (2017).
15. Greer, E. L. & Brunet, A. Different dietary restriction regimens extend lifespan by both independent and overlapping genetic pathways in C. elegans. *Aging Cell* **8**, 113–127 (2009).
16. Weindruch, R. The retardation of aging by caloric restriction: Studies in rodents and primates. *Toxicol. Pathol.* **24**, 742–745 (1996).
17. Mattison, J. A. *et al.* Caloric restriction improves health and survival of rhesus monkeys. *Nat. Commun.* **8**, (2017).
18. Wang, X. *et al.* Identification of genes expressed in the hermaphrodite germ line of C. elegans using SAGE. *BMC Genomics* **10**, (2009).
19. Hunt-Newbury, R. *et al.* High-throughput in vivo analysis of gene expression in Caenorhabditis elegans. *PLoS Biol.* **5**, 1981–1997 (2007).
20. Portman, D. Profiling C. elegans gene expression with DNA microarrays. *WormBook* 1–11 (2006). doi:10.1895/wormbook.1.104.1

21. Murphy, C. T. *et al.* Genes that act downstream of DAF-16 to influence the lifespan of Caenorhabditis elegans. *Nature* **424**, 277–284 (2003).

22. McElwee, J., Bubb, K. & Thomas, J. H. Transcriptional outputs of the Caenorhabditis elegans forkhead protein DAF-16. *Aging Cell* **2**, 111–121 (2003).

23. Kumsta, C. & Hansen, M. C. elegans rrf-1 mutations maintain RNAi efficiency in the soma in addition to the germline. *PLoS One* **7**, (2012).

24. Evans, T. Transformation and microinjection. *WormBook* 1–15 (2006). doi:10.1895/wormbook.1.108.1

25. Stinchcomb, D. T., Shaw, J. E., Carr, S. H. & Hirsh, D. Extrachromosomal DNA transformation of Caenorhabditis elegans. *Mol. Cell. Biol.* **5**, 3484–3496 (1985).

26. Seydoux, G. & Schedl, T. The germline in C. Elegans: Origins, proliferation, and silencing. *Int. Rev. Cytol.* **203**, 139–185 (2001).

27. Libina, N., Berman, J. R. & Kenyon, C. *Tissue-Specific Activities of C. elegans DAF-16 in the Regulation of Lifespan*. *Cell* **115**, (2003).

28. Robert, V. & Bessereau, J. L. Targeted engineering of the Caenorhabditis elegans genome following Mos1-triggered chromosomal breaks. *EMBO J.* **26**, 170–183 (2007).

29. Frøkjær-Jensen, C. *et al.* Single-copy insertion of transgenes in Caenorhabditis elegans. *Nat. Genet.* **40**, 1375–1383 (2008).

30. Paix, A., Folkmann, A., Rasoloson, D. & Seydoux, G. High Efficiency, Homology-Directed Genome Editing in Caenorhabditis elegans Using CRISPR-Cas9 Ribonucleoprotein Complexes. *Genetics* **201**, 47–54 (2015).

31. Dickinson, D. J., Ward, J. D., Reiner, D. J. & Goldstein, B. Engineering the

Caenorhabditis elegans genome using Cas9-triggered homologous recombination. *Nat. Methods* **10**, 1028–1034 (2013).

32. Dickinson, D. J., Pani, A. M., Heppert, J. K., Higgins, C. D. & Goldstein, B. Streamlined genome engineering with a self-excising drug selection cassette. *Genetics* **200**, 1035–1049 (2015).

33. Dickinson, D. J. & Goldstein, B. CRISPR-based methods for caenorhabditis elegans genome engineering. *Genetics* **202**, 885–901 (2016).

34. Vicencio, J., Martínez-Fernández, C., Serrat, X. & Cerón, J. Efficient generation of endogenous fluorescent reporters by nested CRISPR in caenorhabditis elegans. *Genetics* **211**, 1143–1154 (2019).

35. Katic, I., Xu, L. & Ciosk, R. CRISPR/Cas9 Genome Editing in Caenorhabditis elegans : Evaluation of Templates for Homology-Mediated Repair and Knock-Ins by Homology-Independent DNA Repair. *G3* **5**, 1649–1656 (2015).

Chapter 2: Generation of *C. elegans* strains for tracking of endogenous spatiotemporal activity

2.1 Abstract

Traditional techniques for generation of C. elegans transgenic lines have multiple limitations such as the introduction of multiple copies of the transgenic gene, overexpression, mosaicism, and lacking of endogenous expression. We used a modified CRISPR/Cas9 approach to circumvent these problems by tagging transcription factors at their endogenous loci. In this manner, we generate endogenously tagged strains for the transcription factors DAF-16 and PHA-4. We used these strains for evaluating the interplay of these transcription factors under conditions of stress. Moreover, we show that our modified pipeline can be used to generate endogenously tagged strains for other transcription factors such as SKN-1.

2.2 Introduction

Transformation has long been used to generate arrays and to cause random integration of transgenes into the genome. This requires the injection of DNA in the germ line of adult animals. Afterwards, the injected DNA is transmitted to a portion of the progeny[1]. Nevertheless, this method results in multi-copy transgenes, and the inability to determine endogenous levels of gene expression[2]. New CRISPR/Cas9 systems have been developed, aimed specifically for the generation of *C. elegans* transgenic lines with fluorescent tags and selectable markers, while still using microinjection for primary delivery[3–8]. These systems enable targeting endogenous loci to introduce single-copy, custom-made gene-fluorophore constructs with selection markers that provide an easy to identify phenotype for knock-in isolation. We to focus on tagging DAF-16, PHA-4, and

SKN-1, as these transcription factors regulate the activity of many downstream longevity genes. Moreover, all of these transcription factors have been found to show spatiotemporal activity under dietary restriction, opening the possibility of finding novel interactions between these proteins[9,10]. To introduce the tag into the endogenous loci of its respective gene we used a CRISPR/Cas9 system based on homologous recombination of a template containing the fluorophore and a self-excising selection cassette[6]. We chose the Cas9 target site by identifying a single guide RNA (sgRNA) near the stop codon of the target gene. Targeting this region permits tagging of all possible isoforms of the gene. Criteria such as specificity, activity, and distance to the stop codon are considered in selecting the sgRNA. Its sequence is introduced into a Cas9-encoding construct (pDD162, Addgene #47549) using site-directed mutagenesis. Subsequently, 500bp homology arms at each side of the stop codon are generated by PCR amplification of genomic DNA from N2 (wildtype) animals. These fragments are isolated, purified, and introduced in a construct containing a selection cassette (pDD282, Addgene #66823) using Gibson assembly. An injection mix containing both plasmids is injected in the gonads of N2 young-adult animals. These animals are transferred to NGM plates and left to produce progeny. Hygromycin is added to the plates to kill untransformed F1 progeny. After 7 days, animals showing the RoI phenotype are transferred to new NGM plate. Putative knock-in animals are transferred to new plates for homozygous selection. Larvae from homozygous plates are heat-shocked to induce excision of the selection cassette. Wild-type adult animals lacking the RoI phenotype are picked and maintained as the strain containing the fluorescent-tagged gene. Finally, sequencing is performed to confirm correct introduction of the fluorescent tag. Using this approach, we have been able to

generate one strain encoding DAF-16 tagged with GFP, another encoding PHA-4 tagged with mKate2, and we have the groundwork to generate another strain with SKN-1 tagged with tagBFP.

2.3 Results

2.3.1 Generation of DAF-16 and PHA-4 strains

We started generating a DAF-16 strain following the method described by Dickinson et al[6] (further described in the methods section of this chapter). This method consists in the generation of a plasmid containing a single-guide RNA and the Cas9 sequence, and another plasmid containing homology arms flanking a selection cassette. This selection cassette is crucial for the success of this method as it contains a fluorescent protein tag, and a self-excising drug selection gene.

We were unsuccessful in using this method directly after generating all the plasmids necessary for injection. The original protocol called for the inclusion of three plasmids with selection markers with the objective of using these to identify for animals with extrachromosomal arrays[6]. These animals would be then selected as not desired. We reasoned that by including these three plasmids (for a total of five plasmids) we were increasing the likelihood of generating extrachromosomal arrays which was an income that we wanted to minimize. Therefore, we decided to exclude these plasmids from the injection mix. Another modification that we included was to increase the concentration of the plasmid containing the cassette and homology arms. We found the right concentration by trial and error; we tested multiple combinations of concentrations for both plasmids until we were able to produce a homozygous knock-in after multiple rounds of microinjection and transformation.

When we proceeded to generate our PHA-4 strain, we used our modified protocol directly. We were able to generate this strain on our first round of injection. This would indicate that the modifications introduced to the original protocol were important to increase the efficiency of this CRISPR/Cas9 approach. Interestingly, updates to the original protocol by Dickinson et al have introduced some of these modifications such as the plasmid concentration[11], and other recent protocols recommend their own variations on plasmid concentration[7].

2.3.2 Changed of food environment increases DAF-16 activity but not PHA-4

With the strains generated with our CRISPR/Cas9 approach, we decided to create a crossed strain having both transgenic genes and test if these strains can be used to quantify gene expression. Thus, we obtained a strain that allows for the imaging of both DAF-16 and PHA-4 concurrently in different color channels (DAF-16 in green for GFP, PHA-4 in red for mKate2). We tested if this strain could be used to quantify activity of these transcriptions factors under stressful conditions. An interesting type of stressor is the type of food provided to the animals. Typically, *C. elegans* is grown in plates containing bacterial lawns of *E. coli* O50. However, animals can also be grown in liquid culture and with other food sources such as *E. coli* HB101. Our reasoning here is that it has been shown that HB101 is considered more nutrient rich than OP50[12], the bacterial diet influences fat storage in *C. elegans*[13], and animals have been shown to prefer some bacterial sources over others[14]. This would indicate that we should be able to observe an effect from having animals from the same original population under different diet sources (**Figure 2.1**).

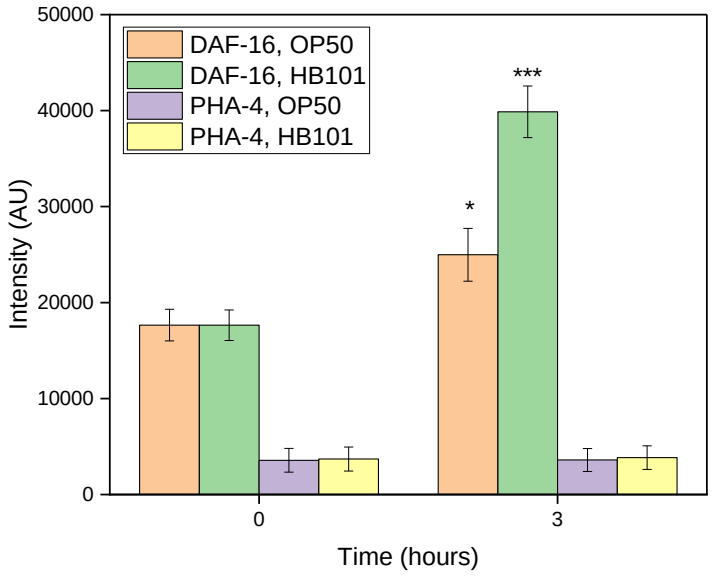

Figure 2.1 Effect of liquid culture and different food source in *C. elegans*. Animals grown on plates with OP50 were switched to liquid culture and provided with ad libitum OP50 or HB101. DAF-16 show increased intensity under both food sources. PHA-4 did not show any significant change in intensity.

We observed that DAF-16 and PHA-4 have different baseline at the start of the experiment. This is most likely because for our experimental conditions mKate2 has a lower intensity than GFP. Interestingly, only DAF-16 shows increased intensity but not PHA-4. This would indicate that the stress caused to animals from switching from a plate to a liquid culture is under the influence of DAF-16. Most likely, this changes induces an amount of food limitation and dietary restriction, which are stressors that induce DAF-16 activity[15]. However, if we focus on DAF-16, we observe that the animals with HB101 showed the larger change in activity of all cases. As mentioned previously, HB101 provides higher nutrition to the animals so we would have expected it to be induce less stress in the nematodes. Nevertheless, it has been shown that a diet if HB101 leads a reduced fat storage and increased lifespan[13,16] so it could be possible that HB101 is

producing an initial amount of stress (in our short experimental time) while the animals get accustomed to their new environment.

2.4 Discussion

In this chapter, we discussed the methods used for generating fluorescently tagged strains to track their endogenous activity. We demonstrated that the available protocols required modification for their successful use in the laboratory. Furthermore, we provide a list of these modifications that will be helpful for researchers using these methods. It is of note that we have the opportunity of discussing these concerns with other researchers and they shared encountering similar problems when using these CRSIPR/Cas9 methods (unpublished data).

We also tested our newly generated strains to highlight how using our approach will help quantify how these transcription factors governed the response to stress in *C. elegans*. Furthermore, we showed that switching animals from one type of media to a different one produces stress. This is important to account for in *C. elegans* studies that require using liquid culture for experiments. The use and valuable information obtained with these strains is expanded in Chapter 4.

2.4 Materials and methods

2.4.1 Strains, media, and culture

C. elegans was maintained on standard Nematode Growth Medium (NGM) plates seeded with OP50 *E. coli* bacteria and kept at 20 ºC until they started to lay eggs. Animals were then bleached using standard protocols to obtain age-synchronized populations[17] for microinjection. Strains used in this work were N2 (C. elegans wild isolate), ASM10 daf-16(del2[daf-16::GFP-C1^3xFlag]) I, ASM12 pha-4(del4[pha-4::mKate2^3xFlag]) V, and

ASM13 (daf-16(del2[daf-16::GFP-C1^3xFlag]) I, pha-4(del4[pha-4::mKate2^3xFlag]) V. OP50 E. coli was grown in LB media following standard procedures[18]. Bacteria were washed thrice with SB media, pelletized, and suspended in S-Medium at a concentration of 100 mg/mL, corresponding to a concentration of 2 x 10^{10} cells/ml.

2.4.2 Generation of DAF-16 transgenic line

We used a CRISPR/Cas9 approach developed by Dickinson *et al.* to insert a GFP-encoding sequence at the 3' end of *daf-16*[6]. We chose the Cas9 target site by identifying all possible single guide RNAs (sgRNA) in a 200bp region centered in the stop codon of the target gene. This region was selected to permit introduction of the fluorescent tag at the C-terminus, tagging in this manner all possible isoforms of the gene. Criteria such as specificity, activity, and distance to the stop codon were considered in selecting the sgRNA using the GuideScan design tool[19]. This 20bp sequence was introduced into a Cas9-encoding construct (pDD162, Addgene #47549) using a NEB Q5 Site-Directed Mutagenesis Kit to generate plasmid pJHR1. 500-700bp long homology arms at each side of the *daf-16* stop codon were then generated by PCR amplification of genomic DNA from N2 animals. These fragments were isolated, purified, and introduced in a construct containing a selection cassette (pDD282, Addgene #66823) using NEBuilder HiFi DNA Assembly Mix to generate plasmid pJHR2.

A mix containing 15ng/µL pJHR1, 50ng/µL pJHR2, and 2.5ng/µL pCFJ90 (mCherry co-injection marker) was injected in the gonads of 100 N2 young-adult animals following standard microinjection procedures[1]. These animals were transferred to NGM plates and left to produce progeny at 25 °C. Hygromycin was added to the plates to kill untransformed F1 progeny. After 7 days, animals showing the Rol phenotype and lacking

red fluorescent extrachromosomal array markers were transferred to new NGM plates without hygromycin. Individual putative knock-in animals were transferred to new plates for homozygous selection. Finally, L1 larvae from homozygous plates (those that contained only animals with the Rol phenotype) were heat-shocked at 34 °C for 4 hours to induce Cre expression, and excision of the selection cassette. Wild-type adult animals lacking the Rol phenotype were picked and maintained as the strain containing the fluorescent-tagged gene. PCR and Sanger sequencing were performed to confirm correct introduction of the tag.

2.4.3 Generation of PHA-4 transgenic line

We followed the same method as for DAF-16 but with the following caveats: the sgRNA sequence was introduced in plasmid pDD162 using a NEB q5 Sire-Directed Mutagenesis kit to generate plasmid pJHR4. 500-700bp long homology arms at each side of the *pha-4* stop codon were then generated by PCR amplification of genomic DNA from N2 animals. These fragments were isolated, purified, and introduced in a construct containing a selection cassette (pDD285, Addgene #66826) using NEBuilder HiFi DNA Assembly Mix to generate plasmid pJHR6. The injection mix contained 15ng/µL pJHR4, and 50ng/µL pJHR6.

2.4.4 Generation of *C. elegans* males and crosses

Around 20 hermaphrodites at the L4 stage were heat-shocked at 34C for 4 hours. These animals were left to recover at 20C for 3 days. The progeny was subsequently scored for the presence of males following established procedures[20]. For the generation of crosses, five males of the first strain were put in the same plate with one hermaphrodite

of the second strain. The progeny was separated in new plates for two generations and scored for heterozygous animals by fluorescent microscopy.

2.6 References

1. Evans T. Transformation and microinjection. *WormBook*. 2006:1-15. doi:10.1895/wormbook.1.108.1

2. Stinchcomb DT, Shaw JE, Carr SH, Hirsh D. Extrachromosomal DNA transformation of Caenorhabditis elegans. *Mol Cell Biol*. 1985;5(12):3484-3496. doi:10.1128/mcb.5.12.3484

3. Paix A, Folkmann A, Rasoloson D, Seydoux G. High Efficiency, Homology-Directed Genome Editing in Caenorhabditis elegans Using CRISPR-Cas9 Ribonucleoprotein Complexes. *Genetics*. 2015;201(1):47-54. doi:10.1534/genetics.115.179382

4. Paix A, Wang Y, Smith HE, et al. Scalable and Versatile Genome Editing Using Linear DNAs with Microhomology to Cas9 Sites in Caenorhabditis elegans. *Genetics*. 2014;198(December):1347-1356. doi:10.1534/genetics.114.170423

5. Dickinson DJ, Ward JD, Reiner DJ, Goldstein B. Engineering the Caenorhabditis elegans genome using Cas9-triggered homologous recombination. *Nat Methods*. 2013;10(10):1028-1034. doi:10.1038/nmeth.2641

6. Dickinson DJ, Pani AM, Heppert JK, Higgins CD, Goldstein B. Streamlined genome engineering with a self-excising drug selection cassette. *Genetics*. 2015;200(4):1035-1049. doi:10.1534/genetics.115.178335

7. Schwartz ML, Davis MW, Rich MS, Jorgensen EM. High-efficiency CRISPR gene editing in C. elegans using Cas9 integrated into the genome. Chisholm AD, ed. *PLOS Genet*. 2021;17(11):e1009755. doi:10.1371/journal.pgen.1009755

8. Vicencio J, Martínez-Fernández C, Serrat X, Cerón J. Efficient generation of endogenous fluorescent reporters by nested CRISPR in caenorhabditis elegans. *Genetics*. 2019;211(4):1143-1154. doi:10.1534/genetics.119.301965

9. Panowski SH, Wolff S, Aguilaniu H, Durieux J, Dillin A. PHA-4/Foxa mediates diet-restriction-induced longevity of C. elegans. *Nature*. 2007;447(7144):550-555. doi:10.1038/nature05837

10. Lee SS, Kennedy S, Tolonen AC, Ruvkun G. DAF-16 target genes that control C-elegans life-span and metabolism. *Science (80-)*. 2003;300(5619):644-647. doi:10.1126/science.1083614

11. Dickinson DJ, Goldstein B. CRISPR-based methods for caenorhabditis elegans genome engineering. *Genetics*. 2016;202(3):885-901. doi:10.1534/genetics.115.182162

12. So S, Tokumaru T, Miyahara K, Ohshima Y. Control of lifespan by food bacteria, nutrient limitation and pathogenicity of food in C. elegans. *Mech Ageing Dev*. 2011;132(4):210-212. doi:10.1016/j.mad.2011.02.005

13. Brooks KK, Liang B, Watts JL. The influence of bacterial diet on fat storage in C. elegans. *PLoS One*. 2009;4(10):e7545. doi:10.1371/journal.pone.0007545

14. Shtonda BB, Avery L. Dietary choice behavior in Caenorhabditis elegans. *J Exp Biol*. 2006;209(1):89-102. doi:10.1242/jeb.01955

15. Greer EL, Brunet A. Different dietary restriction regimens extend lifespan by both independent and overlapping genetic pathways in C. elegans. *Aging Cell*.

2009;8(2):113-127. doi:10.1111/j.1474-9726.2009.00459.x

16. Brejning J, Nørgaard S, Schøler L, et al. Loss of NDG-4 extends lifespan and stress resistance in Caenorhabditis elegans. *Aging Cell*. 2014;13(1):156-164. doi:10.1111/acel.12165

17. Porta-de-la-Riva M, Fontrodona L, Villanueva A, Cerón J. Basic Caenorhabditis elegans methods: Synchronization and observation. *J Vis Exp*. 2012;(64):e4019. doi:10.3791/4019

18. Amrit FRG, Ratnappan R, Keith SA, Ghazi A. The C. elegans lifespan assay toolkit. *Methods*. 2014;68(3):465-475. doi:10.1016/j.ymeth.2014.04.002

19. Perez AR, Pritykin Y, Vidigal JA, et al. GuideScan software for improved single and paired CRISPR guide RNA design. *Nat Biotechnol*. 2017;35(4):347-349. doi:10.1038/nbt.3804

20. Anderson JL, Morran LT, Phillips PC. Outcrossing and the maintenance of males within C. elegans populations. In: *Journal of Heredity*. Vol 101. Oxford Academic; 2010:S62-S74. doi:10.1093/jhered/esq003

Chapter 3: Endogenous DAF-16 Spatiotemporal Activity Quantitatively Predicts Lifespan Extension Induced by Dietary Restriction

3.1 Abstract

In many organisms, dietary restriction (DR) leads to lifespan extension through the activation of cell protection and pro-longevity gene expression programs. In the nematode *C. elegans*, the DAF-16 transcription factor is a key aging regulator that governs the Insulin/IGF-1 signaling pathway and undergoes translocation from the cytoplasm to the nucleus of cells when animals are exposed to food limitation. However, how large is the influence of dietary restriction on DAF-16 activity, and its subsequent impact on lifespan has not been quantitatively determined. In this chapter, we assess the endogenous activity of DAF-16 under various DR regimes by coupling CRISPR/Cas9-enabled fluorescent tagging of DAF-16 with quantitative image analysis and machine learning (as explained in Chapter 2). Our results indicate that DR regimes induce strong endogenous DAF-16 activity, although DAF-16 is less responsive in aged individuals. DAF-16 activity is in turn a robust predictor of mean lifespan in *C. elegans*, accounting for 78% of its variability under DR. Analysis of tissue-specific expression aided by a machine learning tissue classifier reveals that, under DR, the DAF-16 influence on lifespan extension mainly originates from the intestine and neurons. DR also drives DAF-16 activity in unexpected locations such as the germline and intestinal nucleoli.

3.2 Introduction

C. elegans exposed to plentiful food and a stress-free environment can sustain growth and reproduction. Under harsh environmental conditions such as food limitation, oxidative and heat stress, and others, several genetic pathways activate to promote cell

protection and survival in *C. elegans*. These pathways are governed by transcription factors such as DAF-16, PHA-4, and SKN-1[1]. Previous work has shown that these genetic pathways can be manipulated to modulate gene expression and extend lifespan[2–4]. Dietary restriction (DR) is the best-known environmental factor that can extend lifespan in many species[5–8]. In *C. elegans*, DAF-16 is a key pro-longevity transcription factor regulates the Insulin/IGF-1 signaling pathway. Under various forms of stress, DAF-16 migrates from the cytoplasm to the nucleus where it can regulate gene expression programs that lead to lifespan extension[9,10]. DAF-16 has been shown to be activated by DR, but only under certain regimes[11–13]. Likewise, systems approaches that have been used to identify and manipulate the regulatory networks of the DR response, confirm the involvement DAF-16[14]. However, how large is the influence of DR on DAF-16 activation and its subsequent effect on lifespan extension has not been quantitatively determined. In addition, whether the spatiotemporal activity of key aging transcription factors is sufficient to predict the lifespan extension conveyed by their stress-induced activities is still unclear. Elucidating the contributions of these components to *C. elegans* survival, would permit interventions that target lifespan augmentation, and shed light on the relative importance of different pathways towards longevity. With these considerations, we analyze lifespan in *C. elegans* as the outcome of cumulative molecular activity of DAF-16 prompted by exposure to DR.

Various approaches have been successfully used to probe gene expression in *C. elegans* cells, tissues, and at different developmental stages, such as DNA microarrays, real-time PCR, RNAseq, and serial analysis of gene expression (SAGE)[15–19]. Since these methods are destructive in nature, as they require extraction of DNA and RNA, they are

not suitable to obtain the spatial information required to assess nuclear translocation of cytoplasmic DAF-16. Previous studies have also used strains with fluorescently tagged DAF-16, which carry transgenic arrays that typically have hundreds of copies of the gene[20] and label only specific isoforms[21–23]. Here, we measure endogenous activity of all DAF-16 isoforms by tagging the *daf-16* locus at the 3' end using CRISPR/Cas9[24]. Coupled with spatiotemporal quantification of nuclear fluorescence through quantitative image analysis and machine learning, this approach enables *in vivo* analysis of all DAF-16 activity in *C. elegans* at endogenous levels, in a tissue-specific manner. This approach reveals that DAF-16 spatiotemporal activity (measured as lifelong total nuclear intensity) is a strong predictor of lifespan in *C. elegans* populations exposed to DR in liquid culture, accounting for 78% of DR-induced lifespan variability[25]. Furthermore, we show that the main contributors to this DAF-16 activity are neurons and intestinal cells, indicating that the observed lifespan extension originates mainly from the translocation and activity of DAF-16 in these cell types. Finally, we demonstrate that DAF-16 activity is observed in unexpected locations such as germ cells and intestinal nucleoli, where DAF-16 could be undergoing yet to be described interactions affecting the aging process.

3.3 Results

3.3.1 DR regimes modulate endogenous DAF-16 activity

To study the quantitative link between endogenous DAF-16 activity, and lifespan, we first aimed to analyze the response of endogenous DAF-16 to multiple DR regimes by varying food concentration and exposure time. Using CRISPR/Cas9, we generated a strain with the endogenous *daf-16* locus labeled with GFP at the 3' end, and measured the response of DAF-16 using a custom image processing algorithm that quantifies

nuclear intensity throughout the entire animal. Accurate analysis of DAF-16::GFP levels is challenging, as single copy reporters lead to extremely dim images. Since GFP intensities from DAF-16 were lower or similar than those from autofluorescent lipid droplets, we performed image acquisition in the green and red channels (as explained in Chapter 2), allowing subtraction of autofluorescence from the GFP signal. Analysis was performed on every slice of a z-stack covering the entire animal, and four separate z-stacks per channel were acquired per animal to cover the entire worm length. Information from the four z-stacks were aggregated for each worm.

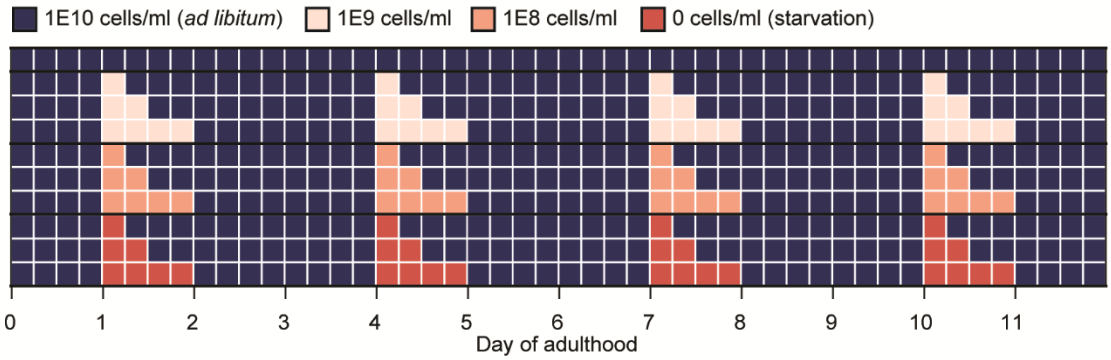

Figure 3.1 Diagram of DR regimes tested in this study. Animals were exposed to three levels of DR: 1E9, 1E8, or 0 OP50 cells/ml; for three exposure times: 6, 12, or 24 hours. After each exposure, animals were put back in an *ad libitum* concentration (1E10 OP50 cells/ml). Exposure to DR was performed at days 1, 4, 7, and 10 of adulthood.

Animals were exposed to DR conditions at day 1 of adulthood and every third day thereafter (**Figure 3.1**). All DR conditions induced an increase in the total nuclear intensity of DAF-16 compared to well-fed animals used as control (**Figure 3.2 A, B**). To validate that the increased DAF-16 nuclear intensity in fact represents transcriptional activity, we analyzed the expression levels of known DAF-16 targets under a subset of DR conditions (**Figure 3.3**) through RT-qPCR. A strong increase in expression was observed for all

tested genes, including the robust *daf-16* target *sod-3*[26]. This increase in expression of *daf-16* targets was partially inhibited by *daf-16* silencing using RNAi by feeding. Partial inhibition suggests that these genes are also modulated by other transcription factors, or that *daf-16* silencing is inefficient, a likely scenario due to reduced intake of dsRNA-expressing bacteria under DR conditions. Despite these limitations, our results clearly indicate that the DR conditions evaluated induced DAF-16 activity in cell nuclei[27,28]. Notably, *mlt-1* and *rpn-6.1* are genes that are involved in determination of *C. elegans* lifespan, while *aakg-4* is involved in cellular response to glucose starvation[29]. Indicating that DAF-16 is activating genes related to response to DR and longevity.

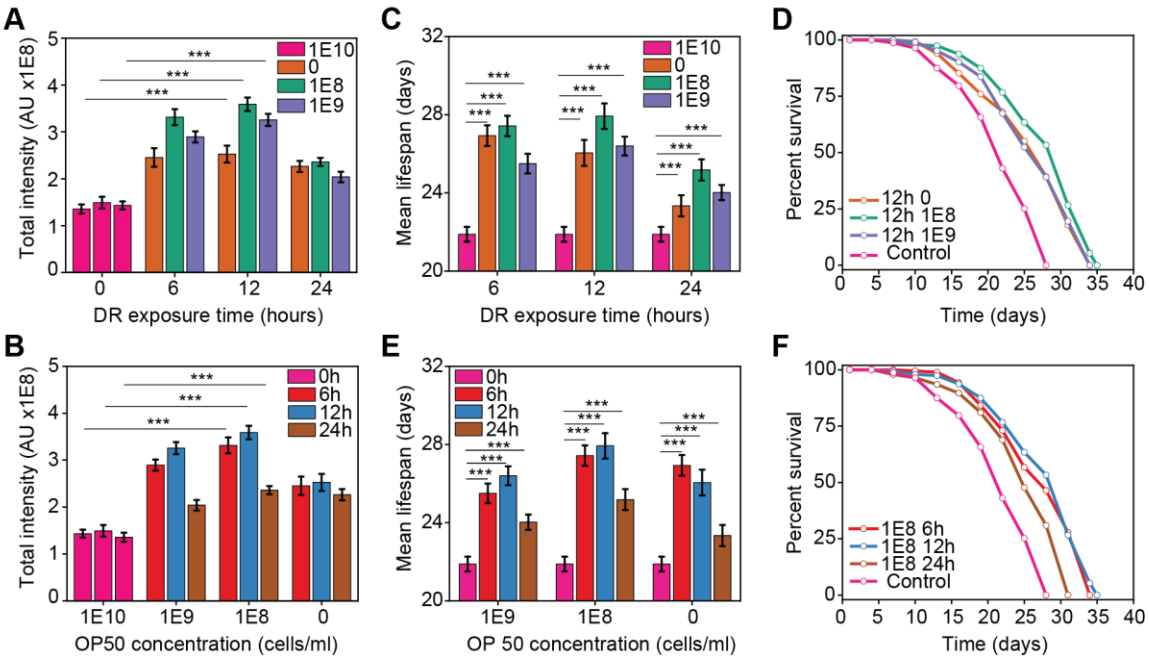

Figure 3.2 DR regimes modulate endogenous DAF-16 activity. A) DAF-16 total intensity as a function of exposure time to DR for various food concentrations at day 1 of adulthood. B) DAF-16 total intensity as a function of food concentration for various exposure times at day 1 of adulthood. C) Mean lifespan as a function of exposure time at various food concentrations. D) Lifespan curves for populations under various food concentrations with 12 hours of exposure to DR. E) Mean lifespan as a function of food concentration at various exposure times. F) Lifespan curves for populations under various exposure times to DR with a 10^8 OP50 cells/ml food concentration. $p < 0.001$ (***). Error bars are SEM. All p-values were calculated using Tukey HSD for all pairwise comparisons after one-way ANOVA (unequal variances) comparison. Control population (pink) is *ad libitum* (1E10 cells/ml, 0 h exposure time).

The strongest DAF-16 response, as measured by DAF-16::GFP nuclear localization, was observed for intermediate DR exposure times, peaking at 12 hours. The longest exposure (24 hours) showed a higher response than the control, but not as pronounced as 6 and 12 hours. Longer DR exposures could result in malnutrition, and lead to reduced DAF-16 responsiveness. Alternatively, DAF-16 could be translocating from nuclei back to the cytoplasm, a phenomenon that has been previously observed during long-term starvation[30]. We observed a similar pattern when varying food concentration. While all DR concentrations induce a response in DAF-16, the maximum DAF-16 response is observed for a mid-level concentration (10^8 OP50 cells/ml) (**Figure 3.2 B**). This non-monotonic response to food concentration has been previously observed[11,31], and our work suggests this is also true when varying DR exposure time. While prior work has shown that DAF-16 activity does not play a role in starvation-induced longevity when animals are cultured in solid media[32], our results suggest that starvation does induce DAF-16 activity in liquid media culture. This suggests that DAF-16 could be induced under starvation when additional conditions are met which differ from solid media, such as an increased energy consumption from swimming[33,34].

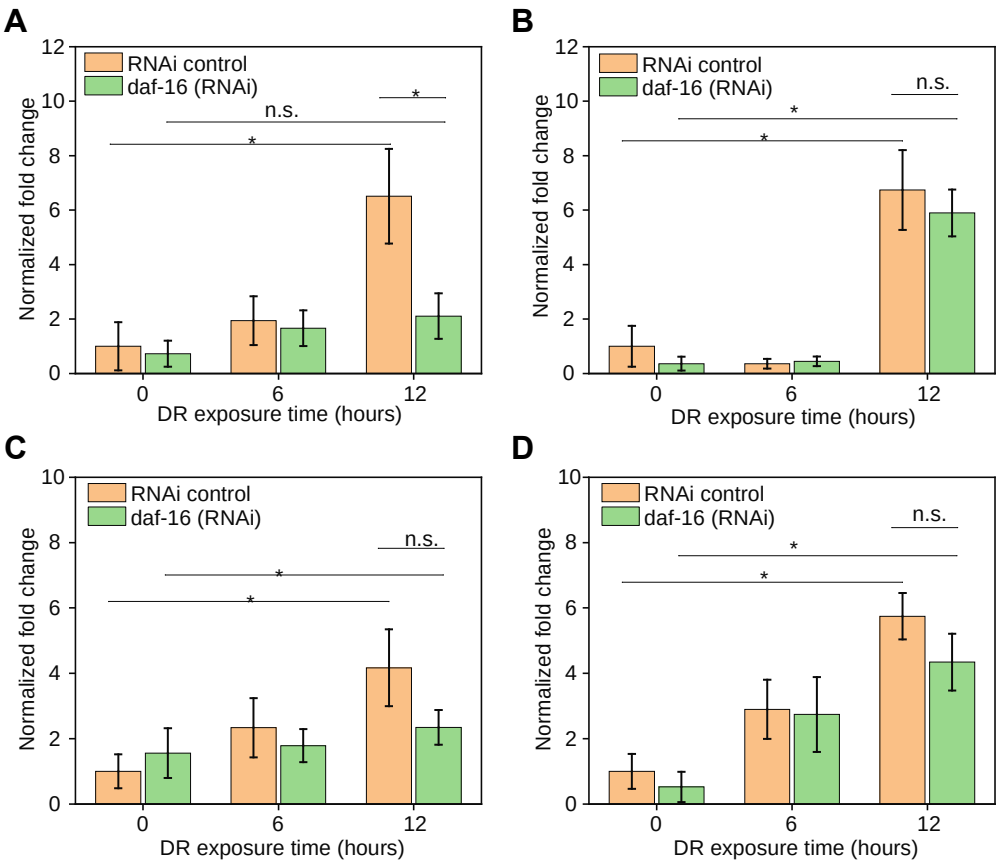

Figure 3.3 Expression of DAF-16 target genes increases under DR. A) to D) Normalized fold change for *sod-3*, *mlt-1*, *rpn-6.1*, and *aakg-4* under a food concentration of 10^8 HT115 cells/ml for 6 and 12 hours. Error bars are SEM. $p > 0.05$ (n.s.), $p < 0.05$ (*). All p-values were calculated using Tukey HSD for all pairwise comparisons after one-way ANOVA (unequal variances) comparison.

To determine how important the magnitude of DAF-16 activity is in modulating lifespan, we measured mean lifespan under the different DR regimes mentioned previously. All DR regimes lead to an extension in mean lifespan when compared to the control (**Figure 3.2 C-F, Figure 3.4**) as expected based on prior work[13,35]. In line with the results of DAF-16 activity, the largest lifespan extension was driven by the mid-level concentration of 10^8 OP50 cells/ml (**Figure 3.2 C, D, Figure 3.4**), and for 6 and 12 hours regimes (**Figure 3.2 E, F, Figure 3.4**). The 24 hours regime also induced lifespan extension, but not as significantly as 6 or 12 hours (**Figure 3.2 F**). It has been previously

observed that long-exposure to starvation increases the likelihood of matricidal hatching, which leads to the animals' death[36]. While we avoid this potential problem by exposing animals to FUdR, long-exposure to starvation could be inducing deleterious effects that are not fully abrogated by the beneficial pathways activated by DR in *C. elegans*.

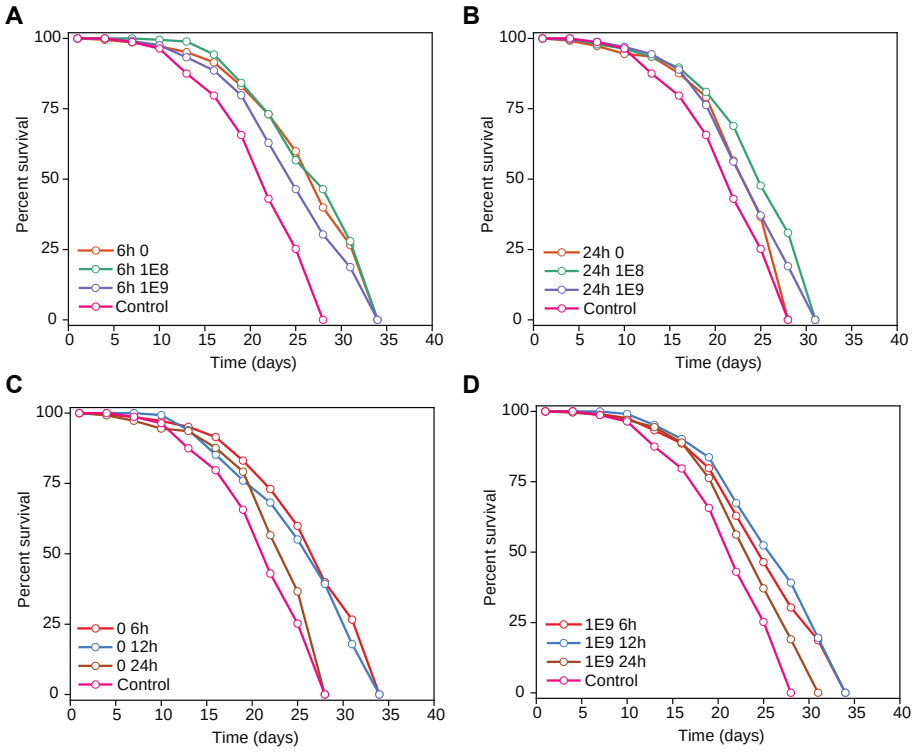

Figure 3.4 Lifespan curves for various DR regimes. A) Varying food concentration with 6 hours exposure time. B) Varying food concentration with 24 hours exposure time. C) Varying exposure time with a food concentration of 0 OP50 cells/ml. D) Varying exposure time with a food concentration of 10^9 OP50 cells/ml.

3.3.2 Cumulative lifelong DAF-16 nuclear activity determines lifespan under DR

We assessed the role of DAF-16 cumulative activity in lifespan extension by adding the total intensity of DAF-16 for all identified nuclei per animal at days 1, 4, 7, and 10 of adulthood, and comparing it to the corresponding mean lifespan (**Figure 3.5 A**). We found that the cumulative activity of nuclear DAF-16 predicts mean lifespan with an R^2 of 0.78 for the DR regimes explored in this study, using a linear regression. This suggests that lifespan extension due to DR is mostly modulated by cumulative DAF-16 lifelong spatiotemporal activity. The remainder of lifespan variability could come from DAF-16 activity at days we did not evaluate or, more likely, from the activity of other signaling pathways that also mediate longevity under DR, such as the target-of-rapamycin (TOR) pathway regulated by PHA-4[12,37,38] and the oxidative stress response regulated by SKN-1[39,40].

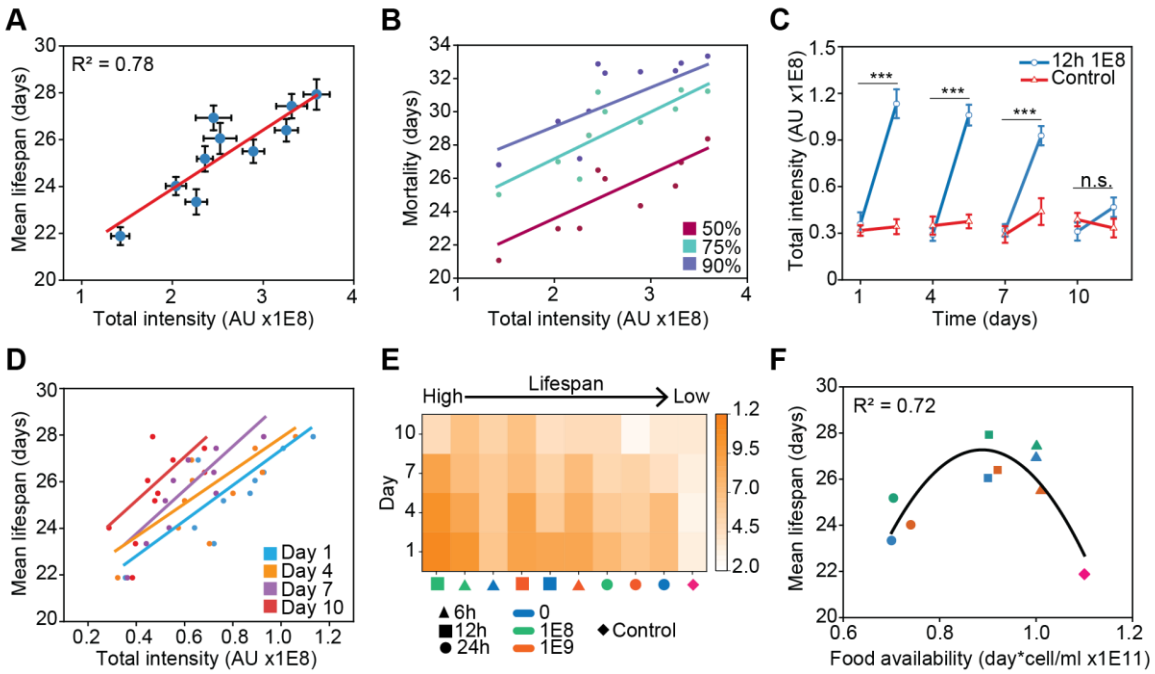

Figure 3.5 Cumulative lifelong DAF-16 nuclear activity determines lifespan. A) Mean lifespan of *C. elegans* as a function of lifelong DAF-16 total intensity under various DR regimes. B) Mortality of *C. elegans* populations as a function of DAF-16 lifelong total intensity. C) DAF-16 total intensity at a 10^8 OP50 cells/ml food concentration with 12 hours of exposure time compared to an *ad libitum* control at 1, 4, 7, and 10 days of adulthood. D) Mean lifespan as a function of DAF-16 total intensity in individual days. E) Heat map of DAF-16 total nuclear intensity per day under different DR regimes, in order of higher to lower lifespan (left to right). F) Mean lifespan as a function of total food available during the first 11 days of animal adulthood. 6 hours (triangles) and 12 hours (squares) regimes are at the peak of the curve while 24 hours (circles) regimes and the control (diamond) are at the lower ends of the curve. Error bars are SEM. $p > 0.05$ (n.s.), $p < 0.001$ (***). All p-values were calculated using Tukey HSD for all pairwise comparisons after one-way ANOVA (unequal variances) comparison. Linear and quadratic polynomial fits were performed in Origin 2020b.

We next evaluated if DAF-16 lifelong activity better quantifies other lifespan metrics. We compared DAF-16 total intensity to mortality quantiles (**Figure 3.5 B**) at 50%, 75%, and 90%, which produced R^2 of 0.48, 0.69, and 0.68 respectively. This suggests the DAF-16 response better captures when a *C. elegans* population perishes once it is already in decline or after 75% of the population has died. Previous studies indicate that DAF-16 has an important role in determining mortality and senescence in *C. elegans*[15] and *D. Melanogaster*[41] at their late life stages. Considering this, our results would indicate that DAF-16 activity is relevant to determine mortality in old animals but not in the case of younger ones.

As mentioned previously, animals underwent DR repeatedly at days 1, 4, 7, and 10 of adulthood (**Figure 3.1**). We observed that DAF-16 nuclear activity in animals previously exposed to DR returned to control levels after being well fed for 3 days. However, DAF-16 responsiveness to DR diminished at each following DR exposure (**Figure 3.5 C**). It has been shown that animals that have been previously exposed to DR show increased resistance to stress[42]. DAF-16 responsiveness could possibly be lower on repeated exposure to DR because the animals have already built resilience to stress from previous exposure. Alternatively, DAF-16 responsiveness could be reduced in aged worms, since the ability of animals to mount a response to stress has been shown to diminish with increasing age[43,44] . By day 10 of adulthood, once animals have passed their reproductive period, no significant change in DAF-16 activity was observed (**Figure 3.5 C**).

We next analyzed the contributions of DAF-16 activity in specific days to mean lifespan (**Figure 3.5 D**). Linear regressions of lifespan vs DAF-16 activity from individual

days results in R^2 of 0.71, 0.63, 0.75, and 0.45 at 1, 4, 7, and 10 days respectively. This analysis indicates that the DAF-16 response relevant for lifespan extension occurs during days 1, 4, and 7 for the DR regimes analyzed here. Likely, this results from a lack of responsiveness of DAF-16 at day 10. We analyzed the DAF-16 responsiveness from each day in all DR regimes and sorted the results by their corresponding mean lifespan (**Figure 3.5 E**). In all cases, DAF-16 activity is significantly reduced at day 10, which occurs after animals stopped egg production (at days 7-8 of adulthood in our experiments). It has been shown that reproduction and lifespan are intertwined in *C. elegans*[45–47]. Potentially, a loss of DAF-16 responsiveness could stem from animals turning-off prioritization of cell protection under stress after their reproductive period is over.

The regimes that result in the longest mean lifespan show the strongest DAF-16 response (6 and 12 hours in **Figure 3.5 E**). Notably, the regime of 6 hours with 0 OP50 cells/ml exhibits the third longest mean lifespan but its DAF-16 response is low compared to the rest. Brief starvation has been shown to stimulate autophagy and prolong lifespan in *D. Melanogaster*[48]. Potentially, the lifespan extension observed in this particular regime is influenced to a lower extent by DAF-16 while other transcription factors, such as the autophagy modulator PHA-4[12,37], play a larger role.

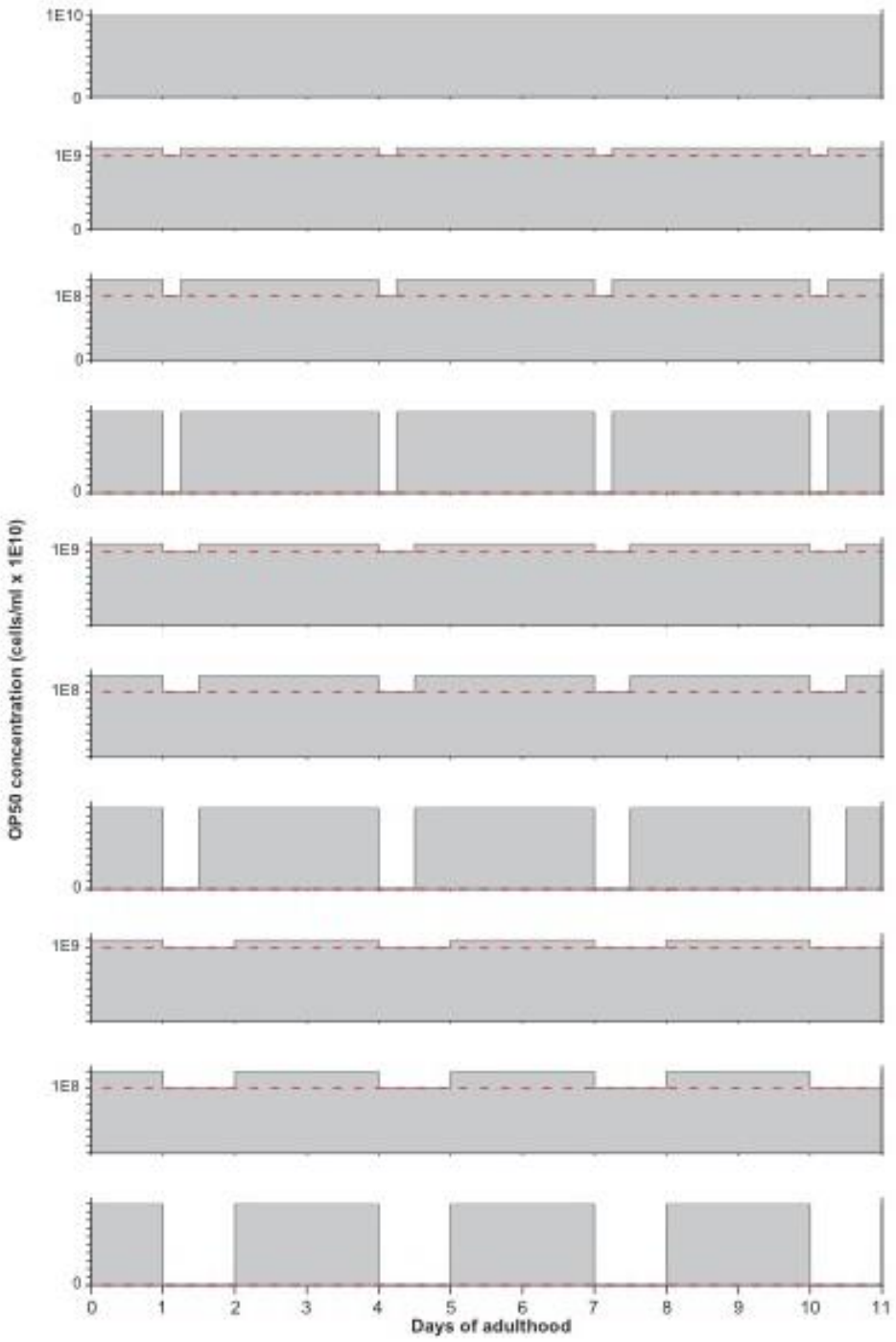

Figure 3.6 Graphic representation of food availability for each of the DR regimes evaluated. Grey areas were calculated for each DR regime and used in Figure 3.5 F.

We next analyzed if total food availability could also be a good quantitative predictor of mean lifespan. We calculated the total amount of food available to animals up to day 11 of adulthood (end of the last exposure to DR), in other words we measured the areas under the curve for each DR regime in **Figure 3.6**. Fitting the data with a quadratic polynomial resulted in an R^2 of 0.72 (**Figure 3.5 F**), with the highest lifespan values corresponding to intermediate levels of food availability, as expected[3]. This analysis suggests that total food availability, rather than timing or level of food restriction, is more important in modulating lifespan. Presumably, DR regimes different than the ones explored in **Figure 3.1**, but with similar areas under their curve could lead to equivalent mean lifespans.

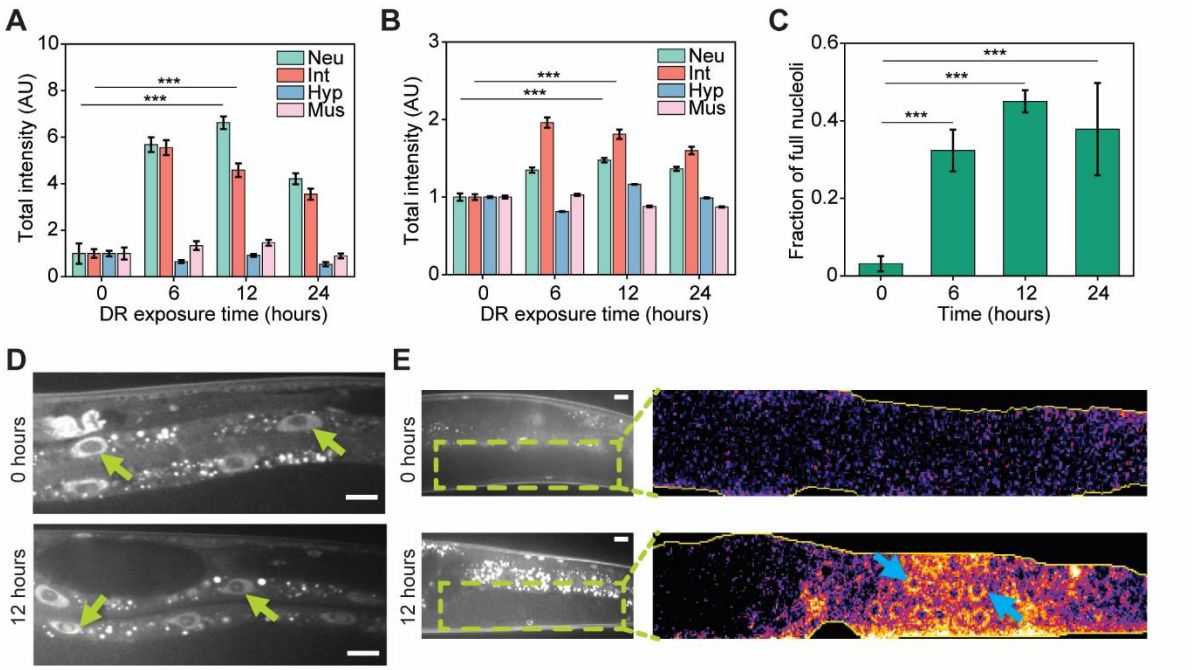

Figure 3.7 Tissue-specific analysis of DAF-16 reveals crucial role of intestine cells and neurons, nucleolar accumulation, and germline localization under liquid culture DR. A) DAF-16 normalized total intensity as a function of exposure time for various tissues. Neuron and intestine cells show the largest contribution to DAF-16 total intensity compared to hypodermis and muscle cells. B) DAF-16 total intensity per cell as a function of exposure time for various tissues. C) Fraction of intestinal nucleoli showing DAF-16 presence as a function of exposure times at a 10^8 OP50 cells/ml food concentration. D) Examples of animals with empty nucleoli (0 hours) and DAF-16 in the nucleoli (12 hours) at a 10^8 OP50 cells/ml food concentration. E) Inset highlights the gonad of a well-fed animal (0 hours) and one exposed to a food concentration of 10^8 cells/ml (12 hours). DAF-16 in in the germline can be discerned in the DR-exposed animal (light-blue arrows). Error bars are SEM. $p < 0.001$ (***). All p-values were calculated using Tukey HSD for all pairwise comparisons after one-way ANOVA (unequal variances) comparison. Scale bars are 20 µM.

3.3.3 Intestinal cells and neurons have the largest DAF-16 activity and contribution to lifespan

Since we observe DAF-16 in a variety of tissues, we then asked which cell-type contributes more to lifespan. Using machine learning, we developed a cell-type classifier to quantify endogenous DAF-16 activity with tissue-specificity. When adding the total intensity of nuclear DAF-16 of all cells of a given type, we observed that neurons and intestinal cells exhibited the largest responses (**Figure 3.7 A**). Neurons reach a peak around 12 hours, while intestinal cells rapidly peak at 6 hours and remain mostly stable afterwards. Since we are quantifying total intensity from all nuclei of each cell type, both the number and size of the nuclei play a role in the comparison of DAF-16 tissue-specific activity. The higher response from neurons could stem from their higher number, with hundreds of neurons per animal as opposed to 20 intestinal cells. To account for this, we analyzed total intensity on a per cell basis. In this case, the largest individual contribution comes from intestinal cells (**Figure 3.7 B**), albeit this result could be explained by intestinal cells being the largest cells in *C. elegans*[49]. This is confirmed by neurons having a higher mean intensity than intestinal cells (**Figure 3.8**). From this analysis, we can conclude that the lifespan extension exhibited by animals under the DR conditions analyzed comes mainly from DAF-16 activity in intestinal cells and neurons. This is further supported by the contributions of total intensity by cell type to mean lifespan (**Figure 3.9**), where we obtained linear regression R^2 values of 0.78, 0.64, 0.47, and 0.00 for neuron, intestinal, muscle, and hypodermal cell types respectively. Note that this low R^2 value for muscle cells is likely the result of an outlier corresponding with the control experiment. These results are in alignment with previous studies indicating that DAF-16 activity in the

intestine of *C. elegans* increases the lifespans of *daf-16*(-) insulin/IGF-1-pathway mutants[21], and that insulin signaling in neurons is important to drive lifespan[50].

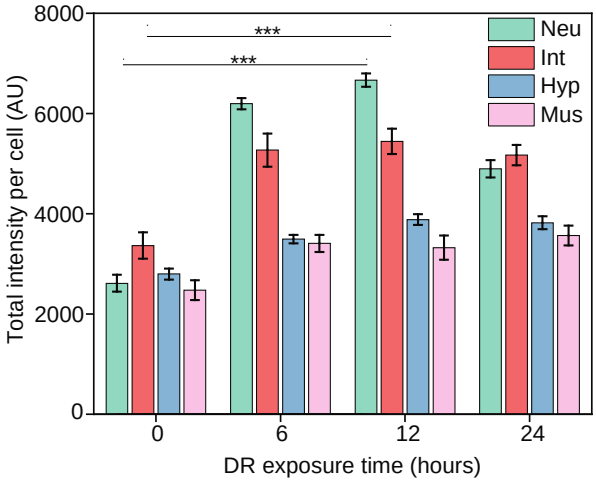

Figure 3.8 Mean intensity per cell type at various exposure times. Intestinal cells and neurons show the largest mean intensity compared to other cell types. Error bars are SEM. $p < 0.001$ (***). All p-values were calculated using Tukey HSD for all pairwise comparisons after one-way ANOVA (unequal variances) comparison.

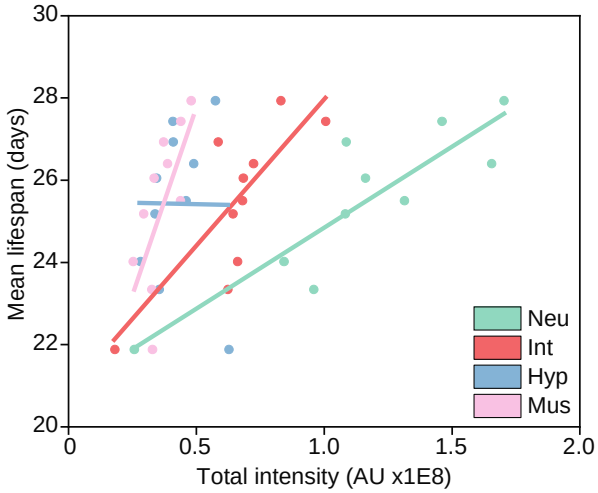

Figure 3.9 Mean lifespan dependence on total intensity by cell type. Intestinal cells and neurons show the largest contribution to mean lifespan. Linear fits were performed in Origin 2020b.

3.3.4 DAF-16 shows activity in the germline and intestinal nucleoli

During our experimental analysis, we observed that DAF-16 migration was not restricted to cell nuclei but also to the nucleolus in intestinal cells (**Figure 3.7 C-D**). We observed that DAF-16 accumulates in 30-50% of intestinal nucleoli under the DR conditions used (**Figure 3.7 C).** This phenomenon was not observed with a transgenic strain that expresses DAF-16::GFP under the *daf-16* promoter, MAH97, developed with transgenic approaches that typically result in hundreds of copies of the reporter in a random genomic location. In these conditions, nucleolar localization is likely hidden due to the high brightness of such reporters, suggesting that DAF-16 activity in intestinal nucleoli can only be observed at endogenous levels of expression. The presence of nucleolar DAF-16 in the intestine could be an important player in the mechanisms of lifespan extension observed under DR, as it has been shown that the nucleolus plays an important role in lifespan extension[51–53]. Similarly, we observed DAF-16 in the germline of animals under DR (**Figure 3.7 E**), although at extremely dim levels. This presence of DAF-16 was not observed in the MAH97 strain expressing DAF-16 tagged with GFP described above, potentially due to germline silencing of transgenic DNA[54–56]. Tagging the endogenous DAF-16 locus could enable the reporter to bypass these silencing mechanisms.

3.4 Discussion

In this work, we have utilized CRISPR/Cas9 and computer vision to quantitatively analyze the link between the endogenous spatiotemporal activity of the main IIS regulator, DAF-16, and longevity in *C. elegans.* We show that the transcription factor DAF-16 accounts by itself for 78% of the variability in lifespan observed in *C. elegans* under the

DR regimes explored here. Previous studies have modulated lifespan by manipulating food concentration or intervening on the genetic pathways governing aging[2,14]. Our quantitative analysis reveals that modulation of a single transcription factor, through DR interventions, accounts for 78% of lifespan variability. Moreover, this work shows that this robust lifespan prediction is achieved by assessing endogenous DAF-16 spatiotemporal activity in a longitudinal manner and is directly affected by the food abundance throughout the animals' life. Notably, the DAF-16 activity that is more relevant for lifespan extension occurred during *C. elegans* reproductive age, highlighting the close relationship between lifespan and reproduction observed in these animals[45]. We explored the activity of DAF-16 in different cell types, showing that intestinal cells and neurons have the largest contributions to DAF-16 activity leading to lifespan extension. This indicates that the mechanisms that govern DAF-16-dependent longevity in *C. elegans* under DR mainly take place in these cell types. This is emphasized by our finding of DAF-16 migrating into intestinal nucleoli, where some of these lifespan-modulating phenomena could be occurring.

Finally, our work opens the possibility of further exploration of other genetic pathways, transcription factors, and environmental factors in a holistic manner. For instance, it is unclear if the predictive power of endogenous DAF-16 activity holds under other environmental or genetic perturbations that also modulate lifespan. Moreover, determining whether the contributions of other longevity and stress signaling pathways are additive, or if these interact in a synergistic or antagonistic manner to determine lifespan will enable better understanding of longevity modulation in an integrative manner.

3.5 Materials and Methods

3.5.1 Strains, media, and culture

C. elegans was maintained on standard Nematode Growth Medium (NGM) plates seeded with OP50 *E. coli* bacteria and kept at 20 ºC until they started to lay eggs. Animals were then bleached using standard protocols to obtain age-synchronized populations[57]. This process was repeated 3 times in total to avoid transgenerational epigenetic effects related to longevity[58]. L4 animals were then transferred to a cell culture flask containing 4ml of SB media with 10^{10} cells/ml of OP50 bacteria and 100 µM 5-fluorodeoxyuridine (FUdR) and kept at 20 ºC for 1 day[59,60]. Cultures were then used for dietary restriction and lifespan experiments. Strains used in this work were ASM10 *daf-16* (del2 [*daf-16*::GFP-C1^3xFlag]) I and N2 (*C. elegans* wild isolate). OP50 *E. coli* was grown in LB media following standard procedures[61]. Bacteria were washed thrice with SB media, pelletized, and suspended in S-Medium at a concentration of 100 mg/mL, corresponding to a concentration of 2 x 10^{10} cells/ml.

3.5.2 Generation of transgenic line

We used a CRISPR/Cas9 approach developed by Dickinson *et al.* to insert a GFP-encoding sequence at the 3' end of *daf-16*[24]. We chose the Cas9 target site by identifying all possible single guide RNAs (sgRNA) in a 200bp region centered in the stop codon of the target gene. This region was selected to permit introduction of the fluorescent tag at the C-terminus, tagging in this manner all possible isoforms of the gene. Criteria such as specificity, activity, and distance to the stop codon were considered in selecting the sgRNA using the GuideScan design tool[62]. This 20bp sequence was introduced into a

Cas9-encoding construct (pDD162, Addgene #47549) using a NEB Q5 Site-Directed Mutagenesis Kit to generate plasmid pJHR1. 500-700bp long homology arms at each side of the *daf-16* stop codon were then generated by PCR amplification of genomic DNA from N2 animals. These fragments were isolated, purified, and introduced in a construct containing a selection cassette (pDD282, Addgene #66823) using NEBuilder HiFi DNA Assembly Mix to generate plasmid pJHR2.

A mix containing 15ng/μL pJHR1, 50ng/μL pJHR2, and 2.5ng/μL pCFJ90 (mCherry co-injection marker) was injected in the gonads of 100 N2 young-adult animals following standard microinjection procedures[63]. These animals were transferred to NGM plates and left to produce progeny at 25 °C. Hygromycin was added to the plates to kill untransformed F1 progeny. After 7 days, animals showing the Rol phenotype and lacking red fluorescent extrachromosomal array markers were transferred to new NGM plates without hygromycin. Individual putative knock-in animals were transferred to new plates for homozygous selection. Finally, L1 larvae from homozygous plates (those that contained only animals with the Rol phenotype) were heat-shocked at 34 °C for 4 hours to induce Cre expression, and excision of the selection cassette. Wild-type adult animals lacking the Rol phenotype were picked and maintained as the strain containing the fluorescent-tagged gene. PCR and Sanger sequencing were performed to confirm correct introduction of the tag.

3.5.3 Dietary restriction and fluorescence imaging

Approximately 200 worms in day 1 of adulthood kept in liquid culture were washed 3 times with SB media and moved to a flask containing 4ml of SB media with a reduced food concentration to induce DR (10^9, 10^8 or 0 OP50 cells/ml) for a fixed amount of time

(6, 12, or 24 hours). After the DR period concluded, additional OP50 was added to raise the concentration to an *ad libitum* level (10^{10} OP50 cells/ml). FUdR concentration was raised to 100 µM total concentration to prevent offspring production[64]. Worms were then kept at 20 ºC for 3 days at *ad libitum* food concentration. DR exposure was repeated on days 4, 7, and 10 of adulthood. At the start and end of each DR exposure, approximately 20-30 worms were immobilized using 10 µL of 2 mM tetramisole on dried 2% agarose pads of approximately 1 cm diameter. Confocal fluorescence microscopy was performed with a Leica DMi8 microscope paired with an 89 North LDI Laser Diode Illuminator coupled with a CrestOptics X-Light V2 confocal imager and an Orca-Flash 4.0 digital CMOS camera. The exposure time and laser intensity were kept constant throughout all experiments at 100 ms and 100%, respectively. Images containing 30 slices (Z-stacks with 3 µm spacing) were acquired with a MATLAB GUI (Graphical User Interface). Images were acquired in the green and red channels sequentially. This enables later subtraction of autofluorescence present in both channels with a custom MATLAB script.

3.5.4 Lifespan experiments

Approximately 200 worms per flask were kept in liquid culture in the same conditions described in the previous section. Animal mobility was analyzed in a stereoscope through visual inspection. Nematodes were scored as alive (active and swimming), dead (rigid and not moving), and censored (lost to manipulation). This was performed every third day, starting on day 1 of adulthood. Lifespan curves were constructed using Online Application for Survival Analysis 2[65] to obtain the mean lifespan for each population.

3.5.5 Quantitative image processing

Images were analyzed using a MATLAB script, customized to segment cell nuclei in each slice of the z-stack. The algorithm's most important steps are: 1) Subtraction of red channel image from green channel image to eliminate autofluorescence present in both images; 2) Generation of a binary mask from the subtracted image; 3) Identification of nuclei by retaining segmented objects that: a) filled up at least 50% of their bounding box, b) had eccentricity values under 0.85, and c) had solidity values above 0.75. The threshold values were determined based on visual assessment of the characteristics of nuclei. Object characteristics were extracted using "regionprops"; 4) Use of the "imopen" function to smooth edges. 5) Deletion of objects smaller than neurons and larger than intestinal cells using the "bwareaopen" function. These operations enable for the selection of nuclei (ellipse or circle-like objects) while eliminating other features such as autofluorescence, animal edges, embryos, etc. in a stepwise manner. To avoid over-estimation, nuclei present in multiple slices were identified by comparing their centroids. If multiple centroids with similar values in the ± 4 pixels range were identified in multiple slices, only the object with the largest area was retained for properties extraction. The MATLAB regionprops function was then used to quantify the total intensity in the segmented nuclei and the data extracted was stored in a MATLAB nested structure. Total intensity was calculated as the sum of the intensity of the pixels from all cell nuclei extracted per worm.

3.5.6 Cell type classification and nucleolus analysis

To classify nuclei belonging to specific tissues, we used a Fine Tree multi-class classification algorithm. A ground truth set of 600 cell nuclei and their corresponding class

(intestine, neuron, hypodermis, or muscle) was manually generated. The Fine Tree algorithm was trained using MATLAB Classification Learner, by using the following object properties as features: area, eccentricity, and equivalent diameter. The generated Fine Tree algorithm resulted in a 96.1% accuracy when predicting cell types with a validation set.

For nucleolar analysis, DAF-16-filled nucleoli in intestinal cells were counted manually using FIJI. A nucleolus was considered “empty” when the nucleus’ center was empty. A nucleolus was considered “filled” when the nucleus center had fluorescence due to GFP-tagged DAF-16.

3.5.7 RNAi by feeding

Age-synchronized worms were grown from the egg stage to the L4 stage at 20 ºC in NGM plates containing HT115 bacteria. Animals were then transferred to flasks containing HT115 bacteria with an empty vector (control) or HT115 bacteria carrying the *daf-16* RNAi vector from the Ahringer library (acquired from Source Biosciences)[66], and grown until day 1 of adulthood. Animals were then exposed to DR for 6 or 12 hours at a food concentration of 10^8 HT115 cells/ml (control or *daf-16* RNAi) as previously described.

3.5.8 RNA isolation and quantitative PCR (qPCR)

Approximately 50 animals that were previously subjected to RNAi treatment (control or *daf-16* RNAi) were transferred to Trizol (Invitrogen) and vortexed twice for 30 seconds. Total RNA was isolated using Direct-Zol RNA MicroPrep Kit (Zymo Research) according to the manufacturer’s protocol. Quantitative PCR was performed on a CFX384 Touch Real-Time PCR Detection System (Bio-Rad Laboratories) using Luna Universal

One-Step RT-qPCR Kit (New England BioLabs) according to the manufacturer's protocol. RT-qPCR data was analyzed using the ΔΔCt method. Target genes were selected using the FOXODB database of DAF-16 direct targets[67]. Gene expression levels were normalized using *ama-1* as housekeeping gene.

3.5.9 Data analysis and statistics

Linear regressions were performed in Origin 2020b using the FitLinear function. Polynomial fits were performed in Origin 2020b using the FitPolynomial function. Significance tests such as t-Test and ANOVA were performed using the Data Analysis Add-on in MS Excel 2016. Lifespan analysis was performed with the Online Application for Survival Analysis 2[65] by using number of dead and censored animals as input; obtaining mean lifespan with a Kaplan-Meier estimator.

3.6 References

1. Kenyon CJ. The genetics of ageing. *Nature*. 2010;464(7288):504-512. doi:10.1038/nature08980

2. Sagi D, Kim SK. An engineering approach to extending lifespan in C. elegans. *PLoS Genet*. 2012;8(6):1002780. doi:10.1371/journal.pgen.1002780

3. Win MTT, Yamamoto Y, Munesue S, Han D, Harada SI, Yamamoto H. Validated liquid culture monitoring system for lifespan extension of Caenorhabditis elegans through genetic and dietary manipulations. *Aging Dis*. 2013;4(4):178-185. /pmc/articles/PMC3733581/. Accessed December 7, 2021.

4. Stroustrup N, Anthony WE, Nash ZM, et al. The temporal scaling of Caenorhabditis elegans ageing. *Nature*. 2016;530(7588):103-107. doi:10.1038/nature16550

5. Masoro EJ, Yu BP, Bertrand HA. Action of food restriction in delaying the aging process. *Proc Natl Acad Sci U S A*. 1982;79(13):4239-4241. doi:10.1073/pnas.79.13.4239

6. Weindruch R. The retardation of aging by caloric restriction: Studies in rodents and primates. *Toxicol Pathol*. 1996;24(6):742-745. doi:10.1177/019262339602400618

7. Masoro EJ. Overview of caloric restriction and ageing. *Mech Ageing Dev*. 2005;126(9 SPEC. ISS.):913-922. doi:10.1016/j.mad.2005.03.012

8. Mattison JA, Colman RJ, Beasley TM, et al. Caloric restriction improves health

and survival of rhesus monkeys. *Nat Commun*. 2017;8. doi:10.1038/ncomms14063

9. Lin K, Hsin H, Libina N, Kenyon C. Regulation of the Caenorhabditis elegans longevity protein DAF-16 by insulin/IGF-1 and germline signaling. *Nat Genet*. 2001;28(2):139-145. doi:10.1038/88850

10. Hsu AL, Murphy CT, Kenyon C. Regulation of aging and age-related disease by DAF-16 and heat-shock factor. *Science (80-)*. 2003;300(5622):1142-1145. doi:10.1126/science.1083701

11. Greer EL, Dowlatshahi D, Banko MR, et al. An AMPK-FOXO Pathway Mediates Longevity Induced by a Novel Method of Dietary Restriction in C. elegans. *Curr Biol*. 2007;17(19):1646-1656. doi:10.1016/j.cub.2007.08.047

12. Panowski SH, Wolff S, Aguilaniu H, Durieux J, Dillin A. PHA-4/Foxa mediates diet-restriction-induced longevity of C. elegans. *Nature*. 2007;447(7144):550-555. doi:10.1038/nature05837

13. Greer EL, Brunet A. Different dietary restriction regimens extend lifespan by both independent and overlapping genetic pathways in C. elegans. *Aging Cell*. 2009;8(2):113-127. doi:10.1111/j.1474-9726.2009.00459.x

14. Hou L, Wang D, Chen D, et al. A systems approach to reverse engineer lifespan extension by dietary restriction. *Cell Metab*. 2016;23(3):529-540. doi:10.1016/j.cmet.2016.02.002

15. McElwee J, Bubb K, Thomas JH. Transcriptional outputs of the Caenorhabditis

elegans forkhead protein DAF-16. *Aging Cell*. 2003;2(2):111-121. doi:10.1046/j.1474-9728.2003.00043.x

16. Portman D. Profiling C. elegans gene expression with DNA microarrays. *WormBook*. 2006:1-11. doi:10.1895/wormbook.1.104.1

17. Wang X, Zhao Y, Wong K, et al. Identification of genes expressed in the hermaphrodite germ line of C. elegans using SAGE. *BMC Genomics*. 2009;10. doi:10.1186/1471-2164-10-213

18. Guthmueller KL, Yoder ML, Holgado AM. Determining genetic expression profiles in C. elegans using microarray and real-time PCR. *J Vis Exp*. 2011;3791(53):1-7. doi:10.3791/2777

19. Possik E, Pause A. Measuring Oxidative Stress Resistance of Caenorhabditis elegans in 96-well Microtiter Plates. *J Vis Exp*. 2015;99(99):527463791-52746. doi:10.3791/52746

20. Stinchcomb DT, Shaw JE, Carr SH, Hirsh D. Extrachromosomal DNA transformation of Caenorhabditis elegans. *Mol Cell Biol*. 1985;5(12):3484-3496. doi:10.1128/mcb.5.12.3484

21. Libina N, Berman JR, Kenyon C. *Tissue-Specific Activities of C. Elegans DAF-16 in the Regulation of Lifespan*. Vol 115.; 2003. doi:10.1016/S0092-8674(03)00889-4

22. Kwon ES, Narasimhan SD, Yen K, Tissenbaum HA. A new DAF-16 isoform regulates longevity. *Nature*. 2010;466(7305):498-502. doi:10.1038/nature09184

23. Kumsta C, Hansen M. C. elegans rrf-1 mutations maintain RNAi efficiency in the soma in addition to the germline. *PLoS One*. 2012;7(5). doi:10.1371/journal.pone.0035428

24. Dickinson DJ, Pani AM, Heppert JK, Higgins CD, Goldstein B. Streamlined genome engineering with a self-excising drug selection cassette. *Genetics*. 2015;200(4):1035-1049. doi:10.1534/genetics.115.178335

25. Huayta J, San-Miguel A. Endogenous DAF-16 Spatiotemporal Activity Quantitatively Predicts Lifespan Extension Induced by Dietary Restriction. *bioRxiv*. 2021;4(1):6. doi:10.1101/2021.12.20.473576

26. Zhang P, Judy M, Lee SJ, Kenyon C. Direct and indirect gene regulation by a life-extending foxo protein in C. elegans: Roles for GATA factors and lipid gene regulators. *Cell Metab*. 2013;17(1):85-100. doi:10.1016/j.cmet.2012.12.013

27. Li W, Gao B, Lee SM, Bennett K, Fang D. RLE-1, an E3 Ubiquitin Ligase, Regulates C. elegans Aging by Catalyzing DAF-16 Polyubiquitination. *Dev Cell*. 2007;12(2):235-246. doi:10.1016/j.devcel.2006.12.002

28. Vilchez D, Morantte I, Liu Z, et al. RPN-6 determines C. elegans longevity under proteotoxic stress conditions. *Nature*. 2012;489(7415):263-268. doi:10.1038/nature11315

29. Tullet JMA, Araiz C, Sanders MJ, et al. DAF-16/FoxO Directly Regulates an Atypical AMP-Activated Protein Kinase Gamma Isoform to Mediate the Effects of Insulin/IGF-1 Signaling on Aging in Caenorhabditis elegans. *PLoS Genet*. 2014;10(2):e1004109. doi:10.1371/journal.pgen.1004109

30. Weinkove D, Halstead JR, Gems D, Divecha N. Long-term starvation and ageing induce AGE-1/PI 3-kinase-dependent translocation of DAF-16/FOXO to the cytoplasm. *BMC Biol*. 2006;4(1):1-13. doi:10.1186/1741-7007-4-1

31. Henderson ST, Johnson TE. daf-16 integrates developmental and environmental inputs to mediate aging in the nematode Caenorhabditis elegans. *Curr Biol*. 2001;11(24):1975-1980. doi:10.1016/S0960-9822(01)00594-2

32. Lee GD, Wilson MA, Zhu M, et al. Dietary deprivation extends lifespan in Caenorhabditis elegans. *Aging Cell*. 2006;5(6):515-524. doi:10.1111/j.1474-9726.2006.00241.x

33. Ghosh R, Emmons SW. Episodic swimming behavior in the nematode C. elegans. *J Exp Biol*. 2008;211(23):3703-3711. doi:10.1242/jeb.023606

34. Laranjeiro R, Harinath G, Burke D, Braeckman BP, Driscoll M. Single swim sessions in C. elegans induce key features of mammalian exercise. *BMC Biol*. 2017;15(1):30. doi:10.1186/s12915-017-0368-4

35. Kaeberlein TL, Smith ED, Tsuchiya M, et al. Lifespan extension in Caenorhabditis elegans by complete removal of food. *Aging Cell*. 2006;5(6):487-494. doi:10.1111/j.1474-9726.2006.00238.x

36. Chen J, Caswell-Chen EP. Why Caenorhabditis elegans adults sacrifice their bodies to progeny. *Nematology*. 2003;5(4):641-645. doi:10.1163/156854103322683355

37. Hansen M, Chandra A, Mitic LL, Onken B, Driscoll M, Kenyon C. A role for

autophagy in the extension of lifespan by dietary restriction in C. elegans. *PLoS Genet*. 2008;4(2). doi:10.1371/journal.pgen.0040024

38. Sheaffer KL, Updike DL, Mango SE. The Target of Rapamycin Pathway Antagonizes pha-4/FoxA to Control Development and Aging. *Curr Biol*. 2008;18(18):1355-1364. doi:10.1016/j.cub.2008.07.097

39. An JH, Blackwell TK. SKN-1 links C. elegans mesendodermal specification to a conserved oxidative stress response. *Genes Dev*. 2003;17(15):1882-1893. doi:10.1101/gad.1107803

40. Bishop NA, Guarente L. Two neurons mediate diet-restriction-induced longevity in C. elegans. *Nature*. 2007;447(7144):545-549. doi:10.1038/nature05904

41. Giannakou ME, Goss M, Jacobson J, Vinti G, Leevers SJ, Partridge L. Dynamics of the action of dFOXO on adult mortality in Drosophila. *Aging Cell*. 2007;6(4):429-438. doi:10.1111/j.1474-9726.2007.00290.x

42. Smith ED, Kaeberlein TL, Lydum BT, et al. Age- and calorie-independent life span extension from dietary restriction by bacterial deprivation in Caenorhabditis elegans. *BMC Dev Biol*. 2008;8(1):1-13. doi:10.1186/1471-213X-8-49

43. Dues DJ, Andrews EK, Schaar CE, Bergsma AL, Senchuk MM, Van Raamsdonk JM. Aging causes decreased resistance to multiple stresses and a failure to activate specific stress response pathways. *Aging (Albany NY)*. 2016;8(4):777-795. doi:10.18632/aging.100939

44. Li S-T, Zhao H-Q, Zhang P, et al. DAF-16 stabilizes the aging transcriptome and

is activated in mid-aged Caenorhabditis elegans to cope with internal stress. *Aging Cell*. February 2019:e12896. doi:10.1111/acel.12896

45. Hsin H, Kenyon C. Signals from the reproductive system regulate the lifespan of C. elegans. *Nature*. 1999;399(6734):362-366. doi:10.1038/20694

46. Luo S, Murphy CT. Caenorhabditis elegans reproductive aging: Regulation and underlying mechanisms. *Genesis*. 2011;49(2):53-65. doi:10.1002/dvg.20694

47. Wang MC, Oakley HD, Carr CE, Sowa JN, Ruvkun G. Gene Pathways That Delay Caenorhabditis elegans Reproductive Senescence. *PLoS Genet*. 2014;10(12). doi:10.1371/journal.pgen.1004752

48. Eisenberg T, Schroeder S, Andryushkova A, et al. Nucleocytosolic depletion of the energy metabolite acetyl-coenzyme A stimulates autophagy and prolongs lifespan. *Cell Metab*. 2014;19(3):431-444. doi:10.1016/j.cmet.2014.02.010

49. Zhang N, Khan LA, Membreno E, et al. The C. elegans intestine as a model for intercellular lumen morphogenesis and in vivo polarized membrane biogenesis at the single-cell level: Labeling by antibody staining, RNAi loss-of-function analysis and imaging. *J Vis Exp*. 2017;2017(128):56100. doi:10.3791/56100

50. Iser WB, Gami MS, Wolkow CA. Insulin signaling in Caenorhabditis elegans regulates both endocrine-like and cell-autonomous outputs. *Dev Biol*. 2007;303(2):434-447. doi:10.1016/J.YDBIO.2006.04.467

51. Kim Y Il, Bandyopadhyay J, Cho I, Lee J, Park DH, Cho JH. Nucleolar GTPase NOG-1 regulates development, fat storage, and longevity through Insulin/IGF

signaling in C. elegans. *Mol Cells*. 2014;37(1):51-57. doi:10.14348/molcells.2014.2251

52. Tiku V, Jain C, Raz Y, et al. Small nucleoli are a cellular hallmark of longevity. *Nat Commun*. 2016;8(1):1-9. doi:10.1038/ncomms16083

53. Tiku V, Antebi A. Nucleolar Function in Lifespan Regulation. *Trends Cell Biol*. 2018;28(8):662-672. doi:10.1016/j.tcb.2018.03.007

54. Kelly WG, Fire A. Chromatin silencing and the maintenance of a functional germline in Caenorhabditis elegans. *Development*. 1998;125(13):2451-2456. doi:10.1242/dev.125.13.2451

55. Seydoux G, Schedl T. The germline in C. Elegans: Origins, proliferation, and silencing. *Int Rev Cytol*. 2001;203:139-185. doi:10.1016/S0074-7696(01)03006-6

56. Aljohani MD, El Mouridi S, Priyadarshini M, Vargas-Velazquez AM, Frøkjær-Jensen C. Engineering rules that minimize germline silencing of transgenes in simple extrachromosomal arrays in C. elegans. *Nat Commun*. 2020;11(1):1-14. doi:10.1038/s41467-020-19898-0

57. Porta-de-la-Riva M, Fontrodona L, Villanueva A, Cerón J. Basic Caenorhabditis elegans methods: Synchronization and observation. *J Vis Exp*. 2012;(64):e4019. doi:10.3791/4019

58. Greer EL, Maures TJ, Ucar D, et al. Transgenerational epigenetic inheritance of longevity in Caenorhabditis elegans. *Nature*. 2011;479(7373):365-371. doi:10.1038/nature10572

59. Stiernagle T. Maintenance of C. elegans. *WormBook*. 2006. doi:10.1895/wormbook.1.101.1

60. Gruber J, Ng LF, Poovathingal SK, Halliwell B. Deceptively simple but simply deceptive - Caenorhabditis elegans lifespan studies: Considerations for aging and antioxidant effects. *FEBS Lett*. 2009;583(21):3377-3387. doi:10.1016/j.febslet.2009.09.051

61. Amrit FRG, Ratnappan R, Keith SA, Ghazi A. The C. elegans lifespan assay toolkit. *Methods*. 2014;68(3):465-475. doi:10.1016/j.ymeth.2014.04.002

62. Perez AR, Pritykin Y, Vidigal JA, et al. GuideScan software for improved single and paired CRISPR guide RNA design. *Nat Biotechnol*. 2017;35(4):347-349. doi:10.1038/nbt.3804

63. Evans T. Transformation and microinjection. *WormBook*. 2006:1-15. doi:10.1895/wormbook.1.108.1

64. Mitchell DH, Stiles JW, Santelli J, Rao Sanadi D. Synchronous growth and aging of Caenorhabditis elegans in the presence of fluorodeoxyuridine. *Journals Gerontol*. 1979;34(1):28-36. doi:10.1093/geronj/34.1.28

65. Han SK, Lee D, Lee H, et al. OASIS 2: Online application for survival analysis 2 with features for the analysis of maximal lifespan and healthspan in aging research. *Oncotarget*. 2016;7(35):56147-56152. doi:10.18632/oncotarget.11269

66. Fraser AG, Kamath RS, Zipperlen P, Martinez-Campos M, Sohrmann M, Ahringer J. Functional genomic analysis of C. elegans chromosome I by systematic RNA

interference. *Nature*. 2000;408(6810):325-330. doi:10.1038/35042517

67. Li YH, Zhang GG. Towards understanding the lifespan extension by reduced insulin signaling: Bioinformatics analysis of DAF-16/FOXO direct targets in Caenorhabditis elegans. *Oncotarget*. 2016;7(15):19185-19192. doi:10.18632/oncotarget.8313

Chapter 4: Machine Learning for Tracking of Subtle Gene Expression Patterns and Tissue Morphological Changes

4.1 Abstract

Tracking of transcription factors such as DAF-16 tagged with a fluorophore under stressful conditions has been typically achieved by manually counting of cell nuclei containing DAF-16 or by measuring intensity of overexpressing strains. In this chapter we show that application of a custom-made MATLAB algorithm enables capture of subtle changes in endogenous DAF-16 translocation from cytoplasm to cell nuclei for a single-copy strain, while a with a Fine Tree classifier enables classification of cells into different tissues. Additionally, we demonstrate that a machine learning approach with a Mask R-CNN algorithm allows for the segmentation of *C. elegans* pharynx in bright field images, which leads to the reduction of processing time and bias in the analysis of morphological changes of this organ.

4.2 Introduction

C. elegans response to stress is governed by transcription factors such as DAF-16, PHA-4, SKN-1, and HSF-1[1]. These proteins possess characteristic expression patterns. For example, DAF-16 migrates from the cytoplasm of cells to their nuclei when *C. elegans* are exposed to conditions of reduced insulin signaling and some forms of dietary restriction[2,3]. In contrast, PHA-4 is always present in the nuclei of cells located in the animal's head (pharynx muscle cells and neurons), with it increasing in the same location when the nematodes are exposed to some types of food limitation[4,5]. Typically, quantification of the expression patterns and activity of these transcription factors has been performed by observation or manual counting of cells of strains containing a

fluorescent-tag attached to the gene of interest[6–8]. For instance, studies report the presence of DAF-16 in cell nuclei by assessing it in 3 levels: 'absent', 'present in some nuclei', and 'present in all nuclei'[8]. Although this type of measurement provides insights in the activity of DAF-16, it does not provide quantitative information that can be used to elaborate predictions on the behavior of this transcription factor. Other studies have taken advantage of image analysis tools to extract further information from fluorescent microscopy such as intensity[9,10]. However, these approaches run in the issues mentioned in Chapter 1: using strains with gene overexpression, mosaicism, silencing in the germline, and not being able to evaluate endogenous levels of expression[11]. With these considerations, we used a CRISPR/Cas9 approach to generate a transgenic strain with a green fluorescent (GFP) tag added at the endogenous locus of DAF-16, thus avoiding the problems mentioned previously. Nevertheless, this approach comes with the new challenge of observing subtle changes in intensity of a dim DAF-16 reporter, paired with the observation of different expression patterns at the cellular and subcellular levels. We decided to use a combination of custom-made MATLAB algorithms and machine learning to overcome this problem.

Machine learning has been used to perform complex classification tasks in fields with data-intensive methods, requiring use of computer vision, and other applications[12]. Machine learning has been used in *C. elegans* to perform tasks such as identification of subtle phenotypes of subcellular landmarks[13], analysis of neuronal phenotypes induced by stressors[14], classification of the sex of *C. elegans*[15], or to identify and classify tissues[16]. Other algorithms have been developed to identify and count individuals such as the WormToolbox[17]. Deep learning tools such as convolutional neural networks have been

used for segmentation and classification of *C. elegans* in applications such as detection, and tracking in behavioral studies[18,19]. Furthermore, decision trees, a type of supervised machine learning have been employed to differentiate between multiple categories after training an algorithm with a ground truth set. This approach has seen use in classification of behavioral phenotypes[20,21], and detection of movement types and navigation patterns in *C. elegans*[22]. We aim at taking advantage of these powerful tools to assess the contribution of different *C. elegans* tissues such as neurons, intestinal, hypodermal, and muscle cells to DAF-16 activity under dietary restriction.

Additionally, convolutional neural networks (CNN) have been used for image segmentation in the medical field to classify different tissues in an organ[23], and in agriculture to detect plant diseases based on how these affect the morphology of leaves[24]. This demonstrates that a deep learning approach based on CNNs can be used to segment regions of interest such as different tissues or organs in *C. elegans*. For example, neuronal phenotypes induced by aging and cold shock in these nematodes[14], and neuron tracing of complex dendritic trees have been both achieved recently using CNNs[25]. We decided to also use a CNN-based algorithm to identify and segment the pharynx of *C. elegans*, as this approach has been used successfully for segmentation of difficult to discern features. This is relevant to perform aging studies because morphological changes in the *C. elegans* pharynx and other related metrics such as pumping rate are extensively used to assess healthspan in these animals[16,26–28].

4.3 Results

4.3.1 Quantitative image processing enables segmentation of subtle features

To study the quantitative link between endogenous DAF-16 activity, and lifespan, we first aimed to analyze the response of endogenous DAF-16 to multiple dietary restriction regimes by varying food concentration and exposure time. Using CRISPR/Cas9, we generated a strain with the endogenous *daf-16* locus labeled with GFP at the 3' end (this was expanded in Chapter 2) and measured the response of DAF-16 using a custom image processing algorithm that quantifies nuclear intensity throughout the entire animal. Accurate analysis of DAF-16::GFP levels is challenging, as single copy reporters lead to extremely dim images. Since GFP intensities from DAF-16 were lower or similar than those from autofluorescent lipid droplets, we performed image acquisition in the green and red channels, allowing subtraction of autofluorescence from the GFP signal. Four separate z-stacks per channel were acquired per animal as this is necessary to cover the entire worm length: head, upper mid-body, lower mid-body, and tail sections. Information from the four z-stacks were aggregated for each worm. Images were analyzed using a custom-made MATLAB script (**Figure 4.1**). This script proceeds to segment cell nuclei in each slice of the z-stack. The algorithm's most important steps are: 1) Subtraction of red channel image from green channel image. This enables deletion of autofluorescence present in the images due to lipid droplets. These are present in both channels but DAF-16::GFP is present only in the green channel. Therefore, this step allows separation of DAF-16 from lipid droplets. 2) Generation of a binary mask from the subtracted image using neighborhood thresholding. This step enables segmentation of cell nuclei and other features such as animal edges but does not keep undesirable

features such as bacteria and other debris that could be present in the original image. 3) Identification of nuclei by retaining segmented objects that: a) filled up at least 50% of their bounding box, as nuclei have a circle-like it would be expected that a perfect circle would occupy ~79% of its bounding box. Using 50% accounts for those nuclei that could have a ellipse-like shape. b) had eccentricity values under 0.85 to eliminate objects such as animals' edges with eccentricities near 1.0 (a line), and instead selecting for circle-liked objects that have an eccentricity closer to 0.0 (a circle). And c) had solidity values above 0.75, with this parameter taking into account features that could have passed the previous filters but would have an empty ellipse-like shape (for example, a developing embryo). These threshold values were determined based on visual assessment of the characteristics of nuclei. Object characteristics from the original raw image were extracted using the "regionprops" function. 4) Use of the "imopen" function to smooth edges of all nuclei because the previous steps provide features with rough edges but cell nuclei have smooth edges, this step corrects this. 5) Deletion of objects smaller than neurons and larger than intestinal cells using the "bwareaopen" function, these objects were usually bacteria present in liquid culture were the animals are maintained. As seen above, these operations as a whole enable for the selection of nuclei (ellipse or circle-like objects) while eliminating other features such as autofluorescence, animal edges, embryos, etc. in a stepwise manner. To avoid over-estimation, nuclei present in multiple slices were identified by comparing their centroids. If multiple centroids with similar values in the ± 4 pixels range were identified in multiple slices, only the object with the largest area was retained for properties extraction. The MATLAB regionprops function was then used to quantify the total intensity in the segmented nuclei and the data extracted was stored in

a MATLAB nested structure. Total intensity was calculated as the sum of the intensity of the pixels from all cell nuclei extracted per worm.

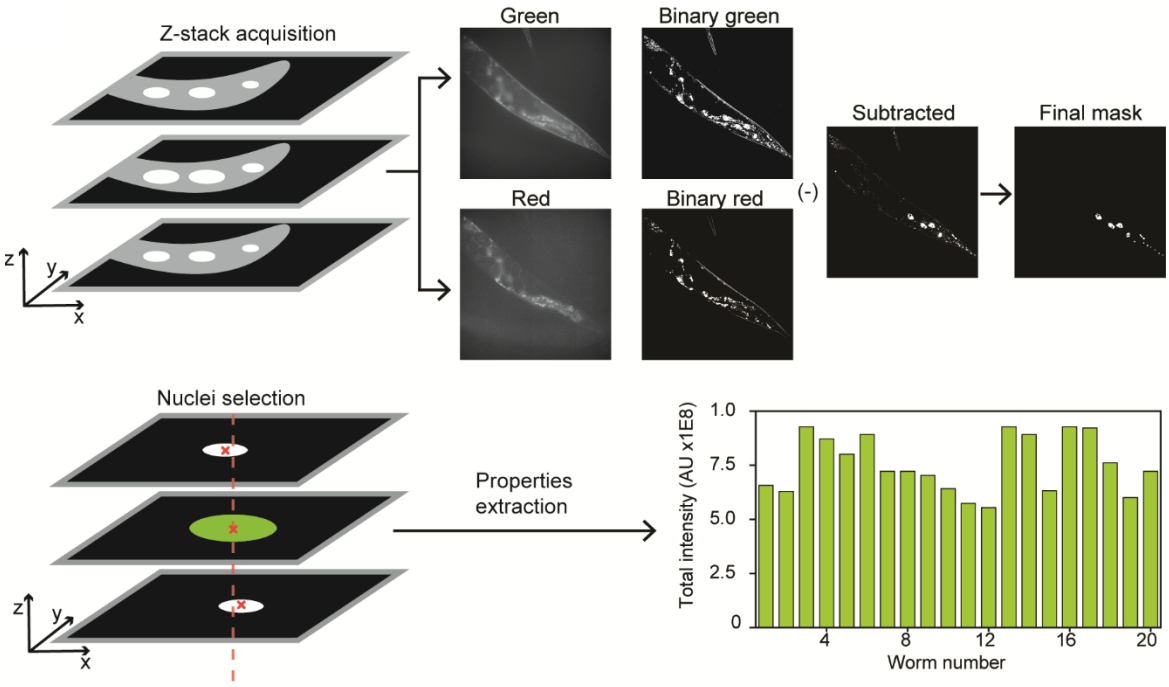

Figure 4.1 Quantitative analysis of endogenous DAF-16 under dietary restriction regimes. Four Z-stacks of 30 slices are taken of each animal. Each slice in the green channel has a corresponding red channel slice. Both are converted to binary images and subtracted from each other to eliminate autofluorescence. The resulting image is treated with morphological functions and objects are filtered based on extent, solidity, and eccentricity. An image containing only cell nuclei is obtained, and largest nuclei are retained if they appear in several slices. Pixel-based intensity is then aggregated to obtain total DAF-16 intensity in all of the animal's identified nuclei.

4.3.2 Machine learning enables cell type classification

Previous DAF-16 studies have demonstrated that its activity is tissue-dependent and that certain DAF-16 isoforms are active in specific tissues[29]. Furthermore, issue interactions and tissues functioning as signaling centers affect DAF-16 activity and its influence in lifespan[7]. These contributions have not been previously quantified to assess the relevance of specific tissues in DAF-16 activity. We decided to evaluate the

contributions of different cell types to DAF-16 total intensity. To achieve this, we used a Fine Tree multi-class classification algorithm generated using the Classification Learner Tool in MATLAB. A ground truth set of 600 cell nuclei and their corresponding class (intestine, neuron, hypodermis, or muscle) was manually generated by visual inspection by a trained observer. The original raw images were loaded on ImageJ for evaluation, cell nuclei were identified, and classification and assignation to the four classes was based on their spatial location, shape, and size (**Figure 4.2**). The Fine Tree algorithm was trained using the MATLAB Classification Learner, by using the following object properties as features: 1) Area, as intestinal cells are much larger than any other type while neurons are the smallest, hypodermal and muscle cells fall in the middle-sized range. 2) Eccentricity, as muscle and intestinal nuclei tends to be more elliptical-shaped, both neurons and hypodermal cells are closer to a circular shape. And 3) Equivalent diameter, this parameter also evaluates subtle differences between ellipses and circles. The generated Fine Tree algorithm resulted in a 96.1% accuracy when predicting cell types with a validation set (**Figure 4.2**). We used the data thus extracted to evaluate individual contributions to DAF-16 activity in Chapter 3.

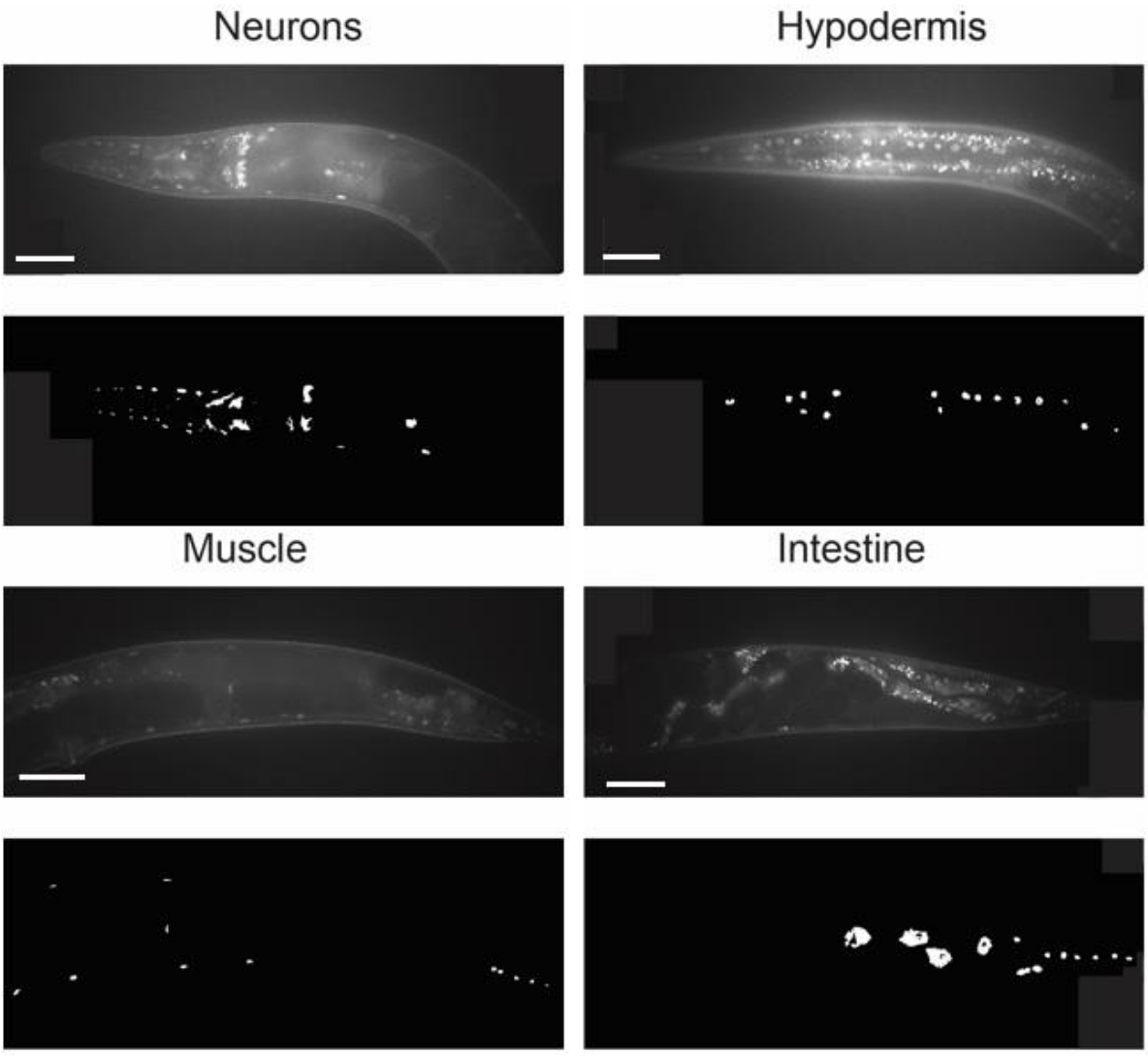

Figure 4.2 Four different cell type classes. These are the cell types evaluated for their contributions to DAF-16 activity. Neurons are more numerous in the head (top left) and tend to be smaller than other cell types. Intestinal cells are the largest (bottom right) and are found along the body, from the end of the head to the tail. Scale bars 50μM

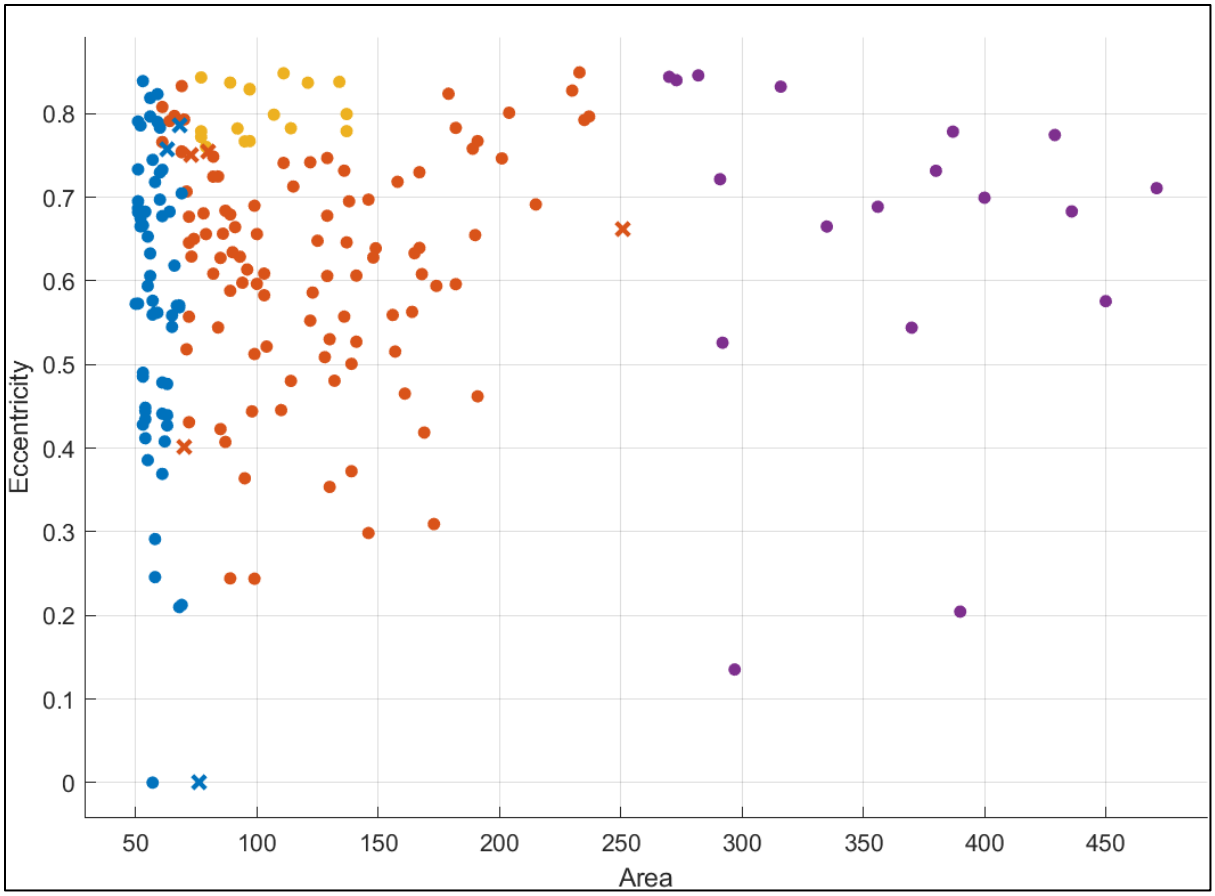

Figure 4.3 Prediction model for Fine Tree classifier. Graphic representation of classification accuracy of prediction model using a Fine Tree classifier with 96.6% accuracy. Four different cell types represented with their true classes: Neurons (blue), muscle (yellow), hypodermal (orange), and intestinal (purple). 'X' indicates a cell that was misclassified with respect to the ground truth.

4.3.3 Segmentation of *C. elegans* pharynx to track morphological changes

The *C. elegans* pharynx goes through morphological changes related to aging. To keep track of these changes, researchers take advantage of the animal's transparent body to observe the pharynx with bright field microscopy. While it is possible to use this method to identify the pharynx from the rest of the animal's body, this does not allow automated analysis. We reasoned that a deep learning algorithm would be useful to detect the pharynx. This approach would require generation of a training set with labeled pharynxes; this step would be time-consuming, and observer-biased. To circumvent this

step, we hypothesized that using segmentation from fluorescently labeled pharynxes would be useful to generate the training set.

We proceeded to generate a strain with such a label. We microinjected the gonad of *C. elegans* with plasmid pCFJ90 containing a red mCherry tag added to the myo-2 gene[30], present in the pharynx. We selected for progeny with extrachromosomal arrays by looking for bright red fluorescence in the pharynx area (**Figure 4.4**). Selected animals were propagated to generate more animals with the array. We performed imaging of an age-synchronized population of these animals on day 1 of adulthood. We focus on the pharynx area acquiring one bright field image and one red fluorescence channel image per worm. A MATLAB-based segmentation algorithm was developed to generate binary masks from the red channel fluorescent images. This was performed by using the 'imbinarize' function. These masks with their corresponding bright field images were used to train a Mask R-CNN-based algorithm for segmentation. The images tested gave Jaccard scores of over 0.85 for all cases (**Figure 4.4**), with a score of 1.00 indicating 100% similarity between the prediction and the ground truth[31]. These results indicate the Mask R-CNN model is robust at segmenting pharynxes from bright field images.

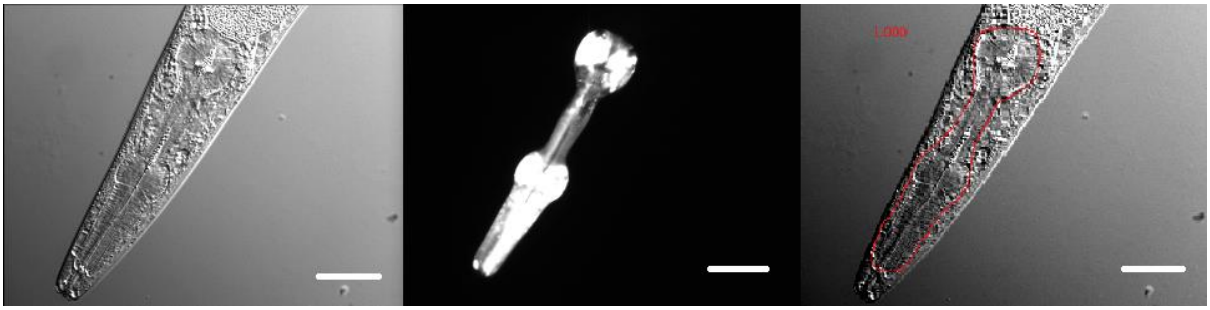

Figure 4.4 Pharynx segmentation with a Mask R-CNN algorithm. Bright field image of an animal's pharynx (left)with its corresponding fluorescent microscopy image (center) with a *myo-2*::mCherry marker highlighting the pharynx. On the right, superimposed image of the Mask R-CNN prediction (red line) over the original bright field image. Scale bar 25µM.

4.4 Discussion

In this chapter we have indicated a number of challenges related to typical image acquisition and processing in *C. elegans* aging research. One is the capture of subtle changes in the activity of DAF-16 that we solved by creating a custom-made MATLAB algorithm that enables segmentation of *C. elegans* cell nuclei even in conditions of low intensity. Allowing to measure how stressful conditions affect DAF-16. Furthermore, we were able to use this nuclei information to segregate DAF-16 by tissue type taking advantage of a Fine Tree algorithm. The combination of these two enables extracting DAF-16 activity data (measured as total intensity) in a high-throughput manner. The conclusions from the information thus acquired were discussed in Chapter 3.

Additionally, we developed a Mask R-CNN-based algorithm that allows for segmentation of *C. elegans* pharynx in bright field image. This opens the possibility of tracking a high volume of images avoiding time-consuming and biased manual segmentation of these images. The application of this approach is in the commonly used method of evaluating pharynx morphological changes to evaluate healthspan in *C. elegans*.

4.5 Materials and Methods

4.5.1 Strains, media, and culture

C. elegans was maintained on standard Nematode Growth Medium (NGM) plates seeded with OP50 *E. coli* bacteria and kept at 20 ºC until they started to lay eggs. Animals were then bleached using standard protocols to obtain age-synchronized populations[32]. This process was repeated 3 times in total to avoid transgenerational epigenetic effects related to longevity[33]. L4 animals were then transferred to a cell culture flask containing 4ml of SB media with 10^{10} cells/ml of OP50 bacteria and 100 µM 5-fluorodeoxyuridine (FUdR) and kept at 20 ºC for 1 day[34,35]. Cultures were then used for dietary restriction and lifespan experiments. Strains used in this work were ASM10 *daf-16* (del2 [*daf-16*::GFP-C1^3xFlag]) I, ASM6 delEx1[sur-5p::DpnI::GFP + (pCFJ90) myo-2p::mCherry], and N2 (*C. elegans* wild isolate). OP50 *E. coli* was grown in LB media following standard procedures[36]. Bacteria were washed thrice with SB media, pelletized, and suspended in S-Medium at a concentration of 100 mg/mL, corresponding to a concentration of 2 x 10^{10} cells/ml.

4.5.2 Dietary restriction and fluorescence imaging

Approximately 20-30 worms were immobilized using 10 µL of 2 mM tetramisole on dried 2% agarose pads of approximately 1 cm diameter. Confocal fluorescence microscopy was performed with a Leica DMi8 microscope paired with an 89 North LDI Laser Diode Illuminator coupled with a CrestOptics X-Light V2 confocal imager and an Orca-Flash 4.0 digital CMOS camera. The exposure time and laser intensity were kept constant throughout all experiments at 100 ms and 100%, respectively. Images containing 30 slices (Z-stacks with 3 µm spacing) were acquired with a MATLAB GUI

(Graphical User Interface). Images were acquired in the green and red channels sequentially. This enables later subtraction of autofluorescence present in both channels with a custom MATLAB script.

4.5.3 Quantitative image processing

Images were analyzed using a MATLAB script, customized to segment cell nuclei in each slice of the z-stack. This is achieved by performing the following operations:

1) Subtraction of red channel image from green channel image

2) Generation of a binary mask from the subtracted image using the 'imbinarize' function

3) Identification of nuclei by segmenting objects that filled up at least 50% of their bounding box, had eccentricity under 0.85, and had solidity values above 0.75

4) Use of the "imopen" function to smooth edges

5) Deletion of objects smaller than neurons and larger than intestinal cells using the "bwareaopen" function

6) If multiple centroids with similar values in the ± 4 pixels range were identified in multiple slices, only the object with the largest area was kept for properties extraction

7) use of the 'regionprops' function to quantify the total intensity in the segmented nuclei

8) Storing of data extracted in a MATLAB nested structure

4.5.4 Cell type classification and nucleolus analysis

To classify nuclei belonging to specific tissues, we used a Fine Tree multi-class classification algorithm. A ground truth set of 600 cell nuclei and their corresponding class (intestine, neuron, hypodermis, or muscle) was manually generated. The Fine Tree algorithm was trained using MATLAB Classification Learner, by using the following object properties as features: area, eccentricity, and equivalent diameter.

4.5.5 Generation of masks for pharynx segmentation

Images of the pharynx in the red channel were read in a MATLAB script. A first mask was generated using the ‘imbinarize’ function. A combination of the ‘imdilate’ and ‘imerode’ functions was used to smooth the edges of the binarized image and to fill up ‘holes’ that could be present in the segmented pharynx. Finally, the ‘bweareaopen’ function was used to eliminate small features and to keep only the largest object (the pharynx) in the image.

4.6 References

1. Uno M, Nishida E. Lifespan-regulating genes in C. elegans. *Aging Mech Dis*. 2016;2(1):16010. doi:10.1038/npjamd.2016.10

2. Kaeberlein TL, Smith ED, Tsuchiya M, et al. Lifespan extension in Caenorhabditis elegans by complete removal of food. *Aging Cell*. 2006;5(6):487-494. doi:10.1111/j.1474-9726.2006.00238.x

3. Masoro EJ. Overview of caloric restriction and ageing. *Mech Ageing Dev*. 2005;126(9 SPEC. ISS.):913-922. doi:10.1016/j.mad.2005.03.012

4. Mair W, Panowski SH, Shaw RJ, Dillin A. Optimizing dietary restriction for genetic epistasis analysis and gene discovery in C. elegans. *PLoS One*. 2009;4(2):4535. doi:10.1371/journal.pone.0004535

5. Panowski SH, Wolff S, Aguilaniu H, Durieux J, Dillin A. PHA-4/Foxa mediates diet-restriction-induced longevity of C. elegans. *Nature*. 2007;447(7144):550-555. doi:10.1038/nature05837

6. Lin K, Hsin H, Libina N, Kenyon C. Regulation of the Caenorhabditis elegans longevity protein DAF-16 by insulin/IGF-1 and germline signaling. *Nat Genet*. 2001;28(2):139-145. doi:10.1038/88850

7. Libina N, Berman JR, Kenyon C. *Tissue-Specific Activities of C. Elegans DAF-16 in the Regulation of Lifespan*. Vol 115.; 2003. doi:10.1016/S0092-8674(03)00889-4

8. Weinkove D, Halstead JR, Gems D, Divecha N. Long-term starvation and ageing

induce AGE-1/PI 3-kinase-dependent translocation of DAF-16/FOXO to the cytoplasm. *BMC Biol*. 2006;4(1):1-13. doi:10.1186/1741-7007-4-1

9. Li S-T, Zhao H-Q, Zhang P, et al. DAF-16 stabilizes the aging transcriptome and is activated in mid-aged Caenorhabditis elegans to cope with internal stress. *Aging Cell*. February 2019:e12896. doi:10.1111/acel.12896

10. Uno M, Tani Y, Nono M, et al. Neuronal DAF-16-to-intestinal DAF-16 communication underlies organismal lifespan extension in C. elegans. *iScience*. 2021;24(7):102706. doi:10.1016/j.isci.2021.102706

11. Kumsta C, Hansen M. C. elegans rrf-1 mutations maintain RNAi efficiency in the soma in addition to the germline. *PLoS One*. 2012;7(5). doi:10.1371/journal.pone.0035428

12. Jordan MI, Mitchell TM. Machine learning: Trends, perspectives, and prospects. *Science (80-)*. 2015;349(6245):255-260. doi:10.1126/science.aaa8415

13. San-Miguel A, Kurshan PT, Crane MM, et al. Deep phenotyping unveils hidden traits and genetic relations in subtle mutants. *Nat Commun*. 2016;7:12990. doi:10.1038/ncomms12990

14. Saberi-Bosari S, Flores KB, San-Miguel A. Deep learning-enabled analysis reveals distinct neuronal phenotypes induced by aging and cold-shock. *BMC Biol*. 2020;18(1). doi:10.1186/s12915-020-00861-w

15. Hahm JH, Kim S, Diloreto R, et al. C. elegans maximum velocity correlates with healthspan and is maintained in worms with an insulin receptor mutation. *Nat*

Commun. 2015;6:8919. doi:10.1038/ncomms9919

16. Huang C, Xiong C, Kornfeld K. Measurements of age-related changes of physiological processes that predict lifespan of Caenorhabditis elegans. *Proc Natl Acad Sci U S A*. 2004;101(21):8084-8089. doi:10.1073/pnas.0400848101

17. Wählby C, Kamentsky L, Liu ZH, et al. An image analysis toolbox for high-throughput C. elegans assays. *Nat Methods*. 2012;9(7):714-716. doi:10.1038/nmeth.1984

18. Fudickar S, Nustede EJ, Dreyer E, Bornhorst J. Mask r-cnn based c. Elegans detection with a diy microscope. *Biosensors*. 2021;11(8):257. doi:10.3390/bios11080257

19. Bates K, Le K, Lu H. Deep learning for robust and flexible tracking in behavioral studies for C. elegans. Webb B, ed. *PLOS Comput Biol*. 2022;18(4):e1009942. doi:10.1371/journal.pcbi.1009942

20. Baek JH, Cosman P, Feng Z, Silver J, Schafer WR. Using machine vision to analyze and classify Caenorhabditis elegans behavioral phenotypes quantitatively. *J Neurosci Methods*. 2002;118(1):9-21. doi:10.1016/S0165-0270(02)00117-6

21. Geng W, Cosman P, Berry CC, Feng Z, Schafer WR. Automatic tracking, feature extraction and classification of C. elegans phenotypes. *IEEE Trans Biomed Eng*. 2004;51(10):1811-1820. doi:10.1109/TBME.2004.831532

22. Huang KM, Cosman P, Schafer WR. Machine vision based detection of omega

bends and reversals in C. elegans. *J Neurosci Methods*. 2006;158(2):323-336. doi:10.1016/j.jneumeth.2006.06.007

23. Mortazi A, Bagci U. Automatically designing CNN architectures for medical image segmentation. In: *Lecture Notes in Computer Science (Including Subseries Lecture Notes in Artificial Intelligence and Lecture Notes in Bioinformatics)*. Vol 11046 LNCS. Springer Verlag; 2018:98-106. doi:10.1007/978-3-030-00919-9_12

24. Sharma P, Berwal YPS, Ghai W. Performance analysis of deep learning CNN models for disease detection in plants using image segmentation. *Inf Process Agric*. 2020;7(4):566-574. doi:10.1016/j.inpa.2019.11.001

25. Yuval O, Iosilevskii Y, Meledin A, Podbilewicz B, Shemesh T. Neuron tracing and quantitative analyses of dendritic architecture reveal symmetrical three-way-junctions and phenotypes of git-1 in C. elegans. *PLoS Comput Biol*. 2021;17(7):e1009185. doi:10.1371/journal.pcbi.1009185

26. Chow DK, Glenn CF, Johnston JL, Goldberg IG, Wolkow CA. Sarcopenia in the Caenorhabditis elegans pharynx correlates with muscle contraction rate over lifespan. *Exp Gerontol*. 2006;41(3):252-260. doi:10.1016/j.exger.2005.12.004

27. Scharf A, Piechulek A, Von Mikecz A. Effect of nanoparticles on the biochemical and behavioral aging phenotype of the nematode caenorhabditis elegans. *ACS Nano*. 2013;7(12):10695-10703. doi:10.1021/nn403443r

28. Johnston J, Iser WB, Chow DK, Goldberg IG, Wolkow CA. Quantitative image analysis reveals distinct structural transitions during aging in Caenorhabditis elegans tissues. *PLoS One*. 2008;3(7):e2821. doi:10.1371/journal.pone.0002821

29. Kwon ES, Narasimhan SD, Yen K, Tissenbaum HA. A new DAF-16 isoform regulates longevity. *Nature*. 2010;466(7305):498-502. doi:10.1038/nature09184

30. Frøkjær-Jensen C, Wayne Davis M, Hopkins CE, et al. Single-copy insertion of transgenes in Caenorhabditis elegans. *Nat Genet*. 2008;40(11):1375-1383. doi:10.1038/ng.248

31. Yan Z, Wu Q, Ren M, Liu J, Liu S, Qiu S. Locally private Jaccard similarity estimation. In: *Concurrency and Computation: Practice and Experience*. Vol 31. John Wiley & Sons, Ltd; 2019:e4889. doi:10.1002/cpe.4889

32. Porta-de-la-Riva M, Fontrodona L, Villanueva A, Cerón J. Basic Caenorhabditis elegans methods: Synchronization and observation. *J Vis Exp*. 2012;(64):e4019. doi:10.3791/4019

33. Greer EL, Maures TJ, Ucar D, et al. Transgenerational epigenetic inheritance of longevity in Caenorhabditis elegans. *Nature*. 2011;479(7373):365-371. doi:10.1038/nature10572

34. Stiernagle T. Maintenance of C. elegans. *WormBook*. 2006. doi:10.1895/wormbook.1.101.1

35. Gruber J, Ng LF, Poovathingal SK, Halliwell B. Deceptively simple but simply deceptive - Caenorhabditis elegans lifespan studies: Considerations for aging and antioxidant effects. *FEBS Lett*. 2009;583(21):3377-3387. doi:10.1016/j.febslet.2009.09.051

36. Amrit FRG, Ratnappan R, Keith SA, Ghazi A. The C. elegans lifespan assay

toolkit. *Methods*. 2014;68(3):465-475. doi:10.1016/j.ymeth.2014.04.002

Chapter 5: Stress Response in *C. elegans* Shows Antagonistic and Silencing Effects Under Combinatorial Conditions

5.1 Abstract

Chemical agents released into the environment can induce oxidative stress in organisms, which is detrimental for health. Although environmental exposures typically include multiple chemicals, organismal studies on oxidative stress derived from chemical agents commonly study exposures to individual compounds. In this work, we explore how chemical mixtures drive the oxidative stress response under various conditions in the nematode *C. elegans*, by quantitatively assessing levels of *gst-4* expression. Our results indicate that naphthoquinone mixtures drive responses differently than individual components, and that altering environmental conditions, such as increased heat and reduced food availability, result in dramatically different oxidative stress responses mounted by *C. elegans*. When exposed to heat, the oxidative stress response is diminished. Notably, when exposed to limited food, the oxidative stress response specific to juglone is significantly heightened, while identified antagonistic interactions between some naphthoquinone components in mixtures are abolished. This implies that organismal responses to xenobiotics is confounded by environment and stressor interactions. Given the high number of variables under study, and their potential combinations, a simplex centroid design was used to capture such non-trivial response over the design space. This makes the case for the adoption of Design of Experiments approaches as they can greatly expand the experimental space probed in noisy biological readouts, and in combinatorial experiments. Our results also reveal gaps in our current knowledge of the organismal oxidative stress response, which can be addressed by

employing sophisticated design of experiments approaches to identify significant interactions.

5.2 Introduction

Oxidative stress, which has deleterious effects on health[1–3], can be induced by ROS (Reactive Oxygen Species) generated from oxidant chemicals. The effects of oxidant exposures on biological systems have been an important area of study, although these effects have been mostly analyzed by employing chemical exposures of individual components.[4] However, realistic environmental exposures are mixtures of multiple components.[5–7] In addition, environmental factors, such as diet and temperature, can modulate the mechanisms by which chemicals induce toxicity and activate defense responses in living organisms.[7,8] It is still unclear how chemical mixtures drive oxidative stress and how environmental conditions modify such responses. In this work, we analyze how mixtures of oxidant species, in particular naphthoquinones, differentially drive the oxidative stress response in the model organism *C. elegans*.

Naphthoquinones are strong oxidants. They are used as precursors of toxic industrial chemicals.[9] They are also a product of fossil fuel combustion and atmospheric photochemical conversions, and are thus found in ambient particulate matter.[10] Environmental exposures to naphthalene (a precursor for naphthoquinones) are important, as it is found in the atmosphere and in cigarette smoke.[11–13] Naphthalene toxicity is thought to occur through the action of napthoquinones.[14,15] Naphthoquinones have been hypothesized to induce oxidative stress through two distinct mechanisms[16,17]: depletion of glutathione (an antioxidant that neutralizes ROS and counteracts xenobiotics

by conjugation) through Michael reaction, or production of ROS through redox cycling.[16] It is unclear if differences in the cytotoxic mechanisms amongst naphthoquinones could be reflected as differences in organismal responses to naphthoquinone mixtures. Naphtoquinone exposures at low concentrations can also induce beneficial effects. Simultaneous exposure to naphthoquinone derivatives such as juglone and plumbagin drive SKN-1/NRF-2 transcription factor-mediated hormesis in *C. elegans* at low concentrations, but turn toxic at higher concentrations.[18] Naphthoquinones have also been shown to have anti-inflammatory effects in other model organisms.[19] For example, allergen induced rats treated with juglone had a reduction in pulmonary eosinophils and bronchoalveolar lavage fluid.[20] Given their prevalence as derivatives of naphthalene, and the differential responses to naphthoquinone exposures, it is critical to study the effects of naphthoquinone mixtures on organismal health.

The model system *C. elegans* facilitates studies on toxicity in a live organism with a well characterized nervous system, cell lineage, and physiology. *C. elegans* has proven to be a powerful model due to its small size, easy maintenance, and mapped genome and neuronal wiring. It enables *in vivo* studies using fluorescent markers due to their transparent bodies and ease of genetic manipulation.[21] *C. elegans* has also been useful to study chemical mixture toxicity through growth and fertility assays.[22–25] *C. elegans* and humans share concordant pathways, such as the insulin/IGF-1 signaling pathway (IIS), which regulates lifespan and healthspan extension driven by dietary restriction.[26] Two-thirds of human proteins have homologs in *C. elegans*.[26] *C. elegans* has been used to study mechanisms of toxicity identification, such as those produced by phorbol esters.[26] Finally, toxicological studies have shown up to 69% concordance between *C. elegans*

and mammalian toxicological data.[27] Another study identified concordance between *C. elegans* data and that from rabbits and rats to be in the 45-53% range, just slightly lower than the concordance between rabbit and rat data (58%).[28]

Defense mechanisms to metabolize and eliminate xenobiotics are evolutionarily conserved from single cell organisms to humans.[29] In mammalian cells, NRF-1, NRF-2, and NRF-3 are a class of NF-E2-related factor 2 (NRF) transcription regulators employed for such defense mechanisms.[30] In *C. elegans,* the oxidative stress response pathway is activated to counteract the toxicity caused by oxidative stressors.[31]The SKN-1 transcription factor, the functional ortholog of mammalian NRF-2, is major regulator of the oxidative stress response in *C. elegans*.[30,32,33] It should be noted that SKN-1 diverges from NRF-2 in the way it binds to DNA. However, the similarities allow us to study SKN-1 in *C. elegans* as a model for mammalian NRF-2.[30] SKN-1 has also been linked to other much broader homeostatic functions such as reducing stress, counteracting lipid accumulation, mitochondrial biogenesis and mitophagy, among others.[30] SKN-1 activity in response to chemicals and heavy metals has been studied by examining expression of SKN-1-regulated genes using endogenously expressed fluorescent reporters. SKN-1 driven expression is mostly studied in the intestine, where digestion and detoxification occur.[4,34–36] Multiple antioxidant response elements (AREs) containing genes are downstream targets of SKN-1, such as *gst-4* and *gcs-1*, which encode for drug-metabolizing glutathione S-transferase (GST-4) and gamma-glutamyl cysteine synthetase (GCS-1), important in glutathione synthesis, respectively. For example, prior work by Crombie et al. focused on studying the effect of environmental factors on the oxidative stress response to juglone using a two level full factorial design, by monitoring

gst-4 expression.[37] *gst-4* is commonly used as proxy for SKN-1 activity and thus activation of the oxidative stress response.[38–40]

In this study, we analyzed the effects of naphthoquinone mixtures on the *C. elegans* oxidative stress response under various environmental conditions, as determined by a *gst-4* translational fluorescent reporter. We follow a Design of Experiments (DoE) approach that enables systematic examination of the input factors to determine the individual and combinatorial influence on the measured response,[41,42] while avoiding the unfeasible number of experiments required for full factorial designs with multi-level factors. This approach minimizes the number of experimental runs necessary to measure interactions between three naphthoquinones and two environmental conditions, while enabling comparisons from independent biological populations. We quantify response surfaces for these ternary mixtures under different conditions. We find that naphthoquinone mixtures drive antagonistic interactions, but these interactions are drastically modified by dietary restriction. On the other hand, heat stress abolishes oxidative stress response to both individual components and mixtures of naphthoquinones. This *gst-4* response is independent of the IIS factor DAF-16. The ROS levels and resistance to acute oxidative stress that result from exposure to naphthoquinone mixtures are also modulated by environmental factors, in the opposite direction as *gst-4* expression.

5.3 Results

5.3.1 Dose dependency of *gst-4* response

To identify relevant concentrations of chemical mixtures of plumbagin, 1, 4-naphthoquinone, and juglone, (**Figure 5.1 A, B, C**) we first determined the dose-dependent *gst-4* activity to individual components (**Figure 5.1 D**). Animals were exposed for 8 hours, based on prior studies that suggest this time is sufficient to observe a *gst-4* response.[43,44] *gst-4* belongs to a class of enzymes used to catalyze conjugation of glutathione with xenobiotics. Prior work determined that *gst-4* expression is increased in animals stressed with xenobiotics, while external ROS generated by hypoxanthine/XOD system, UV light, and heat did not elicit a response.[40] As expected, we identified that as the naphthoquinones concentration increases, *gst-4* activity also increases and eventually saturates (**Figure 5.1 D**), as described in previous studies.[43,44] To assess the effect of mixture proportions on oxidative stress response, the total naphthoquinone dosage should remain constant. Based on these results, we fixed a combined total dosage of 30 μM for mixture experiments, which allows studying the interactions of components at different proportions without potential saturation of the *gst-4* response. Sublethal doses in the range of 20-30 μM for the 3 compounds under study are known to drive SKN-1-dependent expression of *gst-4*, and also induce a hormetic effect driven by SKN-1.[4,18,37]

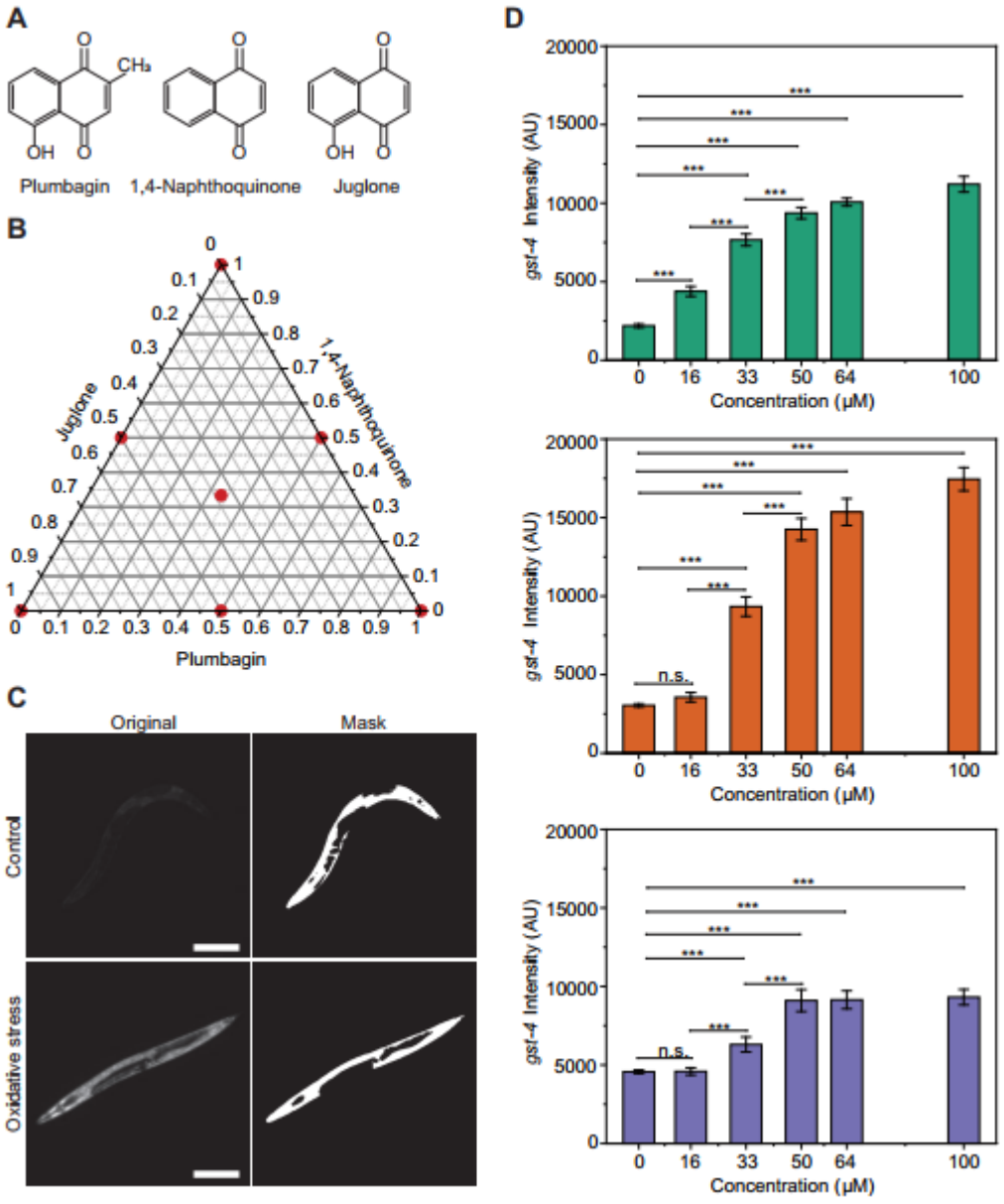

Figure 5.1 *gst-4* response is dose dependent. A) Compounds used for oxidative assays. B) Simplex centroid design. C) CL2166 worms under control and oxidative stress with corresponding masks for extracting *gst-4* expression levels. D) *gst-4* dose-dependent response to Plumbagin, 1, 4-Naphthoquinone, and Juglone (top to bottom). $p > 0.05$ (n.s.), $p < 0.001$ (***). Error bars are SEM. All p-values were calculated using Tukey HSD for all pairwise comparisons after one-way ANOVA (Unequal Variances) comparison in JMP 14.2. Scale bars are 200 μm.

5.3.2 Naphthoquinone mixtures show antagonistic effects under *ad libitum* feeding and physiological temperature conditions.

The first mixture experiments were performed under *ad libitum* feeding and no heat stress conditions based on the simplex centroid design. The average and standard deviations of the baseline *gst-4* responses of controls run for each of the ten sets of experiments were compared to determine if runs were comparable to each other. All measurements are within statistical control (**Figure 5.2**). We used a Scheffe model fit to develop a response surface (**Figure 5.3 A**). The response surface indicates that the individual naphthoquinones induce a higher *gst-4* response than binary and ternary mixtures, suggesting an antagonistic interaction (**Figure 5.3 A)**. Since animals were maintained at 25 ºC and shifted to 20 ºC for chemical exposure, a control exposure experiment at 25 ºC was tested to determine if the temperature shift could play a role in the observed responses. The control experiment maintained at 25 ºC shows the same *gst-4* expression trend as those exhibited by animals shifted to 20 ºC for exposure (**Figure 5.4**): naphthoquinone mixtures are antagonistic in driving the *gst-4* response.

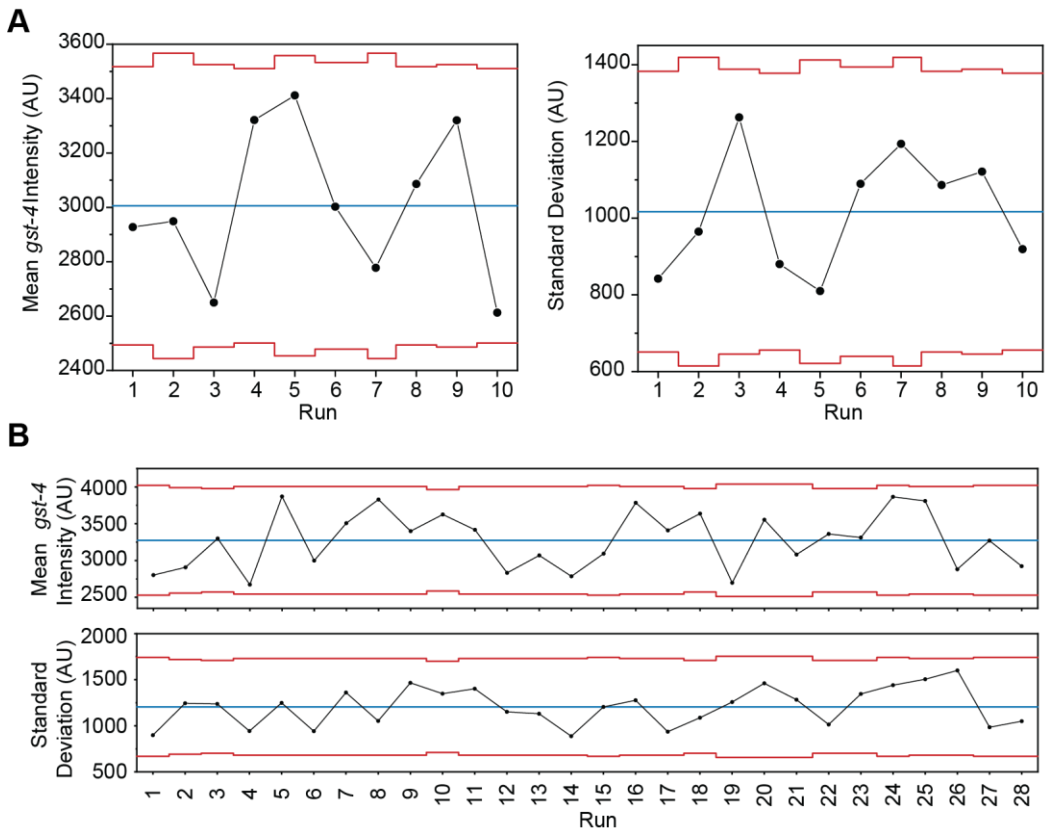

Figure 5.2 Xbar and S-charts for populations tested. A) Xbar and S-chart for 10 populations used for oxidative stress assays. B) Xbar and S-chart for 28 populations used for oxidative stress assays.

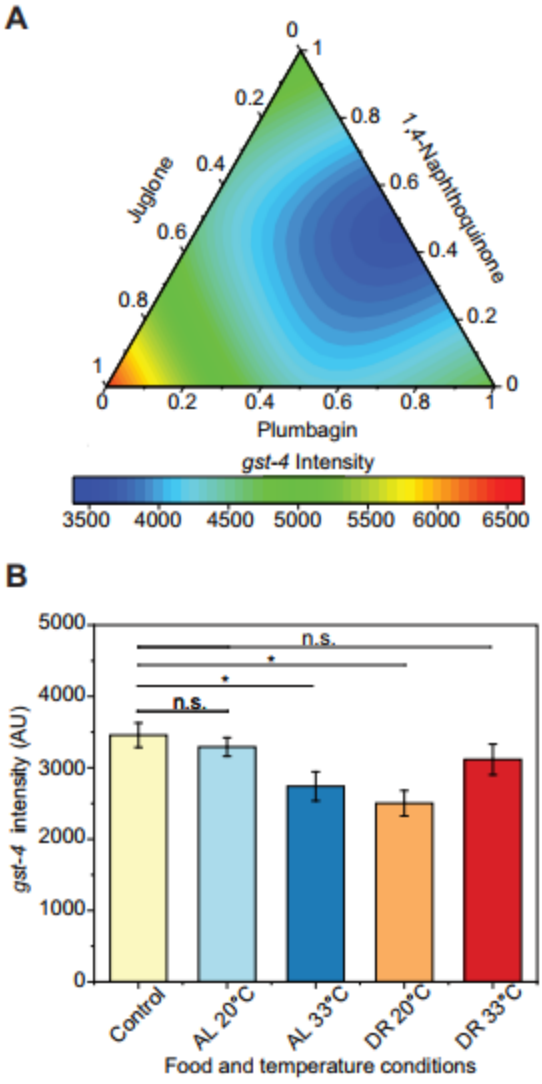

Figure 5.3 Naphthoquinone mixtures show no synergistic effects under *ad libitum* feeding and no heat stress conditions. A) Response surface of *gst-4* expression levels in CL2166 animals under oxidative stress, 20°C, and *ad libitum* feeding. Response surface modeled using standard least squares second order Scheffe model where main effects and interactions were tested for significance. B) Testing for main effect of temperature and food concentration. $p > 0.05$ (n.s.), $p < 0.05$ (*). p-values were calculated using Dunnett's test with *ad libitum*, overall control as control after two-way ANOVA comparison in JMP 14.2. Error bars are SEM.

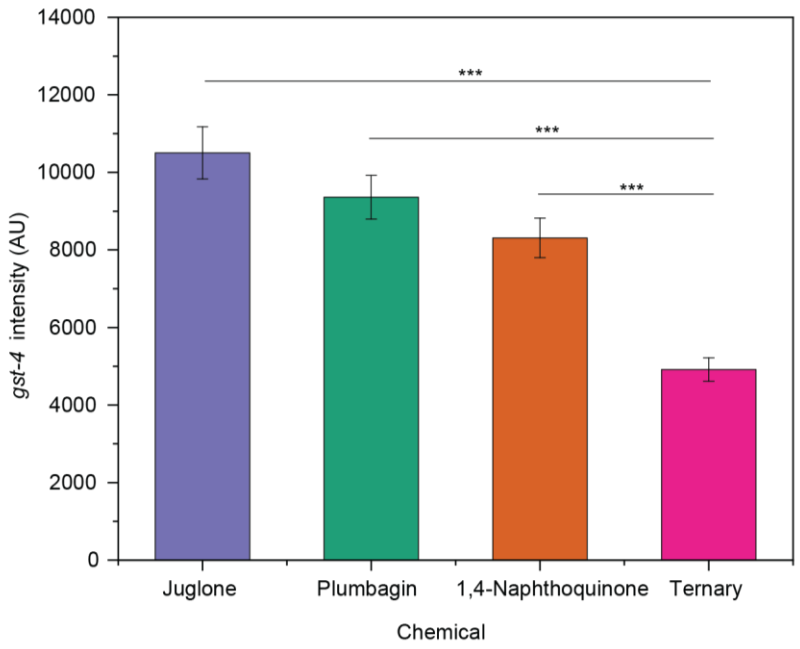

Figure 5.4 *gst-4* response at 25 ºC. *gst-4* response to Plumbagin, 1, 4-Naphthoquinone, Juglone, and ternary mixture at 25 ºC. $p < 0.001$ (***). Values follow the same trend as Figure 2B with a lower value for the ternary mixture (middle point of response surface in Figure 2B), and higher values for individual naphthoquinones (vertex points of response surface in 2B). Error bars are SEM.

5.3.3 Naphthoquinone mixtures induce different *gst-4* responses under different environmental conditions

Temperature and dietary intake have been shown to affect the oxidative stress response in *C. elegans*.[33,37,45] Thus, we tested how exposure to heat stress and dietary restriction modified the *gst-4* response to naphthoquinone mixtures by fitting the *gst-4* expression data to a mixed effects model. The overall control was plotted as Xbar and S chart and indicates that the populations are within statistical limits of each other (**Figure 5.2**).

Heat stress and dietary restriction (DR) significantly affect the oxidative stress response, inducing a lower baseline *gst-4* response than a control of 20 ºC and *ad libitum* conditions (**Figure 5.3 B**). However, heat and dietary restriction induce differential responses in *gst-4* in the presence of naphthoquinone mixtures (**5.5 A, B**). The *ad libitum* and 20 ºC response surface (**Figure 5.5 B**) is the repetition of the first mixture experiment and was confirmed to not be statistically different (**Figure 5.3 A**). The experimentally acquired data is represented as conventional bar plots in **Figure 5.6**. As the temperature is increased to 33 ºC, heat stress inhibits the *gst-4* response to pure components and mixtures, consistent with prior results.[37] Dietary restriction reduces the baseline *gst-4* level (**Figure 5.3 B**).[46] In contrast, reduced food concentration did not affect the *gst-4* response to 1,4-naphthoquinone and plumbagin (**Figure 5.5 B**) and it drastically increased the response to juglone, as compared to *ad libitum* conditions. Furthermore, exposure to binary or ternary mixtures under dietary restriction did not result in antagonistic interactions observed in mixtures at *ad libitum* dietary regime (**Figure 5.5 B, C**). These results suggest that dietary restriction can differentially modulate the oxidative stress response to individual compounds, and significantly modify interactions amongst naphthoquinones.

Figure 5.5 Naphthoquinone mixtures elicit differential response under simultaneous stress exposure. A) Representative CL2166 animals exposed to ternary naphthoquinone mixtures (1,4-Naphthoquinone, Juglone, Plumbagin) at different environmental conditions. B) Response surface of *gst-4* expression levels for CL2166 animals under oxidative stress at different environmental conditions. C) *gst-4* expression levels for CL2166 animals under exposure to the ternary naphthoquinone mixture. D) DCFDA intensity levels for N2 animals exposed to the ternary naphthoquinone mixture. E) DCFDA staining of representative N2 animals exposed to the ternary naphthoquinone mixture. F) Average survival time under exposure to 250 µM Juglone in CL2166 animals pre-exposed to the ternary naphthoquinone mixture at different environmental conditions. G) *gst-4* expression levels under *daf-16* RNAi for CL2166 animals exposed to ternary naphthoquinone mixtures. H) *daf-16* expression levels for MAH97 animals exposed to ternary naphthoquinone mixtures, measured as total intensity in the nuclei of cells per worm. Hatched bars (all close to zero) are responses under *daf-16* RNAi. AL: *ad libitum.* DR: dietary restriction. $p > 0.05$ (n.s.), $p < 0.05$ (*), $p < 0.001$ (***). p-values were calculated using Dunnett's test with *ad libitum*, 20 ºC as control after one-way ANOVA comparison in JMP 14.2.Response surfaces modeled using standard least squares second order Scheffe model where main effects and interactions were tested for significance. Scale bars are 100 µm. Error bars are SEM.

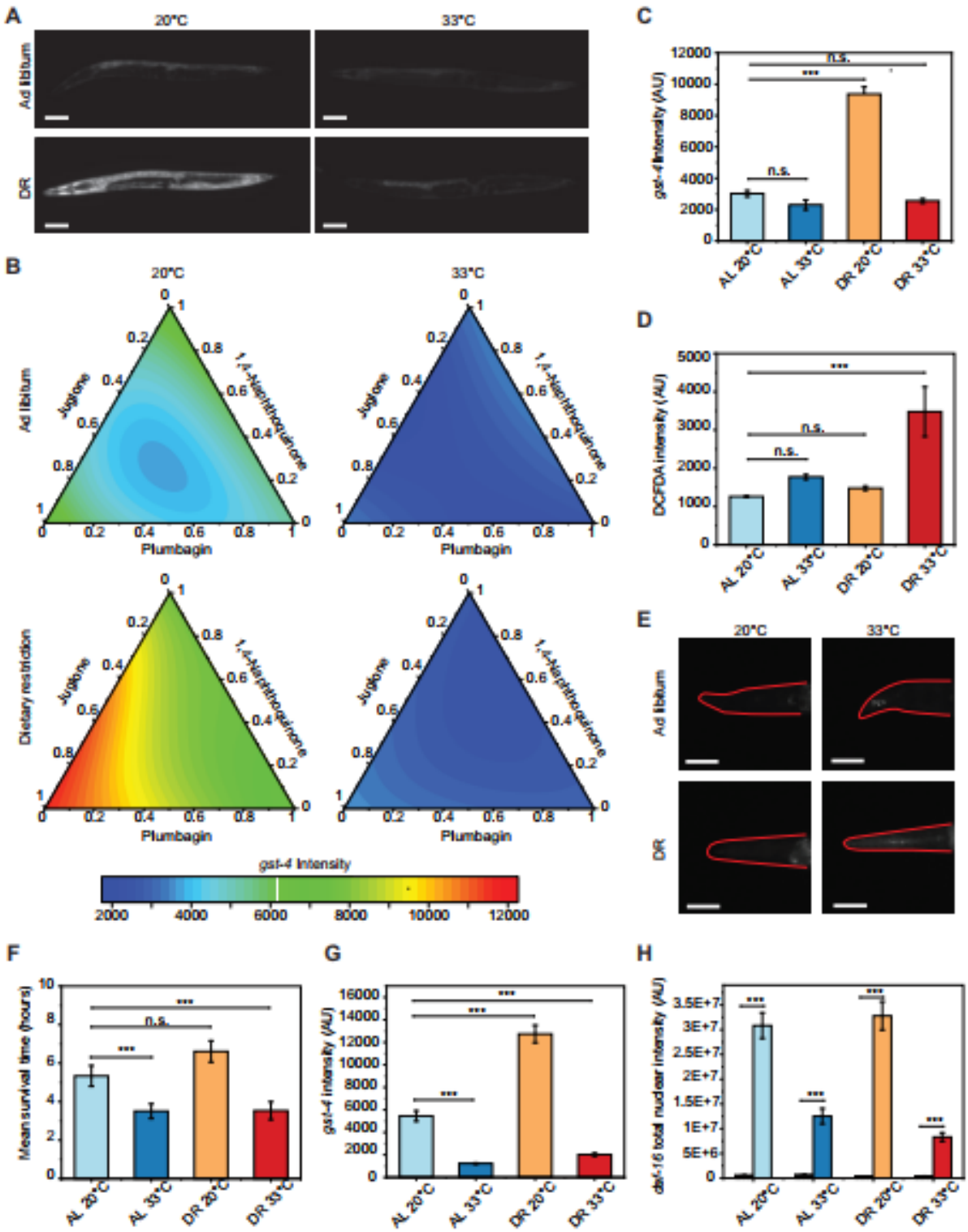
A
20°C
33°C
Ad libitum
DR
B
20°C
33°C
Ad libitum
Dietary restriction
Juglone
1,4-Naphthoquinone
Plumbagin
gst-4 Intensity
2000
4000
6000
8000
10000
12000
C
gst-4 intensity (AU)
n.s.
***
AL 20°C
AL 33°C
DR 20°C
DR 33°C
D
DCFDA intensity (AU)
n.s.
***
E
20°C
33°C
Ad libitum
DR
F
Mean survival time (hours)
n.s.
***
G
gst-4 intensity (AU)
***
H
dvk-16 total nuclear intensity (AU)
***

We next asked whether these environmental modifications of the oxidative stress response to naphthoquinone mixtures could stem from differences in ROS levels, and if the *gst-4* response exhibiting differential responses to mixtures and environmental variables would imply differences in organismal resistance to acute oxidative stress. These questions were addressed by measuring ROS levels through DCFDA staining of N2 animals (**Figure 5.5 D, E**) and by assessing the survival of worms to acute oxidant exposures after exposure to low-level naphthoquinone mixtures (**Figure 5.5 F, 5.7**) These experiments show that the presence of ROS in the worms is highest under conditions of dietary restriction at 33 ºC, which are also conditions with the lowest level of *gst-4* (**Figure 5.5C**). The differences in ROS levels between the populations exposed to heat stress could be explained by an increase formation of ROS in animals under glucose restriction,[47] while high levels of glucose renders *C. elegans* more resilient to oxidative stress.[48] In this case, a parallel can be drawn between glucose and food availability. Animals exposed to acute juglone concentrations exhibit the lowest survival under heat stress (**Figure 5.5 F**), which matches with the lowest observed levels of *gst-4* (**Figure 5.5 C**). These results suggest that environmental conditions that modulate the *gst-4* responses to naphthoquinone mixtures similarly affect the animal's resistance to oxidants, and that ROS levels are also increased in conditions that result in minimal *gst-4* expression and highest susceptibility to acute juglone exposures.

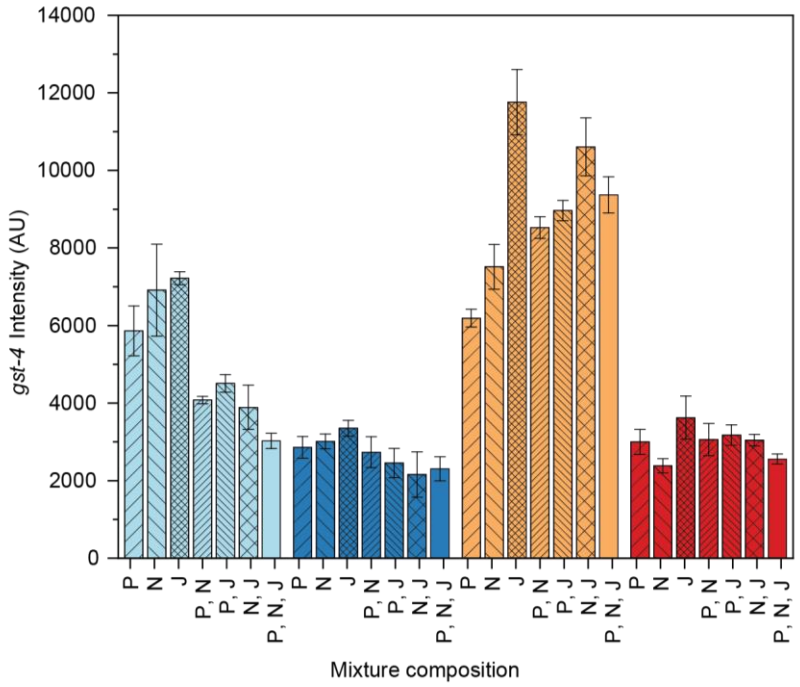

Figure 5.6 Bar plot representation of experimentally acquired *gst-4* expression level. *gst-4* expression levels of animals exposed to naphthoquinone mixtures at different process conditions. From left to right, AL 20ºC (light blue), AL 33ºC (blue), DR 20ºC (orange), DR 33ºC (red). P-Plumbagin, N-1,4-Naphthoquinone, J-Juglone. Error bars are SEM.

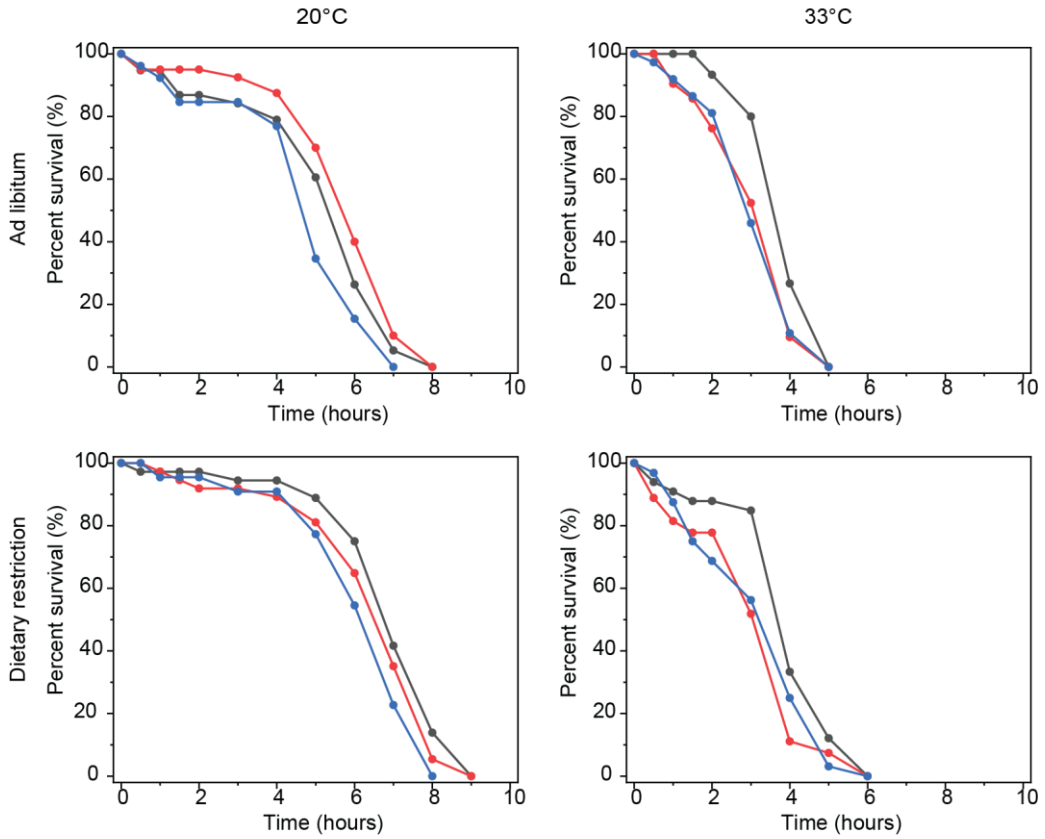

Figure 5.7 Lifespan curves for juglone survival assay. Lifespan curves built with OASIS 2 for CL2166 animals under ternary mixture at different environmental conditions. Each condition was tested three times.

Since dietary restriction modifies the *gst-4* responses to naphthoquinones (individually and in mixtures), we then asked whether this effect could be modulated by the insulin/insulin-like signaling (IIS) pathway that can be activated with specific dietary restriction regimes.[49] To address this question, we tested a possible dependence of the *gst-4* response on *daf-16,* the main regulator of the IIS pathway (**Figure 5.5 G, 5.8**).[50,51] Comparing the *gst-4* responses in the presence (**Figure 5.5C**) and absence (**Figure 5.5 G**) of DAF-16 shows that the DR-dependent induction of *gst-4* under naphthoquinone exposures is independent of DAF-16, suggesting an alternative pathway is at play. Likely *skn-1* itself regulates this interaction, since it is known to play a role in DR-induced lifespan extension.[52] We also measured *daf-16* responses to naphthoquinones mixture exposure by assessing the levels of a DAF-16::GFP fusion protein within intestinal cell nuclei. Like *gst-4, daf-16* responses are inhibited by heat stress (**Figure 5.5 H**). On the other hand, ternary naphthoquinone mixtures induced strong *daf-16* responses in both DR and AL conditions. As mentioned above, under AL conditions, *gst-4* exhibits a reduced signal for ternary mixtures (i.e., antagonistic interactions), which is not observed in *daf-16* activity. This result suggests naphthoquinone mixtures induce strong *daf-16* activity, which is inhibited by heat stress, and the *daf-16* response to oxidants is not modulated by DR, potentially indicating that oxidative stress is prioritized over food intake for downstream signaling.

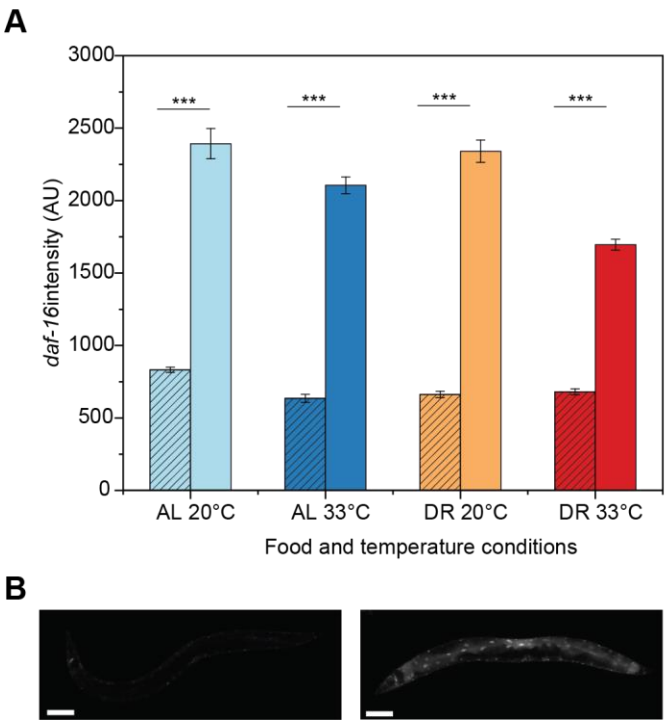

Figure 5.8 *daf-16* response to ternary mixture. A) *daf-16* response to ternary mixture at different environmental conditions. Striated bars represent MAH97 animals under *daf-16* RNAi, clear bars are control animals. B) Representative MAH97 animals under *daf-16* RNAi (left) and control (right). $p < 0.001$ (***). Scale bars are 100 µm. Error bars are SEM.

5.4 Discussion

In this work, we took advantage of a DoE approach to study the oxidative stress response driven by combinatorial exposures to naphthoquinones under a variety of environmental conditions. Unlike traditional full-factorial designs, which would entail an unfeasible number of experiments, using block effects and a simplex centroid design enabled performing experiments in a non-simultaneous and feasible manner. Initially, using mixed second order Scheffe model statistical analysis, we built a response surface to ternary naphthoquinone mixtures under controlled environmental factors. The

observed antagonistic interactions in **Figure 5.3 A** could stem from different mechanisms of toxicity elicited by the mixture components. For instance, there are differences in the chemical reactivity of juglone and plumbagin.[53] Naphthoquinones have been shown to result in toxicity through ROS generation or glutathione depletion.[16,18] Juglone has relatively higher chemical activity and could undergo Michael's addition to glutathione even at lower doses.[53,54] 30 μM of 1, 4-naphthoquinone and plumbagin could cause oxidative stress through redox cycling at lower doses, and only at higher doses cause Michael's addition to glutathione.[53,55] Mixtures of these chemicals could thus result in lower *gst-4* activation than individual mixtures, if *gst-4* induction is more sensitive towards one of these toxicity mechanisms.

We further analyze if the response to naphthoquinones would be modified under different environmental conditions: food availability and temperature, and found drastic changes to response curves. The reduction in *gst-4* expression levels by heat stress observed in **Figure 5.3 B** could be explained by organismal prioritization of the heat shock response over the oxidative stress response, as previously suggested by Crombie et al.[37] The reduction in *gst-4* levels by dietary restriction could be the result of the reduced activity of *cct-4* under dietary restriction, which encodes a chaperonin directly involved in SKN-1–dependent transcription of *gst-4*.[46] We also built response curves to ternary naphthoquinone mixtures under the four environmental conditions, which revealed significant interactions between chemicals. Surprisingly, these interactions were drastically modulated by environmental conditions of temperature and food availability. The identified *gst-4* responses to naphthoquinones is abolished by heat stress, which

could be attributed to prioritization of proteostasis over detoxification, where the HSF-1 driven heat stress response genes are upregulated to prevent protein misfolding.[37]

Dietary restriction also modulated stress response. Under *ad libitum* condition, individual components drove *gst-4* expression to similar levels, however, dietary restriction-induced oxidative stress response show high specificity for juglone, suggesting differences in organismal processing of similar oxidants. Although there is cross-regulation between the diet regulated DAF-16 and oxidative stress regulated SKN-1 pathways,[56,57] RNAi experiments revealed that *gst-4* responses to mixtures are *daf-16*-independent. However, SKN-1 is also known to modulate DR-induced modulation of longevity,[52] and is thus likely integrating signals for DR and oxidative stress and driving the observed interactions. Interestingly, *daf-16* is activated by naphthoquinone mixtures in the absence of heat stress, recapitulating the *gst-4* inhibition by heat stress. In contrast, DR did not elicit higher *daf-16* activation than AL conditions, suggesting organismal responses to oxidants are prioritized over reduced caloric intake. It is still unclear why the DR effects are specific to the oxidant type. Potentially, these differences could stem from differences in toxicity and detection mechanisms through chemosensation, as explained before, coupled with multiple transcriptional pathways interacting at the organismal level.

These findings highlight the importance of experimental analysis in realistic settings, where a variety of chemical components is present, and where environmental conditions vary significantly. In addition, the identified interactions between naphthoquinone mixtures, heat stress, and dietary restriction, shed light on organismal integration and processing of stressors and environmental factors. This could stem from differences in oxidant detection in *C. elegans.* For instance, low levels of H_2O_2 activate

the I2 neuron, while paraquat only elicits a response at a very high concentration.[58] The difference in the *gst-4* response to individual compounds and mixtures could stem from the combined effects of differences in xenobiotic detection and the mechanisms of toxicity by the different naphthoquinones. This result indicates that individual components do not act through a singular mechanism, and that mixtures can drive significantly different organismal responses than individual components, even for highly similar chemical species. A detailed investigation on neuronal SKN-1 could help elucidate whether the interaction mechanisms between chemical mixtures and environments involve neuronal detection.

C. elegans are complex in nature and many factors could affect the response to oxidative stress, such as variation in developmental period, food availability on plate, temperature, as well as biological stochasticity. It is necessary to control and account for such effects as combinatorial mixture experiments cannot be performed using a single population. Control charts have proven to be useful in identifying potential problematic populations, which might show a different response. Such populations can have different biological activity and can affect the results of the experiments being performed. Adding block factors and split plots as random effects to the model also help us compare between populations, even if these exhibit differences that could come from experimental or biological variation. Thus, using a combination of mixture experiments and control charts we have highlighted the differential *gst-4* response by *C. elegans* to oxidative stressor mixtures under different environmental conditions. These results warrant further investigation of the different transcriptional pathways involved and shed light on how organisms respond to variable environments and realistic chemical exposures.

5.5 Materials and Methods

5.5.1 Strain maintenance

C. elegans was maintained on standard Nematode Growth Medium (NGM) plates seeded with OP50 *E. coli* bacteria and maintained at 25 ºC. Worms at day 1 of adulthood were bleached and age synchronized using standard protocols,[59] and grown to the young adult stage before application of oxidative stress. The strains used in the experiments were CL2166: *dvLs19* [pAF15 (gst-4P:GFP::NLS)], MAH97 *muIs109* [daf-16p::GFP::DAF-16 cDNA + odr-1p::RFP], and N2 (wild type) which were obtained from the Caenorhabditis Genetics Center. Animals were exposed to either control (S-Medium) or naphthoquinone mixtures in liquid culture in the presence of HB101 *E. coli* as a food source, based on established procedures.[60] *E. coli* was grown in LB media in the presence of 4 mM streptomycin. Bacteria were washed thrice with SB media, pelletized, and resuspended in S-Medium at a concentration of 100 mg mL^{-1}. Bacteria was then killed by heat treatment at 65 ºC for a period of 45 mins,[37] to avoid bacterial metabolism to confound results.

5.5.2 Chemical preparation

Juglone, 1, 4-naphthoquinone, and plumbagin (**Figure 5.1 A**) were sourced from Fisher Scientific and stored according to supplier guidelines. 100 mM stock solutions were prepared for 1, 4-naphthoquinone and plumbagin by dissolving the powdered compounds in DMSO and stored at -20 ºC. Juglone stock was prepared fresh before the start of each experiment, given its low stability.[4]

5.5.3 Experimental design

An experimental design was generated to study the effect of oxidant mixtures at *ad libitum* feeding (2 x 10^{10} cells mL^{-1}) and no heat stress conditions, using a simplex centroid design (7 points in the experimental space, **Figure 5.1B**). The simplex centroid design was chosen as it entails a low number of experimental points, thus facilitating performing more replicates. This design entailed 40 runs split into 10 groups of 4 runs (where each design point had 5 – 7 replicates). To assign simplex centroid points to groups, we started from an I-optimal design generated in JMP Pro v 14.2 with 21 points in the experimental space, which already assigns each point to a group. These I-block points were then approximated to the closest point in the simplex centroid design, and their assignment to a group from the I-block design was maintained. An additional control run was tested along with each group to account for differences in populations due to any experimental variability (ambient temperature, humidity, etc.). A population of animals from a single NGM plate was thus divided into 5 runs (4 for design points, and one as a control).

To study the effects of process conditions on responses induced by chemical mixtures, a split plot mixture experiment was performed. The whole plot factors were the two environmental stressors and the split plot factors were the naphthoquinone mixtures. Two levels of heat exposures: 20 ºC and sublethal 33 ºC were considered as the first environmental stressor. Two levels of HB101 bacterial diet regime - *ad libitum* (2 x 10^{10} cells mL^{-1}) (AL) and dietary restriction (2 x 10^{9} cells mL^{-1}) (DR) was considered as the second environmental stressor.[37,61] A total of 28 populations of animals were used for the split plot mixture experiments. Each population was split into five runs. One run, at

process conditions 20 ºC and *ad libitum* diet named “overall control”, was used to compare the 28 populations (7 points of simplex centroid design * 4 process conditions). Another run named “experimental control” was reserved for testing the effect of individual environmental stressor, i.e., a specific heat level and diet combination with no oxidant. Thus, each of the four process conditions were replicated 7 times across the 28 populations. The remaining three runs were exposed to the same combination of diet and heat exposure as the experimental control, but each was exposed to a different chemical mixture. These were assigned to groups similar to the previous experiment, using experimental points from a simplex centroid design. Hence, a total of 84 runs (7 points of the simplex centroid design * 3 replicates * 4 process conditions) and 56 control runs were used to study the effects of heat stress and dietary restriction on the naphthoquinone mixtures. The overall controls were plotted as Xbar and S control chart to ensure that populations were statistically comparable with each other (**Figure 5.2**).

5.5.4 Application of oxidative stress and fluorescence imaging

Approximately 30-40 age-synchronized worms were loaded into a well of a 24-well plate containing the oxidant and HB101 bacteria in S-Medium. Control experiments were conducted with an empty vector of 1% v/v DMSO. Animals were exposed to the oxidants for a period of 8 hours at a temperature of 20 ± 1 ºC. For Pgst-4::GFP imaging, worms were immobilized using a drop of 4 mM tetramisole on dried 2% agarose pads. Worms were imaged using a wide field inverted fluorescence microscope Leica DMi8 at 10x magnification after the exposure period. A Spectra X LED illumination system centered at 470 nm was used for excitation, and a Hamamatsu Orca Flash 4.0 16-bit digital CMOS camera was used for image acquisition. A dose response to individual compounds was

first quantified by exposing animals in increasing concentrations from 0 µM to 100 µM for a period of 8 hours. The naphthoquinone mixtures were applied based on the designs described the previous section.

5.5.5 Quantitative image processing

GFP driven by the *gst-4* promoter is observed throughout the animal, and its intensity was quantified to estimate oxidative stress response *in vivo*. Images were analyzed using a MATLAB script that generates a binary mask to identify a single worm per image. The MATLAB regionprops function was then used to quantify the mean intensity of the animal by overlapping the binary mask over the original image (**Figure 5.1C**).

5.5.6 RNAi by feeding

To measure the influence of *daf-16* on the *gst-4* response to environmental conditions, age-synchronized worms were grown from the egg stage to day 1 of adulthood at 20 ºC in NGM plates containing HT115 bacteria containing the dsRNA-producing vector from the Ahringer library (acquired from Source Biosciences).[62,63] Animals were then bleached following standard protocols.[59] The eggs obtained were deposited in new NGM plates containing HB101 bacteria carrying the *daf-16* RNAi vector. Animals were grown to young adulthood at 20 ºC, and then exposed to oxidative stress as previously described.

5.5.7 ROS detection

To measure ROS levels, 30 animals, exposed to oxidants as described above, were washed twice in M9, and then stained for 2 hours in 1 mL of M9 containing 150 µM 2',7'-dichlorofluorescein diacetate (DCFDA, Sigma) while rotating in the dark. Worms

were then washed twice with M9, and transferred to 2% agarose pads on glass slides, covered, and immediately imaged within 30 minutes of washing out the DCFDA.[64,65] Imaging was performed as previously described. Images were analyzed in ImageJ, where average intensity of the head region was scored.

5.5.8 Survival assay and lifespan curves

To measure survival of animals to acute oxidative stress, 50 worms, exposed to oxidants as described above, were washed twice in M9, and then transferred to a 24-well plate containing 1 ml M9 with 250 µM juglone. Animals observed as rigid and immobile after imparting movement to the liquid in the well were scored as dead. Animals were scored for survival every 30 minutes for the first 2 hours and every 1 hour thereafter until all animals were scored as dead.[4,61] Lifespan curves and statistical analysis of mean lifespan were performed using the Online Application for Survival Analysis 2 (OASIS 2).[66]

5.5.9 Statistical analysis

Data was compiled and analyzed using JMP Pro v.14.2. The standard least squares second order Scheffe model accounting for the individual components, mixture interactions, and effect of the process variables was used.[67] The block effect in the first design and the split plot in the second design were taken to be random effects. All effects, including interactions between the mixtures and process variables, with p value smaller than 0.05 during statistical testing ($\alpha < 0.05$) were considered as significant. Since this approach means dealing with multiple *C. elegans* populations (a population is considered animals cultured on the same NGM plate), we monitored both the mean and variability of gene expression to ensure that population responses are within statistical limits of each other. To assess whether different populations were comparable, we used control limits.

A population plotted within the control limits is equivalent to failing to reject the null hypothesis of statistical control (i.e., all populations have equal means), and a population plotted outside the control limits is equivalent to rejecting the null hypothesis. The process mean was monitored using the X bar chart, while process variability was monitored using the S chart.[68] The responses of the controls were plotted using an Xbar (average) and S (standard deviation) control chart (**Figure 5.2**).

5.6 References

1. Chege, P. M. & McColl, G. Caenorhabditis elegans: A model to investigate oxidative stress and metal dyshomeostasis in Parkinson's disease. *Frontiers in Aging Neuroscience* **6**, (2014).
2. Chen, X. *et al.* Recent progress in the development of fluorescent, luminescent and colorimetric probes for detection of reactive oxygen and nitrogen species. *Chemical Society Reviews* **45**, 2976–3016 (2016).
3. Dias, V., Junn, E. & Mouradian, M. M. The role of oxidative stress in parkinson's disease. *Journal of Parkinson's Disease* **3**, 461–491 (2013).
4. Senchuk, M., Dues, D. & Van Raamsdonk, J. Measuring Oxidative Stress in Caenorhabditis elegans: Paraquat and Juglone Sensitivity Assays. *Bio-Protocol* **7**, (2017).
5. Altenburger, R. *et al.* Mixture effects in samples of multiple contaminants – An inter-laboratory study with manifold bioassays. *Environ. Int.* **114**, 95–106 (2018).
6. Goldberg, M. S. On the interpretation of epidemiological studies of ambient air pollution. in *Journal of Exposure Science and Environmental Epidemiology* **17**, S66–S70 (Nature Publishing Group, 2007).
7. Vermeulen, R., Schymanski, E. L., Barabási, A. L. & Miller, G. W. The exposome and health: Where chemistry meets biology. *Science (80-.).* **367**, 392–396 (2020).
8. Turner, M. C. *et al.* Assessing the Exposome with External Measures: Commentary on the State of the Science and Research Recommendations. *Annual Review of Public Health* **38**, 215–239 (2017).

9. Grolig, J. & Wagner, R. Naphthoquinones. in *Ullmann's Encyclopedia of Industrial Chemistry* (Wiley-VCH Verlag GmbH & Co. KGaA, 2000). doi:10.1002/14356007.a17_067

10. Shang, Y., Chen, C., Li, Y., Zhao, J. & Zhu, T. Hydroxyl radical generation mechanism during the redox cycling process of 1,4-naphthoquinone. *Environ. Sci. Technol.* **46**, 2935–2942 (2012).

11. Finlayson-Pitts, B. J. & Pitts, J. N. Chemistry of the upper and lower atmosphere. *Choice Rev. Online* **37**, 37-5725-37–5725 (2000).

12. Preuss, R., Koch, H. M., Wilhelm, M., Pischetsrieder, M. & Angerer, J. Pilot study on the naphthalene exposure of German adults and children by means of urinary 1- and 2-naphthol levels. *Int. J. Hyg. Environ. Health* **207**, 441–445 (2004).

13. Lin, C. Y. *et al.* Characterization of a structurally intact in situ lung model and comparison of naphthalene protein adducts generated in this model vs lung microsomes. *Chem. Res. Toxicol.* **18**, 802–813 (2005).

14. Lin, P. H., Chen, D. R., Wang, T. W., Lin, C. H. & Chuang, M. C. Investigation of the cumulative tissue doses of naphthoquinones in human serum using protein adducts as biomarker of exposure. *Chem. Biol. Interact.* **181**, 107–114 (2009).

15. Wilson, A. S. *et al.* Characterisation of the toxic metabolite(s) of naphthalene. *Toxicology* **114**, 233–242 (1996).

16. Inbaraj, J. J. & Chignell, C. F. Cytotoxic Action of Juglone and Plumbagin: A Mechanistic Study Using HaCaT Keratinocytes. *Chem. Res. Toxicol.* **17**, 55–62 (2004).

17. Fowler, P., Meurer, K., Honarvar, N. & Kirkland, D. A review of the genotoxic

potential of 1,4-naphthoquinone. *Mutation Research - Genetic Toxicology and Environmental Mutagenesis* **834**, 6–17 (2018).

18. Hunt, P. R. *et al.* Extension of lifespan in C. elegans by naphthoquinones that act through stress hormesis mechanisms. *PLoS One* **6**, 21922 (2011).
19. Kumagai, Y., Shinkai, Y., Miura, T. & Cho, A. K. The chemical biology of naphthoquinones and its environmental implications. *Annu. Rev. Pharmacol. Toxicol.* **52**, 221–247 (2012).
20. Esnault, S. *et al.* A critical role for Pin1 in allergic pulmonary eosinophilia in rats. *J. Allergy Clin. Immunol.* **120**, 1082–1088 (2007).
21. Corsi, A. K., Wightman, B. & Chalfie, M. A transparent window into biology: A primer on Caenorhabditis elegans. *Genetics* **200**, 387–407 (2015).
22. Wittkowski, P. *et al.* Caenorhabditis elegans As a Promising Alternative Model for Environmental Chemical Mixture Effect Assessment - A Comparative Study. *Environ. Sci. Technol.* **53**, 12725–12733 (2019).
23. Vingskes, A. K. & Spann, N. The toxicity of a mixture of two antiseptics, triclosan and triclocarban, on reproduction and growth of the nematode Caenorhabditis elegans. *Ecotoxicology* **27**, 420–429 (2018).
24. Lu, C., Svoboda, K. R., Lenz, K. A., Pattison, C. & Ma, H. Toxicity interactions between manganese (Mn) and lead (Pb) or cadmium (Cd) in a model organism the nematode C. elegans. *Environ. Sci. Pollut. Res.* **25**, 15378–15389 (2018).
25. Chen, H. *et al.* A review of toxicity induced by persistent organic pollutants (POPs) and endocrine-disrupting chemicals (EDCs) in the nematode Caenorhabditis elegans. *Journal of Environmental Management* **237**, 519–525

(2019).

26. Hunt, P. R. The C. elegans model in toxicity testing. *Journal of Applied Toxicology* **37**, 50–59 (2017).

27. Boyd, W. A. *et al.* Developmental effects of the ToxCast™ phase I and phase II chemicals in caenorhabditis elegans and corresponding responses in Zebrafish, Rats, and Rabbits. *Environ. Health Perspect.* **124**, 586–593 (2016).

28. Allard, P., Kleinstreuer, N. C., Knudsen, T. B. & Colaiácovo, M. P. A C. elegans screening platform for the rapid assessment of chemical disruption of germline function. *Environ. Health Perspect.* **121**, 717–724 (2013).

29. Klaus, V. *et al.* 1,4-Naphthoquinones as inducers of oxidative damage and stress signaling in HaCaT human keratinocytes. *Arch. Biochem. Biophys.* **496**, 93–100 (2010).

30. Blackwell, T. K., Steinbaugh, M. J., Hourihan, J. M., Ewald, C. Y. & Isik, M. SKN-1/Nrf, stress responses, and aging in Caenorhabditis elegans. *Free Radical Biology and Medicine* **88**, 290–301 (2015).

31. Wu, M. *et al.* Regulator of G protein signaling-1 modulates paraquat-induced oxidative stress and longevity via the insulin like signaling pathway in Caenorhabditis elegans. *Toxicol. Lett.* **273**, 97–105 (2017).

32. Inoue, H. *et al.* The C. elegans p38 MAPK pathway regulates nuclear localization of the transcription factor SKN-1 in oxidative stress response. *Genes Dev.* **19**, 2278–2283 (2005).

33. Przybysz, A. J., Choe, K. P., Roberts, L. J. & Strange, K. Increased age reduces DAF-16 and SKN-1 signaling and the hormetic response of Caenorhabditis

elegans to the xenobiotic juglone. *Mech. Ageing Dev.* **130**, 357–369 (2009).

34. Benedetto, A., Au, C., Avila, D. S., Milatovic, D. & Aschner, M. Extracellular dopamine potentiates Mn-induced oxidative stress, lifespan reduction, and dopaminergic neurodegeneration in a BLI-3-dependent manner in caenorhabditis elegans. *PLoS Genet.* **6**, e1001084 (2010).
35. Possik, E. & Pause, A. Measuring Oxidative Stress Resistance of Caenorhabditis elegans in 96-well Microtiter Plates. *J. Vis. Exp.* **99**, 527463791–52746 (2015).
36. Hasegawa, K. *et al.* Acrylamide-responsive genes in the nematode Caenorhabditis elegans. *Toxicol. Sci.* **101**, 215–225 (2008).
37. Crombie, T. A., Tang, L., Choe, K. P. & Julian, D. Inhibition of the oxidative stress response by heat stress in Caenorhabditis elegans. *J. Exp. Biol.* **219**, 2201–2211 (2016).
38. Tawe, W. N., Eschbach, M. L., Walter, R. D. & Henkle-Dührsen, K. Identification of stress-responsive genes in Caenorhabditis elegans using RT-PCR differential display. *Nucleic Acids Res.* **26**, 1621–1627 (1998).
39. Link, C. D. & Johnson, C. J. Reporter transgenes for study of oxidant stress in Caenorhabditis elegans. in *Methods in Enzymology* **353**, 497–505 (Academic Press Inc., 2002).
40. Leiers, B. *et al.* A stress-responsive glutathione S-transferase confers resistance to oxidative stress in Caenorhabditis elegans. *Free Radic. Biol. Med.* **34**, 1405–1415 (2003).
41. Goos, P. & Jones, B. *Optimal Design of Experiments: A Case Study Approach*. *Optimal Design of Experiments: A Case Study Approach* (2011).

doi:10.1002/9781119974017

42. Goos, P. & Donev, A. N. The D-optimal design of blocked experiments with mixture components. *J. Qual. Technol.* **38**, 319–332 (2006).

43. Hasegawa, K. *et al.* A rapid and inexpensive method to screen for common foods that reduce the action of acrylamide, a harmful substance in food. *Toxicol. Lett.* **175**, 82–88 (2007).

44. Van Raamsdonk, J. M. & Hekimi, S. Superoxide dismutase is dispensable for normal animal lifespan. *Proc. Natl. Acad. Sci.* **109**, 5785–5790 (2012).

45. Paek, J. *et al.* Mitochondrial SKN-1/Nrf mediates a conserved starvation response. *Cell Metab.* **16**, 526–537 (2012).

46. Rollins, J. A., Shaffer, D., Snow, S. S., Kapahi, P. & Rogers, A. N. Dietary restriction induces posttranscriptional regulation of longevity genes. *Life Sci. Alliance* **2**, (2019).

47. Schulz, T. J. *et al.* Glucose Restriction Extends Caenorhabditis elegans Life Span by Inducing Mitochondrial Respiration and Increasing Oxidative Stress. *Cell Metab.* **6**, 280–293 (2007).

48. Gusarov, I. *et al.* Glycogen controls Caenorhabditis elegans lifespan and resistance to oxidative stress. *Nat. Commun.* **8**, 1–12 (2017).

49. Greer, E. L. & Brunet, A. Different dietary restriction regimens extend lifespan by both independent and overlapping genetic pathways in C. elegans. *Aging Cell* **8**, 113–127 (2009).

50. Lee, R. Y. N., Hench, J. & Ruvkun, G. Regulation of C. elegans DAF-16 and its human ortholog FKHRL1 by the daf-2 insulin-like signaling pathway. *Curr. Biol.*

11, 1950–1957 (2001).

51. Lin, K., Hsin, H., Libina, N. & Kenyon, C. Regulation of the Caenorhabditis elegans longevity protein DAF-16 by insulin/IGF-1 and germline signaling. *Nature Genetics* **28**, 139–145 (2001).

52. Bishop, N. A. & Guarente, L. Two neurons mediate diet-restriction-induced longevity in C. elegans. *Nature* **447**, 545–549 (2007).

53. Hernández-Muñoz, L. S., Gómez, M., González, F. J., González, I. & Frontana, C. Towards a molecular-level understanding of the reactivity differences for radical anions of juglone and plumbagin: An electrochemical and spectroelectrochemical approach. *Org. Biomol. Chem.* **7**, 1896–1903 (2009).

54. O'Brien, P. J. Molecular mechanisms of quinone cytotoxicity. *Chemico-Biological Interactions* **80**, 1–41 (1991).

55. Seshadri, P., Rajaram, A. & Rajaram, R. Plumbagin and juglone induce caspase-3-dependent apoptosis involving the mitochondria through ROS generation in human peripheral blood lymphocytes. *Free Radic. Biol. Med.* **51**, 2090–2107 (2011).

56. Benedetto, A. *et al.* New label-free automated survival assays reveal unexpected stress resistance patterns during C. elegans aging. *Aging Cell* **18**, (2019).

57. Tullet, J. M. A. DAF-16 target identification in C. elegans: past, present and future. *Biogerontology* **16**, 221–234 (2015).

58. Bhatla, N. & Horvitz, H. R. Light and Hydrogen Peroxide Inhibit C.elegans Feeding through Gustatory Receptor Orthologs and Pharyngeal Neurons. *Neuron* **85**, 804–818 (2015).

59. Porta-de-la-Riva, M., Fontrodona, L., Villanueva, A. & Cerón, J. Basic Caenorhabditis elegans methods: Synchronization and observation. *J. Vis. Exp.* (2012). doi:10.3791/4019

60. Stiernagle, T. Maintenance of C. elegans. *WormBook* (2006). doi:10.1895/wormbook.1.101.1

61. Keith, S. A., Amrit, F. R. G., Ratnappan, R. & Ghazi, A. The C. elegans healthspan and stress-resistance assay toolkit. *Methods* **68**, 476–486 (2014).

62. Fraser, A. G. *et al.* Functional genomic analysis of C. elegans chromosome I by systematic RNA interference. *Nature* **408**, 325–330 (2000).

63. Kamath, R. S. *et al.* Systematic functional analysis of the Caenorhabditis elegans genome using RNAi. *Nature* **421**, 231–237 (2003).

64. Yoon, D., Lee, M.-H. & Cha, D. Measurement of Intracellular ROS in Caenorhabditis elegans Using 2',7'-Dichlorodihydrofluorescein Diacetate. *Bio-Protocol* **8**, (2018).

65. Lu, T. *et al.* REST and stress resistance in ageing and Alzheimer's disease. *Nature* **507**, 448–454 (2014).

66. Han, S. K. *et al.* OASIS 2: Online application for survival analysis 2 with features for the analysis of maximal lifespan and healthspan in aging research. *Oncotarget* **7**, 56147–56152 (2016).

67. Preece, D. A. & Cornell, J. A. Experiments with Mixtures: Designs, Models, and the Analysis of Mixture Data. *Biometrics* **38**, 288 (1982).

68. Scouse, R. A. Introduction to Statistical Quality Control. *Plast. rubber Int.* **10**, 30–32 (1985).

Chapter 6: Assessment of Early Onset of Pharynx Morphological Changes Caused by Increased Protein Accumulation

6.1 Abstract

In this chapter, we measure healthspan and lifespan metrics of mutants with increased protein aggregation. Our aim is to confirm that this phenotype is correlated with a reduction in the animals' health (measured as pumping rate, pharynx morphological changes, and locomotion) and longevity (measured as mean lifespan). We confirm that these mutants, screened for the protein aggregation phenotype, have an early onset of aging indicators and have a shorten lifespan respect to the wildtype strain. This demonstrates that increased protein aggregation can be used as a metric for aging studies and phenotyping screens.

6.2 Introduction

The process by which organisms undergo structural and functional decline with age is regulated by a complex network of genetic and environmental factors[1]. It is important to identify the mechanisms that govern aging and understanding the biological mechanisms and genetic pathways that are affected by this process. Approaches for genetic screening that rely on novel phenotypes or the development of new tools provide an opportunity to probe an unexplored genotype-phenotype landscape and identify yet uncharacterized genes that regulate the aging process[2].

One characteristic displayed by aging individuals is increased levels of protein aggregation due to a decline in proteostasis[3]. Protein aggregation has recently been used so as a marker for aging[2]. One protein that has shown increased aggregation with age is the Poly(A)-binding protein PAB-1[4]. This protein is expressed and aggregates in

wildtype *C. elegans*. We hypothesized that mutants with increased protein aggregation should also show a reduction in healthspan and lifespan.

In this chapter, we evaluate various metrics to test *C. elegans* mutants with increased protein aggregation. We assayed healthspan indicators and lifespan of these aggregation mutants and identified a reduction in their longevity.

6.3 Results

C. elegans strain DCD214 (uqIs24 [*myo-2*p::tagRFP::*pab-1*]) has expression of tagRFP:*pab-1* in pharyngeal muscles. This protein assembles into stress granules when exposed to heat stress and forms aggregates in aging animals[5]. This protein aggregation is present in aging individuals because of the decline in proteostasis[6,7]. Midkiff et al developed a platform for isolation of *C. elegans* mutants with shortened lifespan trough a forward genetic screen approach, taking advantage of this protein aggregation in aged animals. This way, they identified mutants with a significant reduction in longevity and increased tagRFP:PAB-1 aggregation[2]. These mutant strains are named M3 and M9.

Although Midkiff et al used found a correlation between mutants with increased aggregation and reduced lifespan, there are other metrics that can be analyzed to evaluate how this accelerated aging shown in strains M3 and M9 could possibly be reducing healthspan of the animals. We chose to first evaluate pumping rate as this has been shown to undergo a dramatic decrease and an easy to quantify decline with age[8,9], this is because of an increase accumulation of bacteria in the pharynx[10]. Pumping rate is therefore a robust indicator of animals' health and is well correlated to lifespan[9,11,12].

To assess the likelihood of a diminished health in the pharynx of *C. elegans* we evaluated the pumping rate of the strains DCD214, DCD214 crossed with the short-lived

VS24 (*kat-1*(tm1037)), and strains M3 and M9. We observed no significant difference with the wildtype for the first 6 days of adulthood. However in day 9 there was a sharp decrease in pumping rate for strain M3 (**Figure 6.1**). This decrease in pharyngeal functionality indicates an early onset of senescence in this strain. Similar results were observed for strains M9 and the VS24 cross by day 12. These results demonstrate that these short-lived animals also age more quickly showing pharyngeal decline earlier in their life than the wildtype.

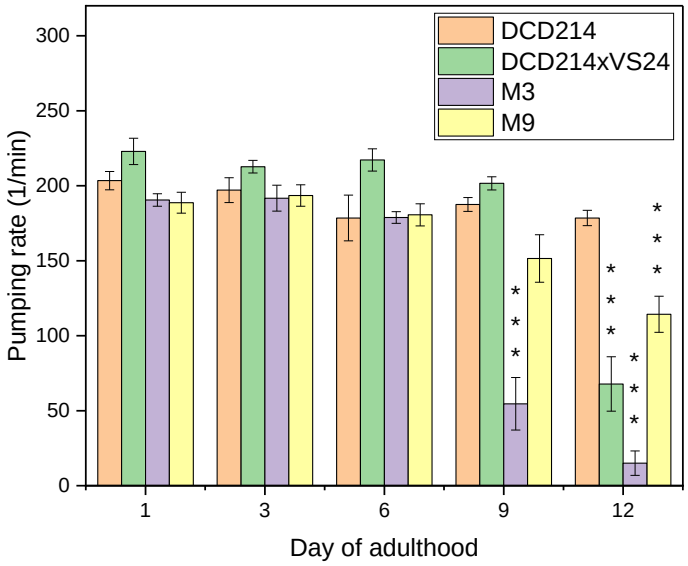

Figure 6.1 Pumping rate decreases with increased protein aggregation. Pumping rates for strain M3 shows a sharp decrease at day 6 of adulthood. Strains DCD214xVS24 and M9 show a similar trend by day 12. $p < 0.001$ (***), error bars are SEM.

In addition to pumping rate, another indicator of pharynx health is the observation of morphological changes in its structure. Aged worms show structural decline related to the presence of vacuole-like pits, bacterial plugging of the pharynx, and the bending of the pharynx' isthmus[9]. We used an structural index to evaluate this decline:

1-least decline, 2-somewhat declined, and 3-most deteriorated (**Figure 6.2**). Our results indicate that morphological changes are observed stating at day 6 of adulthood for all strains respect to the wildtype (**Figure 6.3**). Interestingly, by day 9 only strain M3 showed any significant difference in decline and by day 12 all strains, including the wildtype, showed similar structural decline. Strain DCD214 did not show any significant decline until day 9 indicating that all the mutant strains have early onset of pharyngeal decline. This confirms our observations from Figure 6.1. These results demonstrate that not only are this strains short-lived but they also expend a significant part of their lifespan in diminished health. Furthermore, it is interesting that strain M3 also had a significant deterioration of the pharynx even when all other strains were already showing signs of structural damage by day 9. Notably, strain M3 was also the shortest lived of all the strains evaluated (**Figure 6.5**). However, eventually even the healthier wildtype also shows decline in later stages as its pharynx losses functionality because of age.

Figure 6.2 Morphological changes in the aging pharynx. A healthy pharynx (top) shown no structural damage. In aged animals, we observe vacuole-like structures (red arrow) or pharynx bending (green arrow).

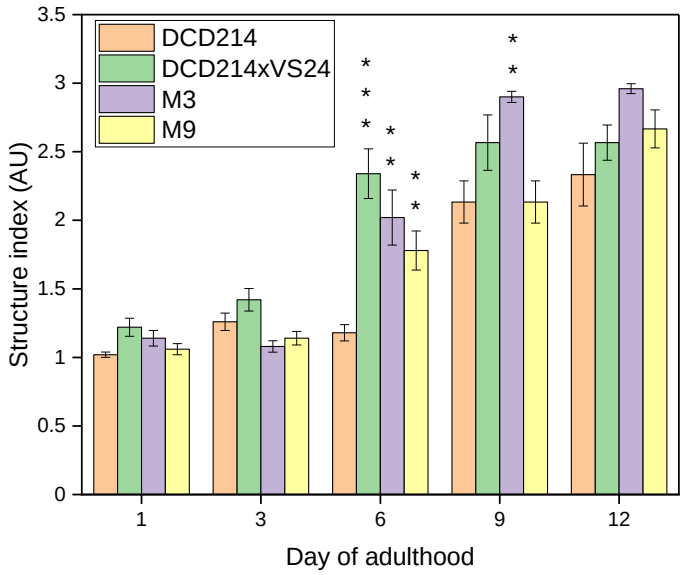

Figure 6.3 Structural integrity of the pharynx diminishes with aging and increased protein aggregation. A structural index of 1 (least deteriorated) to 3 (most deteriorated) shows that the mutant strains have an early onset of structural decline in the pharynx respect to the wildtype strain with the earliest difference observed at day 6 of adulthood. $p < 0.01$ (**), $p < 0.001$ (***), error bars are SEM.

The previous metrics are directly related to the health and functionality of the animals' pharynx. We decided to test a different indicator of healthspan in *C. elegans* by assessing the number of thrashings in liquid of the strains evaluated. It has been shown that healthy animals have a higher frequency of movement in liquid than aged ones[13–15]. In contrast to the previous experiments, we observed an earlier decline in thrashing frequency for the mutant worms in day 3 (**Figure 6.3**). Although the wildtype also showed decline in its thrashing frequency, it is notable that this reduction was not as sharp and steady as with the mutant strains M3 and M9. Strain VS24 did not show a significant difference with the wildtype until day 9, possibly indicating to a relation between increased protein aggregation and loss of proteostasis in strains M3 and M9 and early loss of locomotion rate.

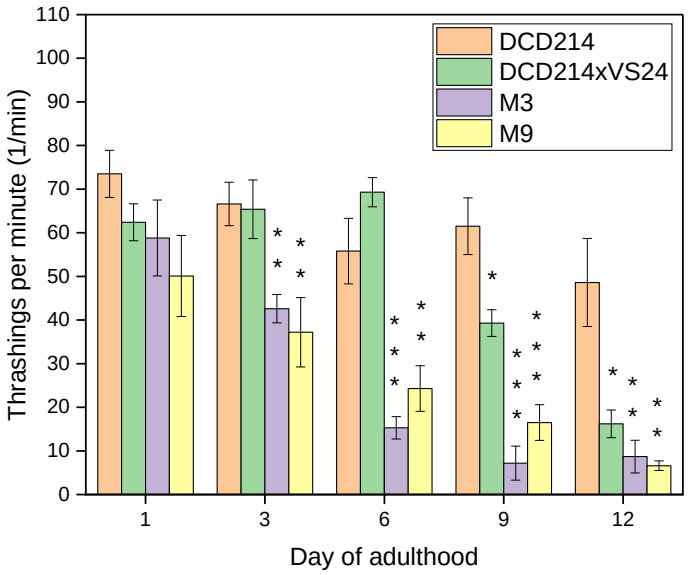

Figure 6.4 Movement in liquid of *C. elegans* diminishes with increased protein aggregation. Movement in liquid, measured as the thrashing frequency shows an early decline by day 3 of adulthood in mutant animals. $p < 0.01$ (**), $p < 0.001$ (***), error bars are SEM.

The previous experiments were aimed to evaluate healthspan metrics in *C. elegans*. These indicate that the mutant strains show an early decline in health as shown in their loss of pharynx functionality and diminished locomotion. We decided to measure lifespan of these strains to confirm if this diminished healthspan is associated with a reduction in longevity (**Figure 6.5**). Our results confirmed that all mutant strains have diminished lifespan with respect to the wildtype. This confirms that strains M3 and M9 are short-lived as previously shown by Midkiff et al[2]. Our results indicate a correlation between increased protein aggregation, diminished healthspan as measure by pharynx health and locomotion, and a reduction in the animals' longevity.

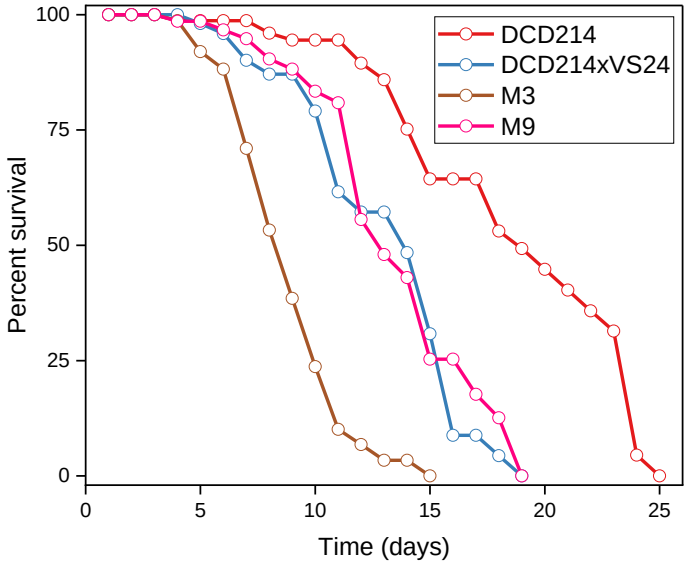

Figure 6.5 Mutant strains have a reduction in longevity. Lifespan for the mutant strains is diminished with strain M3 showing the shortest lifespan of the mutant strains.

5.4 Discussion

In this chapter, we have demonstrated that animals with mutations that lead to increased protein aggregation also have diminished healthspan, and confirmed their reduced longevity. To test this we used metrics such as pharyngeal pumping, observation of structural damage in the animals' pharynx, and movement in liquid measures as thrashing frequency. We demonstrated that increased protein aggregation is a robust predictor of healthspan reduction as all of our metrics show an early onset of aging phenotypes in the mutant worms. This evaluation can be paired with mutant screening such as performed by Midkiff et al[2] to strengthen the identification and validation of mutants with increased protein aggregation.

6.5 Materials and methods

6.5.1 Strains and maintenance

C. elegans strains DCD214 [myo-2p::tagRFP::pab-1], and VS24 [kat-1(tm1037)] were acquired from the CGC (Caenorhabditis 421 Genetics Center). Strains carrying integrated transgene myo-2p::tagRFP::pab-1 as well as kat-1(tm1037) were constructed by crossing DCD214 males with hermaphrodites from strains VS24 according to standard protocols. All other mutants were derived from ethyl methane sulfate (EMS) mutagenesis of the DCD214 strain[2]. Worms were cultured on NGM plates according to standard protocols[16] on lawns of E. 428 coli strain OP50. Worms were grown at 20 ºC. Day 1 of adulthood is defined as the first 24 hours following the conclusion of the L4 larval stage.

6.5.2 Pharyngeal pumping

Pumping assays were performed on agar plates at room temperature (approximately 20 °C) using a Leica M165 FC stereomicroscope. Pumping rate was defined as the number of contractions in the terminal bulb in a 1-min period. Pumping rates were measured in the presence of OP50 bacteria, the standard laboratory diet for *C. elegans.*

6.5.3 Structural analysis of the pharynx

For pharynx structure, 10 animals for each age and genotype were mounted on 2% agarose pads and paralyzed with 1mm tetramisole in M9 buffer. Bright field images were collected of the animal's head focusing on the pharynx using a Hamamatsu Orca Flash 4.0 16-bit digital CMOS camera connected to a Leica DMi8 microscope at 63x magnification. Each image was presented to group-blind respondents who scored the structure as 1—least, 2—somewhat, or 3—most deteriorated. Five respondents' scores

for each animal were averaged to give a single structural deterioration score. Student's *t*-tests were performed to analyze group differences.

6.5.4 Thrashing frequency in liquid

In liquid, every third day, 10 worms were picked from the stock plates at 20°C and transferred to 24-well plates containing 1 mL of M9 solution in each well. The worms were allowed to equilibrate for ~30s, and then the thrashing was recorded using a Lumenera Infinity 3 camera mounted on a Leica M165 FC microscope for 20s. The average thrashings per minute were computed and then plotted for all of the strains.

6.5.5 Lifespan analysis

Worms were age-synchronized and grown at 20 ºC until reaching Day 1 of adulthood. Approximately 100 worms from each population were then counted and picked to a new plate and placed at 20 ºC. For each subsequent day, the number of living, dead, and censored worms were counted. Living worms are defined as worms that responded to a gentle touch from a platinum wire and dead worms are defined as those that did not respond to the same stimulus. Worms were censored if they were not visible (i.e. crawled off the plate or under the agar) or displayed signs of internal hatching. Signs of internal hatching include internal growth of larvae ("bag of worms") as well as worms that undergo apparent rupture. Worms were picked to new plates daily during the egg-laying phase. Following egg-laying, worms were picked to new plates when plates begin to dry or in rare cases where small fungal contaminants appeared. After no living worms remained, mutants' lifespan data was compared to wild-type data using the log-rank statistical test to determine P-values, and to identify worms with reduced lifespan[17].

6.6 References

1. Uno M, Nishida E. Lifespan-regulating genes in C. elegans. *Aging Mech Dis*. 2016;2(1):16010. doi:10.1038/npjamd.2016.10

2. Midkiff DF, San-Miguel A. Identifying C. elegans Lifespan Mutants by Screening for Early-Onset Protein Aggregation. *bioRxiv*. 2021:1-28. doi:10.1101/2021.12.14.472506

3. David DC, Ollikainen N, Trinidad JC, Cary MP, Burlingame AL, Kenyon C. Widespread protein aggregation as an inherent part of aging in C. elegans. *PLoS Biol*. 2010;8(8):47-48. doi:10.1371/journal.pbio.1000450

4. Portman D. Profiling C. elegans gene expression with DNA microarrays. *WormBook*. 2006:1-11. doi:10.1895/wormbook.1.104.1

5. Lechler MC, Crawford ED, Groh N, et al. Reduced Insulin/IGF-1 Signaling Restores the Dynamic Properties of Key Stress Granule Proteins during Aging. *Cell Rep*. 2017;18(2):454-467. doi:10.1016/j.celrep.2016.12.033

6. Mondal S, Hegarty E, Martin C, Gökçe SK, Ghorashian N, Ben-Yakar A. Large-scale microfluidics providing high-resolution and high-throughput screening of Caenorhabditis elegans poly-glutamine aggregation model. *Nat Commun*. 2016;7:13023. doi:10.1038/ncomms13023

7. van Ham TJ, Holmberg MA, van der Goot AT, et al. Identification of MOAG-4/SERF as a regulator of age-related proteotoxicity. *Cell*. 2010;142(4):601-612. doi:10.1016/j.cell.2010.07.020

8. Keith SA, Amrit FRG, Ratnappan R, Ghazi A. The C. elegans healthspan and stress-resistance assay toolkit. *Methods*. 2014;68(3):476-486. doi:10.1016/j.ymeth.2014.04.003

9. Chow DK, Glenn CF, Johnston JL, Goldberg IG, Wolkow CA. Sarcopenia in the Caenorhabditis elegans pharynx correlates with muscle contraction rate over lifespan. *Exp Gerontol*. 2006;41(3):252-260. doi:10.1016/j.exger.2005.12.004

10. Garigan D, Hsu AL, Fraser AG, Kamath RS, Abringet J, Kenyon C. Genetic analysis of tissue aging in Caenorhabditis elegans: A role for heat-shock factor and bacterial proliferation. *Genetics*. 2002;161(3):1101-1112. doi:10.1093/genetics/161.3.1101

11. Huang C, Xiong C, Kornfeld K. Measurements of age-related changes of physiological processes that predict lifespan of Caenorhabditis elegans. *Proc Natl Acad Sci U S A*. 2004;101(21):8084-8089. doi:10.1073/pnas.0400848101

12. Scharf A, Piechulek A, Von Mikecz A. Effect of nanoparticles on the biochemical and behavioral aging phenotype of the nematode caenorhabditis elegans. *ACS Nano*. 2013;7(12):10695-10703. doi:10.1021/nn403443r

13. Dong L, Cornaglia M, Lehnert T, Gijs M. On-chip microfluidic biocommunication assay for studying male-induced demise in C. elegans hermaphrodites. *Lab Chip*. 2016;16(23):4534-4545. doi:10.1039/C6LC01005A

14. Laranjeiro R, Harinath G, Burke D, Braeckman BP, Driscoll M. Single swim sessions in C. elegans induce key features of mammalian exercise. *BMC Biol*. 2017;15(1):30. doi:10.1186/s12915-017-0368-4

15. Ghosh R, Emmons SW. Episodic swimming behavior in the nematode C. elegans. *J Exp Biol*. 2008;211(23):3703-3711. doi:10.1242/jeb.023606

16. Stiernagle T. Maintenance of C. elegans. *WormBook*. 2006. doi:10.1895/wormbook.1.101.1

17. Han SK, Lee D, Lee H, et al. OASIS 2: Online application for survival analysis 2 with features for the analysis of maximal lifespan and healthspan in aging research. *Oncotarget*. 2016;7(35):56147-56152. doi:10.18632/oncotarget.11269

Chapter 7: Conclusions

7.1. Summary and overview of projects

In modern society, the number of elderly adults will continue to increase in the near future, causing higher economic and social impacts on countries. Amongst the causes for these population tendencies is the improvement on health services experienced during the previous decades. Consequently, this has caused a rise in lifespan, defined as the maximum amount of time an organism in a species can live[1]. Furthermore, elderly adults have a higher risk of exhibiting diseases such as Alzheimer's disease, Parkinson's disease, and several forms of dementia[2]; this highlights the relevance of performing aging studies. We have use successfully the model organism *C. elegans* for aging research, a microscopic nematode that has been important in elucidating genetic and environmental factors affecting lifespan[3]. Our work is the first of its kind to use an integrated high-throughput approach to characterize lifespan, while associating this metric to the spatiotemporal activity of longevity genes. This was achieved by combining a CRISPR/Cas9 approach to circumvent the issues encountered with strains generated with methods that are more traditional. Additionally, we used computer vision tools and machine learning to extract high-throughput information from our lifespan and stress assays. No systematic method has been used before to characterize activity of a transcription factor associated with stress to determine and predict an organism's longevity, with our results indicating that DAF-16 accounts for up to 78% of lifespan variability under the dietary restriction regimes evaluated[4]. This could to potential developments such as the determination and choosing of the best interventions for lifespan extension in *C. elegans* (and organisms with the DAF-16

conserved pathway). Furthermore, our approach reveals that it can be adapted and applied to other transcription factors. Generating these strains with endogenous levels of expression will reveal unexpected behavior (such as the migration of DAF-16 to cell nucleoli) or interactions that were previously not possible to assess, for example we showed that DAF-16 activates in the germline, other techniques would not reveal this because of silencing in the germline. We also provide an automated pipeline that combines MATLAB scripts and machine learning for the identification of these behaviors and translocation patterns. Moreover, our systems biology approach enable identification of previously unknown interactions at the subcellular level, such as the migration of DAF-16 in cell nucleoli under dietary restriction. These findings and results will help to understand the fundamental mechanisms by which DAF-16 and other transcription factors regulate the aging process.

Several environmental conditions affect longevity in *C. elegans*. Exposure to these stressors affects the activity of transcription factors, such as DAF-16, PHA-4, SKN-1, and others. These proteins influence the downstream expression of genes related to stress resilience in *C. elegans*. Some examples of these environmental stimuli are dietary restriction (DR), temperature, oxidative stress, etc. However, environmental stressors do not affect organisms in vacuum as they are frequently found in combinations. Understanding how these different stressors interplay with each other is crucial to evaluate their effect when they are present in the environment. Nevertheless, the amount of combinatorial experiments needed to evaluate this interplay can become very large when considering new interactions. We developed a platform to evaluate combinatorial perturbations using a simplex centroid. This approach permits the generation of response

surfaces that are robust in assessing the synergistic or antagonistic effects of these combinations. Using this platform, we show that naphtoquinones have an antagonistic effect on the oxidative stress response of *C. elegans* when use in mixtures. However, dietary restriction reverses this antagonistic effect. Furthermore, we demonstrate that heat stress abolishes the oxidative stress response, possibly the animals favor cell protection against loss of proteostasis over the response to xenobiotics generating oxidative stress[5]. We demonstrated the relevance of evaluating exposure to xenobiotics in context, as these are pollutants found in the environment in conjunction with other environmental factors and conditions.

Our results reveal that if we consider combinatorial exposure to stressors, their behavior is altered, leading to antagonistic, synergistic, or silencing effects. Recently, more research is performed in assessing the effect of the exposome in human health. Our findings should warn future research to consider these combinatorial effects as they could possibly alter significantly the efficacy of the stress response of organisms. We also provide an experimental platform to perform these studies, as we expect the single centroid design to be adopted by the community to evaluate exposure to multiple xenobiotics and stressors in a systematic manner. These results display the importance and relevance of evaluating how organisms respond to variable environmental factors in a more realistic assessment.

Finally, we demonstrate that the increase protein aggregation phenotype identified in mutant strains by Midkiff et al[6] are correlated with the early appearance of aging phenotypes such as diminish pharyngeal pumping, increased structural deterioration of the pharynx, and reduction of locomotion in liquid. Moreover, the mutants with this

phenotype also have a shorten lifespan. This demonstrates that protein aggregation can be used a robust predictor of aging in *C. elegans*.

7.2 Applications beyond the scope of this dissertation

7.2.1 A CRISPR/Cas9 and machine learning approach to quantify endogenous spatiotemporal activity to predict stress-induced lifespan extension

Our systems approach can be easily modified to be used to other transcription factors that govern the aging process. PHA-4 has been shown to increase its activity under conditions of dietary restriction[7], SKN-1 is a transcription factor that regulates the oxidative stress response[8], and HSF-1 has a similar role in the heat stress response[9]. Research with these transcription factors has some of the same issues as the ones mentioned for DAF-16. For example, no availability of strains tagged at the endogenous locus. Our CRISPR/Cas9 approach is modular and can be modified to target these genes; this opens the possibility of observing their endogenous activity patterns. Our custom-made MATLAB algorithm can also be modified to track these proteins. DAF-16 was shown to be present in all tissues for our experiments and our algorithm was developed to account for the differences between cell types and tissues. This means that its use for assessment of total intensity of other genes can be performed by changing parameters such as the binarization threshold. However, other parameters such as classification by cell type do not require much modification.

This means that we can potentially evaluate the contributions of various transcription factors to lifespan extension in *C. elegans* by performing stress assays of the type required for the specific gene, feed this large data sets to or algorithm, and use it to formulate predictions of lifespan based on gene activity. Moreover, this approach can

be applied to combinatorial exposures. For instance, both DAF-16 and PHA-4 activate under different dietary restriction regimes. A strain containing tags for both genes could be used to evaluate any synergistic or additive effect their response may have in lifespan under stressful conditions. We have already develop such a strain and our preliminary data show that DAF-16 and PHA-4 'collaborate' to the dietary restriction response by 'taking over' one another under different levels of food limitation.

Finally, our platform has revealed previously unreported interactions of DAF-16 in cell nucleoli and germline. Recent studies have an increased focus on lifespan extension conveyed by mechanisms happening inside of the nucleoli[10,11]. Our findings indicate a possible role for DAF-16 in the nucleolus that increases lifespan. This result was possible only by using our single-copy strain revealing endogenous activity. It is likely that other strains developed in the same manner will reveal novel interactions at the cellular and subcellular level.

7.2.2 Assessment of antagonistic, synergistic, and silencing effects of combinatorial stress response of *C. elegans*

Combinatorial perturbation experiments require the acquisition of large data sets with multiple replicates. Our approach allows for the generation of response surfaces using a simplex centroid design, facilitating the interpretation of the effects of combinatorial exposures while at the same time reducing the amount of data point needed for significance. This is made more relevant by the fact that naphthoquinones are present in the environment[12,13], so their effects in organisms happen in combination of other factors. Our approach can be used to evaluate other known xenobiotics that could enact the oxidative stress response in *C. elegans*. Some of these are paraquat, acrylamide,

arsenic, chromium, nickel, and benzopyrene, tethrachlorodibenzo-p-dioxin[14]. This is made more relevant as some of these are also carcinogenic and known to be present in the environment as pollutants.

In addition, our platform is not limited to looking primarily to the oxidative stress response. As shown in Chapter 5, we also evaluated the response of DAF-16 to a subset of the main experimental conditions. This highlights that *gst-4* can be replaced for other genes such as *daf-16*, *pha-4*, *hsp-16.2*, *sod-3*, *skn-1*, and others. Performing this will possibly reveal novel interactions between combinatorial exposures. For example, *daf-16* activates under dietary restriction, oxidative stress and heat stress. Evaluating the whole response surface for it could reveal if DAF-16 favors responding to certain types of stress or mixtures of stress.

7.2.3 Quantitative assessment of early healthspan decline and shortened lifespan associated with increased protein aggregation

Our evaluation of the correlation between diminished healthspan and lifespan for the mutant stains with the increased protein aggregation phenotype reveal that this phenotype is possibly a strong predictor of senescence. This confirms that the pipeline developed by Midkiff et al[6] can be used to identify mutants with a reduction in longevity by screening for mutants that undergo protein aggregation during their late life stages. The use of the metrics evaluated in Chapter 6 should strengthen this pipeline as the original study look mainly at lifespan metrics. Using these additional healthspan metrics make the approach more robust.

In addition, the Mask R-CNN algorithm developed in Chapter 4 should prove to be a valuable tool for the *C. elegans* community after further testing of its capabilities is

performed. In Chapter 6 we used trained observers to evaluate the structural damage of the aging pharynx. Using such an enhanced CNN would allowed for unbiased analysis of the morphological changes of the pharynx associated with aging, while providing a better quantification than our structural index.

7.3 References

1. Kenyon CJ. The genetics of ageing. *Nature*. 2010;464(7288):504-512. doi:10.1038/nature08980

2. Arey RN, Murphy CT. Conserved regulators of cognitive aging: From worms to humans. *Behavioural Brain Research*. http://www.sciencedirect.com/science/article/pii/S0166432816303904. Published 2017. Accessed April 12, 2017.

3. Corsi AK, Wightman B, Chalfie M. A transparent window into biology: A primer on Caenorhabditis elegans. *Genetics*. 2015;200(2):387-407. doi:10.1534/genetics.115.176099

4. Huayta J, San-Miguel A. Endogenous DAF-16 Spatiotemporal Activity Quantitatively Predicts Lifespan Extension Induced by Dietary Restriction. *bioRxiv*. 2021;4(1):6. doi:10.1101/2021.12.20.473576

5. Suresh Arulalan K, Huayta J, Stallrich JW, San-Miguel A. Antagonistic effects of chemical mixtures on the oxidative stress response are silenced by heat stress and reversed under dietary restriction. *Exposome*. 2021;1(1). doi:10.1093/exposome/osab005

6. Midkiff DF, San-Miguel A. Identifying C. elegans Lifespan Mutants by Screening for Early-Onset Protein Aggregation. *bioRxiv*. 2021:1-28. doi:10.1101/2021.12.14.472506

7. Panowski SH, Wolff S, Aguilaniu H, Durieux J, Dillin A. PHA-4/Foxa mediates diet-restriction-induced longevity of C. elegans. *Nature*. 2007;447(7144):550-555.

doi:10.1038/nature05837

8. Bishop NA, Guarente L. Two neurons mediate diet-restriction-induced longevity in C. elegans. *Nature*. 2007;447(7144):545-549. doi:10.1038/nature05904

9. Kumsta C, Chang JT, Schmalz J, Hansen M. Hormetic heat stress and HSF-1 induce autophagy to improve survival and proteostasis in C. Elegans. *Nat Commun*. 2017;8. doi:10.1038/ncomms14337

10. Tiku V, Antebi A. Nucleolar Function in Lifespan Regulation. *Trends Cell Biol*. 2018;28(8):662-672. doi:10.1016/j.tcb.2018.03.007

11. Tiku V, Jain C, Raz Y, et al. Small nucleoli are a cellular hallmark of longevity. *Nat Commun*. 2016;8(1):1-9. doi:10.1038/ncomms16083

12. Fowler P, Meurer K, Honarvar N, Kirkland D. A review of the genotoxic potential of 1,4-naphthoquinone. *Mutat Res - Genet Toxicol Environ Mutagen*. 2018;834:6-17. doi:10.1016/j.mrgentox.2018.07.004

13. Gram TE. Chemically reactive intermediates and pulmonary xenobiotic therapy. *Pharmacol Rev*. 1997;49(4):297-341. https://pubmed.ncbi.nlm.nih.gov/9443161/. Accessed August 31, 2021.

14. Henkler F, Brinkmann J, Luch A. The role of oxidative stress in carcinogenesis induced by metals and xenobiotics. *Cancers (Basel)*. 2010;2(2):376-396. doi:10.3390/cancers2020376